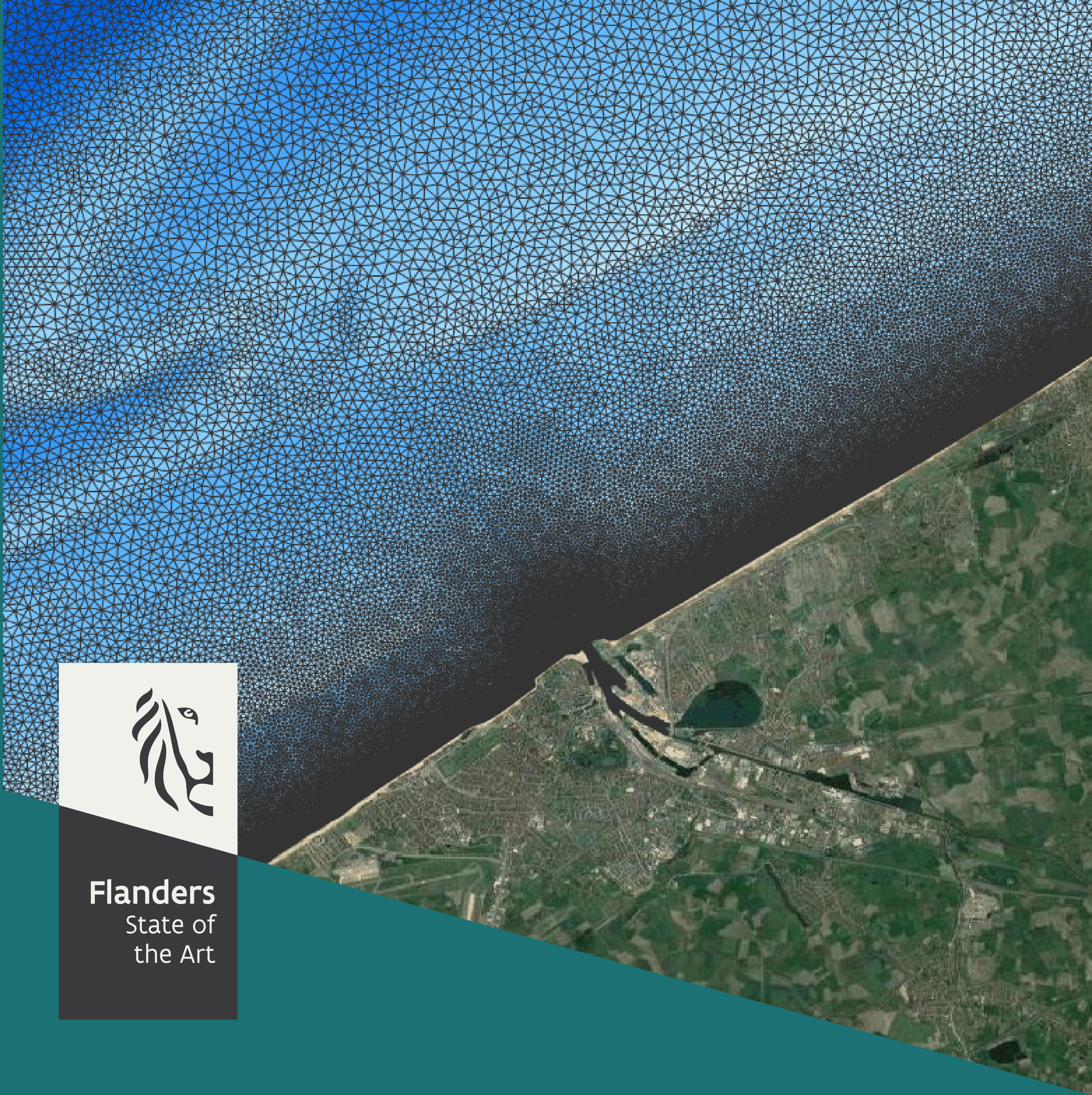

Flanders
State of
the Art

15_068_12
FHR reports

Modelling Belgian Coastal zone and Scheldt mouth area

Sub report 12
Scaldis-Coast model
Model setup and validation of the 2D hydrodynamic model

DEPARTMENT
MOBILITY & PUBLIC WORKS

www.flandershydraulicsresearch.be

Modelling Belgian Coastal zone and Scheldt mouth area Modelling Belgian Coastal zone and Scheldt mouth area

Sub report 12: Scaldis-Coast model – Model setup and validation of the 2D hydrodynamic model

Kolokythas, G.; De Maerschalck, B.; Wang, L.; Fonias, S.; Breugem, A.; Vanlede, J.; Mostaert, F.

Flanders Hydraulics Research
Flanders State of the Art

Legal notice

Copyright and citation

D/2021/3241/067

This publication should be cited as follows:

Kolokythas, G.; De Maerschalck, B.; Wang, L.; Fonias, S.; Breugem, A.; Vanlede, J.; Mostaert, F. (2021). Modelling Belgian Coastal zone and Scheldt mouth area Modelling Belgian Coastal zone and Scheldt mouth area: Sub report 12: Scaldis-Coast model – Model setup and validation of the 2D hydrodynamic model. Version 4.0. FHR Reports, 15_068_12. Flanders Hydraulics Research: Antwerp

Document identification

Customer:	Vlaams-Nederlandse Scheldecomissie (VNSC)	Ref.:	WL2021R15_068_12
Keywords (3-5):	Coastal modelling, Complex Project Kustvisie, Tide		
Knowledge domains:	Hydraulics and sediment > Hydrodynamics > Tides > Numerical modelling		
Text (p.):	66	Appendices (p.):	40
Confidential:	☒ No	☒ Available online	

Author(s):	Kolokythas, G.; De Maerschalck, B.; Wang, L.

Control

	Name	Signature
Reviser(s):	Vanlede, J.	Getekend door:Joris Vanlede (Signature) Getekend op:2021-05-31 16:18:49 +02:0 Reden:Ik keur dit document goed Joris Vanlede
Project leader:	De Maerschalck, B.	Getekend door:Bart De Maerschalck (Sig Getekend op:2021-05-19 10:33:14 +02:0 Reden:Ik keur dit document goed Bart De Maerschalck

Approval

Head of Division:	Mostaert, F.	Getekend door:Frank Mostaert (Signature Getekend op:2021-05-17 16:41:52 +02:0 Reden:Ik keur dit document goed Frank Mostaert

CERTIFIED ISO 9001

Abstract

With the increasing awareness of sea level rise, the Flemish Authorities initiated the *Complex Project Kustvisie* (CPKV) in order to start together with all involved stakeholders to define the overall long-term coastal defence strategy for the Belgian Coast. To analyze the impact of sea level rise on the morphology of the coast and to assess mitigation measures on their efficiency the need for a flexible coastal model for the Belgian coast and Scheldt mouth area was revealed.

Therefore, in 2015 it was decided to build an integral coastal model within the TELEMAC-MASCARET model suite. The present report describes the setup and validation of the two-dimensional hydrodynamic model. The hydrodynamic model forms the basis of the final goal: the morphodynamic model. The hydrodynamic model will be coupled to the TOMAWAC spectral wave model and SISYPHE sediment transport and bed update model.

The model is validated by comparison of the numerically predicted water levels and velocities against measured water levels, stationary velocities and velocities along transects (ADCP sailed) at several locations at the coast and the Western Scheldt estuary. The performance of Scaldis-Coast is found to be good at the Belgian coast but also in The Western Scheldt. For the water levels the total RMSE increases from 9 cm in the North Sea to 13 cm in the Western Scheldt towards Antwerp. The absolute value of the bias of water levels is equal or lower than 5 cm at most stations.

The Scaldis-Coast performs good in predicting the velocities at the considered coastal locations, presenting RMSE of velocity magnitude which is in general around 0.15 m/s.

The hydrodynamic model is available at the Flanders Hydraulics Research model repository: https://wl-subversion.vlaanderen.be/!/#repoSpNumMod/view/head/TELEMAC/Scaldis-Kust/15_068%20Complex%20Model%20Kustvisie%202021/1_2D_HYDRODYNAMICS.

Contents

List of tables

List of figures

1 Introduction

Within the *Complex Project Kustvisie* (CPKV) all involved stakeholders participate in process of defining the overall design of the long-term coastal defence of the Belgian Coast. The project was formerly known as project *Vlaamse Baaien* (Flemish Bays). The *Vlaamse Baaien* project was initiated in 2014 by the Flemish Authorities with the goal to protect the Belgian Coast from (extreme) sea level rise and climate change on the horizon 2050 – 2100. The goal of the project is to create an attractive and natural coast that is climate change resilient with economic benefits like estuarine traffic and renewable energy.

Within this project a wide variety of mitigation strategies can be considered, ranging from extra beach and foreshore nourishments, dunes on beaches to artificial offshore barrier islands. The evaluation of these interventions on currents, waves and morphology revealed the need for a flexible, accurate and versatile global coastal model for the Belgian coast and Western Scheldt mouth area.

Up till 2015, the available models for the Belgian coast, were mostly restricted to selective stretches of the coast or ports, built for specific projects and limited in offshore direction, mostly based on structured grids. Apart from the aforementioned models, large scale continental shelf models with little focus on the near- and onshore coastal areas, were also available.

Therefore, it was decided to build an integral coastal model within the TELEMAC-MASCARET model suite. The model should be suitable to estimate morphological evolutions both on the short scale (days to a year) as on the mid-term scale (up to a decades) both in the tidally driven off-shore part and at the near-shore.

The present report describes the setup and validation of the two-dimensional hydrodynamic tidal model developed with the TELEMAC2D model suite. The hydrodynamic 2D model forms the basis of the final morphodynamic model and delivers input on the currents and water levels for the morphodynamic model. The 2D hydrodynamic model will be coupled to the TOMAWAC wave propagation model and the SISYPHE sediment transport and bed update model. The setup and validation of the wave propagation and the morphodynamic model is described in separate sub-reports. The stand-alone hydrodynamic model only provides the currents driven by tidal and meteorological forcing. Once coupled with the wave propagation model, also wave-induced currents will be calculated.

Recall that the main objective of the hydrodynamic model is providing water levels and currents for the morphodynamic model. For morphodynamics the currents are of higher importance than the water levels. The main area of interest is the coastal area and the Scheldt mouth area. These requirements have some specific impact on the choices made in the calibration phase of the model. Detailed flow patterns inside the ports, like the eddy formation inside the outer port of Zeebrugge, are of less importance. Generally, the salinity in the coastal area has limited effect on the currents, except inside the ports of Zeebrugge and Nieuwpoort where freshwater discharges can lead to local stratification and density driven currents. Therefore, salinity is not considered in the hydrodynamics model.

A list of the preceding reports and memos delivered within project 15_068 is given in Table 1.

Table 1 – List of delivered FHR reports (R) and memos (M) within project 15_068.

Title	ID
Report: Modellering Vlaamse Baaien, Deelrapport 1: Hydrodynamische Modellering Scenario's Oostkust	WL2016R15_068_1
Report: Modellering Belgische Kustzone en Scheldemonding, Deelrapport 2: Morfologische analyse scenario's Vlaamse Baaien	WL2017R15_068_2
Report: Modellering Belgische Kustzone en Scheldemonding, Deelrapport 3: Modellering van de morfologische effecten na aanleg nieuwe Geul van de Walvischstaart	WL2017R15_068_3
Report: Modellering Belgische Kustzone en Scheldemonding, Rekennota: Berekening golfklimaat Vlaamse Baaien scenario's E4 en F1	WL2017R15_068_4
Report: Modellering Belgische Kustzone en Scheldemonding, Sub report 5: Progress report - Scenarios Vlaamse Baaien and model developments	WL2017R15_068_5
Report: Modelling Belgian Coastal zone and Scheldt mouth area: Sub report 6: Progress report 2 - Evaluation of numerical modelling tools and model developments	WL2018R15_068_6
Report: Modelling Belgian Coastal zone and Scheldt mouth area: Sub report 7: Progress report 3 – Model developments: Hydrodynamics, waves and idealized modelling	WL2018R15_068_7
Report: Modelling Belgian Coastal zone and Scheldt mouth area: Sub report 8: Progress report 4 – Model developments: Waves, idealized modelling and morphodynamics	WL2019R15_068_8
Report: Modelling Belgian Coastal zone and Scheldt mouth area: Sub report 9: Progress report 5 – Model developments: Waves, idealized modelling and morphodynamics	WL2019R15_068_9
Report: Modelling Belgian Coastal zone and Scheldt mouth area: Sub report 10 – Summary of the 2D TELEMAC morphodynamic model ScaldisCoast: version 2020 developed for the Complex Projects Coastal Vision and Extra Container Capacity Antwerp	WL2020R15_068_10
Report: Modelling Belgian Coastal zone and Scheldt mouth area: Sub report 11: Progress report 6 – Model developments: Grid optimization, Morphodynamics, Dredging/dumping subroutines, Wave conditions	WL2020_R15_068_11
Report: Modelling Belgian Coastal zone and Scheldt mouth area: Sub report 12: Scaldis-Coast model – Model setup and validation of the 2D Hydrodynamic model	WL2021_R15_068_12
Report: Modelling Belgian Coastal zone and Scheldt mouth area: Sub report 13: Scaldis-Coast model – Model setup and validation of the wave model	WL2021_R15_068_13

Report: Modelling Belgian Coastal zone and Scheldt mouth area: Sub report 14: Scaldis-Coast model – Model setup and validation of the morphodynamic model	WL2021_R15_068_14
Memo: Modelling Belgian Coastal zone and Scheldt mouth area	WL2016M15_068_1
Memo: Beschrijving scenario's Vlaamse Baaien: Oostkust	WL2016M15_068_2
Memo: Berekeningen golfklimaat scenario F1	WL2016M15_068_3
Memo: Gebruik van de rekencluster aMT voor Telemac berekeningen	WL2016M15_068_4
Memo: Modelling of bed morphology evolution at Knokke for a beach nourishment scenario (G2) by XBeach	WL2016M15_068_5
Memo: Berekeningen golfklimaat scenario E4	WL2016M15_068_6
Memo: Morfologische analyse scenario's Vlaamse Baaien	WL2016M15_068_7
Memo: Vlaamse Baaien: invloed eiland ten oosten van Zeebrugge op het Zwin	WL2016M15_068_8
Memo: Sediment transport formulation in XBeach and Delft3D	WL2016M15_068_9
Memo: Impact aanleg nieuwe vaargeul op de morfologie van de Schelde monding en estuarium: Een geïdealiseerde modelstudie	WL2016M15_068_10
Memo: Morfodynamische effecten aanleg nieuwe geul van de Walvischstaart	WL2016M15_068_11
Memo: Morfologische modellering m.b.v. TELEMAC - SISYPHE	WL2016M15_068_12
Memo: Geul van de Walvischstaart: samenvatting morfologisch onderzoek stabiliteit en baggerbeslag	WL2016M15_068_13
Memo: Artikel Tijdingen: Vlaamse Baaien	WL2016M15_068_14
Memo: Toelichting baggerbeslag Geul van de Walvischstaart	WL2017M15_068_15
Memo: Hydrodynamic modelling of 'Vlaamse Baaien' dunebelt scenarios I3 and I4	WL2017M15_068_16
Memo: Dunebelt scenario I4 – Scaldis vs Semi-circular Telemac3D	WL2017M15_068_17
Memo: Overview of existing Telemac hydrodynamic models: NSG-BCG and Scaldis	WL2017M15_068_18
Memo: CSM and ZUNO run of 2009 including 60, 90 and 200 cm sea level rise	WL2017M15_068_19
Memo: Sea level rise impact on Zeebrugge port accessibility - Telemac3D hydrodynamic modelling	WL2017M15_068_20
Memo: Bringing TELEMAC and Gmsh meshing tool closer	WL2017M15_068_21

Memo: Time step sensitivity analysis for TOMAWAC stand alone and TELEMAC3D-TOMAWAC coupled simulations	WL2017M15_068_22
Memo: Unstructured high resolution coastal model for the Belgian Coast and Scheldt Mouth: model requirements	WL2018M15_068_23
Memo: Telemac2D (and 3D) coupling with Sisyphe	WL2017M15_068_24
Memo: TOMAWAC test runs	WL2017M15_068_25
Memo: Bathymetry and Mesh Construction for ScaldisKust	WL2018M15_068_26
Memo: Scaldis-Coast model calibration: Bottom roughness tuning	WL2018M15_068_27
Memo: Preparing SDS wind file for CSM-ZUNO runs	WL2019M15_068_28
Memo: TELEMAC2D-TOMAWAC-SISYPHE coupled run for hydrodynamics and wave validation	WL2019M15_068_29
Memo: Nestor coupling with TELEMAC2D/SISYPHE and set-up	WL2019M15_068_30
Memo: ScaldisCoast: Summary Coastal 2D TELEMAC morphodynamic model for the Belgian Coast and Scheldt mouth area (input CREST final report)	WL2019M15_068_31
Memo: ScaldisCoast: Summary Coastal 2D TELEMAC morphodynamic model for the Belgian Coast and Scheldt mouth area for the Complex Project Coastal Vision	WL2020M15_098_32
Memo: Artikel tijdingen: Storm Ciara	WL2020M15_068_33
Memo: Suspended sediment transport using GAIA	WL2020M15_068_34
Memo: Test runs with new module GAIA in the TELEMAC-MASCARET system	WL2020M15_068_35
Memo: Mixed sediment transport by GAIA: Improvements and a ScaldisCoast application	WL2020M15_068_37

Table 2 – Conference proceedings/presentations

XBeachX 2017	MORPHODYNAMIC ANALYSIS OF INTERVENTION SCENARIOS AT THE BELGIAN COAST UNDER THE MASTERPLAN 'FLEMISH BAYS'	XBeach X Conference
ICCE 2018	IMPACT OF SEA LEVEL RISE ON THE ACCESSIBILITY OF COASTAL PORTS: A CASE STUDY OF THE PORT OF ZEEBRUGGE (BELGIUM)	International Conference on Coastal Engineering
TUC 2018	Neumann (water level gradient) boundaries in TELEMAC 2D and their application to wave-current interaction (Conference proceedings)	Telemac User Conference
EGU 2019	SCALDIS-COAST: AN INTEGRATED NUMERICAL MODEL FOR THE SIMULATION OF THE BELGIAN COAST MORPHODYNAMICS	EGU General Assembly
TUC 2019	TEL2TOM: coupling TELEMAC and TOMAWAC on arbitrary meshes	Telemac User Conference
VLIZ 2019	ScaldisCoast: An unstructured next generation integrated model for the Belgian Coastal Zone	VLIZ Marine Science Day
IAHR 2020	Simulating the morphological evolution of the Belgian coast by means of the integrated numerical model SCALDIS-COAST	IAHR Europe Congress

2 Base grid and bathymetry preparation

2.1 Base grid

2.1.1 Introduction

Base grid is called the computational grid used for the hydrodynamic validation of the presented TELEMAC model named 'Scaldis-Coast'. However, it is called base grid for another reason. That is because the computations for the various scenarios of interventions at the Belgian coast will be performed on modified versions of this base grid. In other words, it is intended for the base grid to be the starting point in the construction of every new model of the scenarios in the framework of the Complex Project Coastal Vision (Complex Project Kustvisie).

The computational grid for the TELEMAC simulations is constructed using the finite element mesh generator GMSH (Geuzaine & Remacle, 2009). One of the main advantages of this meshing tool is the accurate specification of the target element size based on different conditions such as the local bathymetry, the bathymetry gradient, the distance from specified boundary lines, etc.. This attribute minimizes the manual interventions for refinement of the mesh and therefore leads to high quality meshes (avoiding the creation of degenerated cells). Moreover, it allows for efficient generating adapted grid for new scenarios with a limited number of manual interventions.

2.1.2 Outline of the computational domain

The so-called 'Scaldis-Coast' (TELEMAC) model has an outline that resembles the corresponding one of the Scaldis model reported in Smolders *et al.* (2016). As shown in Figure 1 the most noticeable difference between the two outlines is the schematized upstream part of the Scaldis-Coast model. The idea of the schematized upstream part came from its successful implementation in another TELEMAC model, known as the Zeebrugge model, developed by IMDC for the study of the accessibility of the port of Zeebrugge (IMDC, 2015). The computational domain of this model is shown in Figure 2. Although it is expected that the quality of the numerical results at the upstream of Scheldt river will be affected by the schematization, the new model aspires to achieve high quality predictions at the coastal zone and the mouth of Western Scheldt. To this end, the model has been validated by means of an extended comparison with measurements (see sections 3.2.7 and 3.2.8).

Other differences can be noticed at the coast (e.g. the inclusion of Dunkirk port close to the western boundary of the model), the Western and the Eastern Scheldt (at the at the drowned land of Saeftinghe and the Neeltje Jans island). Moreover, small differences which are hardly noticeable resulted from the updated tracking of the land boundaries. Note that the current tracking aims mostly on the detailed and accurate representation of the Belgian coastline and the mouth of Western Scheldt. The offshore (open) boundary of the two domains are identical.

Figure 1 – The outline of the new Scaldis-Coast model (red line) illustrated on top of the computational domain of Scaldis model (Smolders *et al.* 2016) in grey colour.

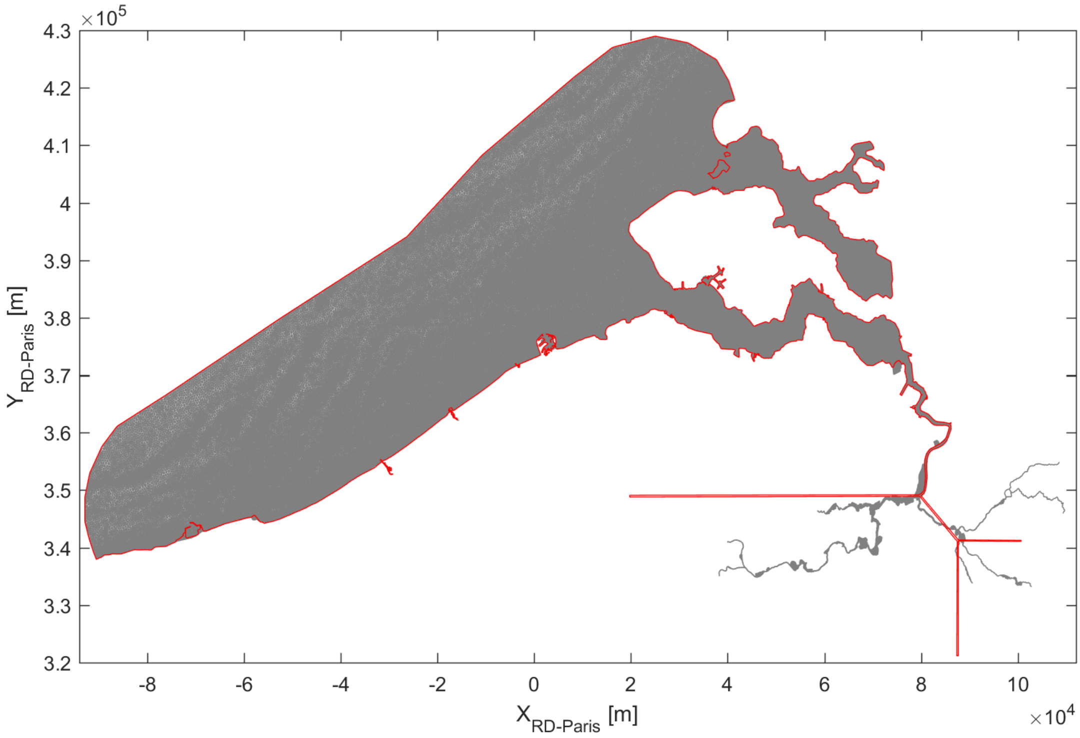

Figure 2 – The computational domain of Zeebrugge model (IMDC, 2015).
The outline of the the new Scaldis-Coast model (red line) is depicted on top of it.

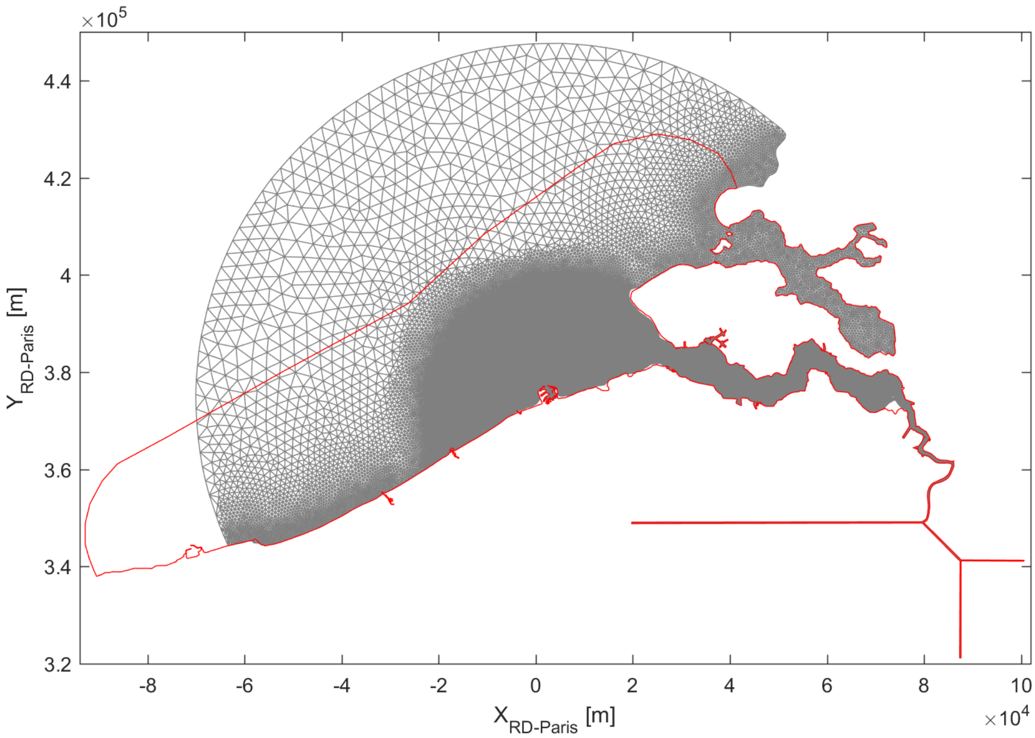

2.1.3 Grid configuration

The computational grid is constructed by use of the finite element grid generator GMSH (Geuzaine & Remacle, 2009). An adaptive mesh refinement is necessary in order to achieve more accurate predictions at the areas of interest, especially close to the coastline where the objective is to accurately resolve beach and foreshore morphodynamics including the effects of groynes and disturbances of the fairways to the seaports and marinas. The local adjustment of the mesh density locally is achieved by using the available options of GMSH (Size Fields) for the prescription of the characteristic size of the elements. In Figure 3, the characteristic element sizes at different regions of the computational domain after mesh refinement by GMSH software, are shown. The computational grid consists of 251 604 nodes (493 842 triangular elements) with the maximum resolution of 25 m being along the Belgian coastline and the minimum resolution of 750 m being along the along the offshore (open) boundary.

Figure 3 – Characteristic element sizes of the base grid after adaptive mesh refinement using GMSH software.

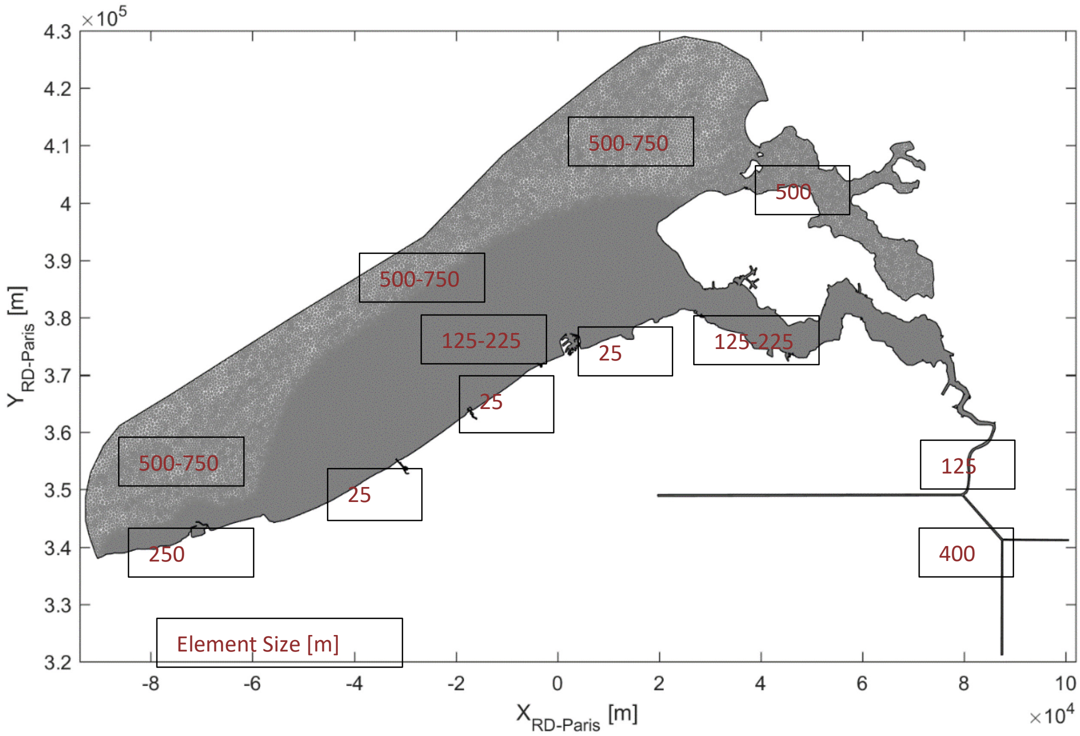

Different techniques were used for the local mesh refinement at different parts of the domain. At the main part of the domain, which includes the area along the offshore boundary, the Belgian coast (prolonged towards the French and the Dutch coast) and the Western Scheldt, the grid size was determined by the local bathymetry slope (see Figure 4). The gradient of the bathymetry is selected as a target value to ensure higher resolution in the vicinity of steep bathymetries like channel slopes. A higher resolution is here justified since it is expected that at locations with steep bathymetry gradients, also flow velocity gradients will occur. The same holds for non-smooth geometries, like harbour breakwaters.

The implementation of the bathymetry gradient based grid, involves three Size Fields of GMSH, i.e., the *Structured*, the *Threshold* and the *Gradient* size fields:

Structured: This field contains bathymetric data on a structured grid provided in an input text file (with specific format) and interpolated linearly on the unstructured mesh.

Threshold: This field is always complementary to another field. Two element sizes (Lcmin, Lcmax) and two distances (DistMin, DistMax) have to be prescribed here. Lcmin size will be imposed up to a distance DistMin from an entity and Lcmax beyond the DistMax distance. Between DistMin and DistMax interpolation of the element size is applied. For the offshore area Lcmin=500m and Lcmax=750m, while for the coastal area and the Western Scheldt Lcmin=125m and Lcmax=225m, are chosen (see Figure 3).

Figure 4 – Element size determination based on the local bathymetry slope by use of GMSH Size Field options (Structured, Gradient, Threshold). Top figure: Focus on the coastal and offshore area (Nieuwpoort is located at bottom right corner); Bottom figure: Focus on part of the Western Scheldt and its mouth.

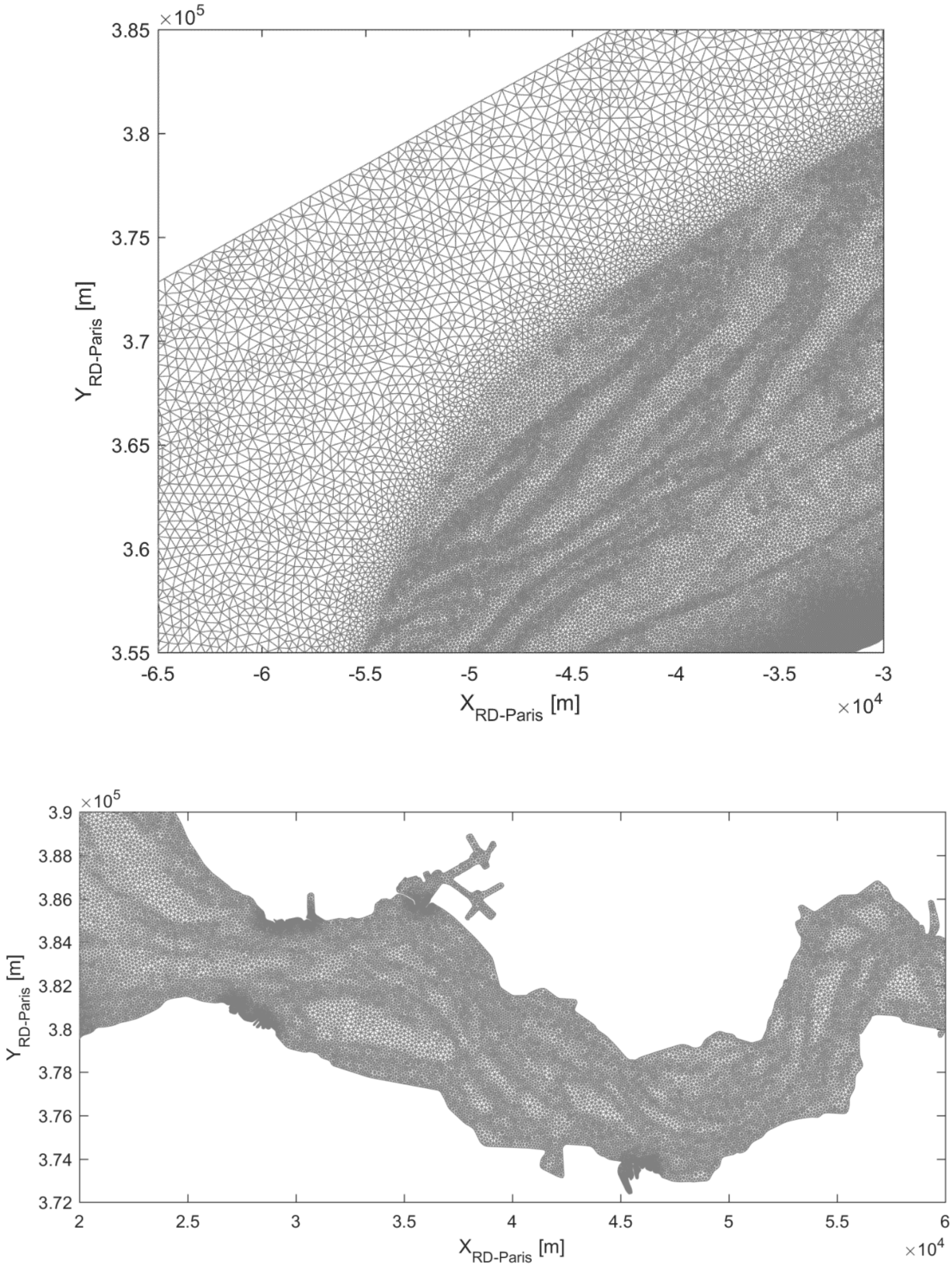

Gradient: This field makes use of the bathymetric data in the *Structured* field in order to calculate the bathymetry gradients. Gradient based grid size can be achieved if *Gradient* field is combined with a *Threshold* field. In this case the DistMin and DistMax parameters correspond to gradients and not to horizontal distances. The chosen values for this case are DistMin=0.01 and DistMax=0.

For the areas which are close to the western and the eastern boundaries of the computational domain, i.e. the French coast and the Eastern Scheldt, uniform grid sizes equal to 250m and 500m, respectively, are applied (Figure 5).

Figure 5 – Computational grid formation at the area around Dunkirk port (French coast) (top figure) and at the Eastern Scheldt (bottom figure).

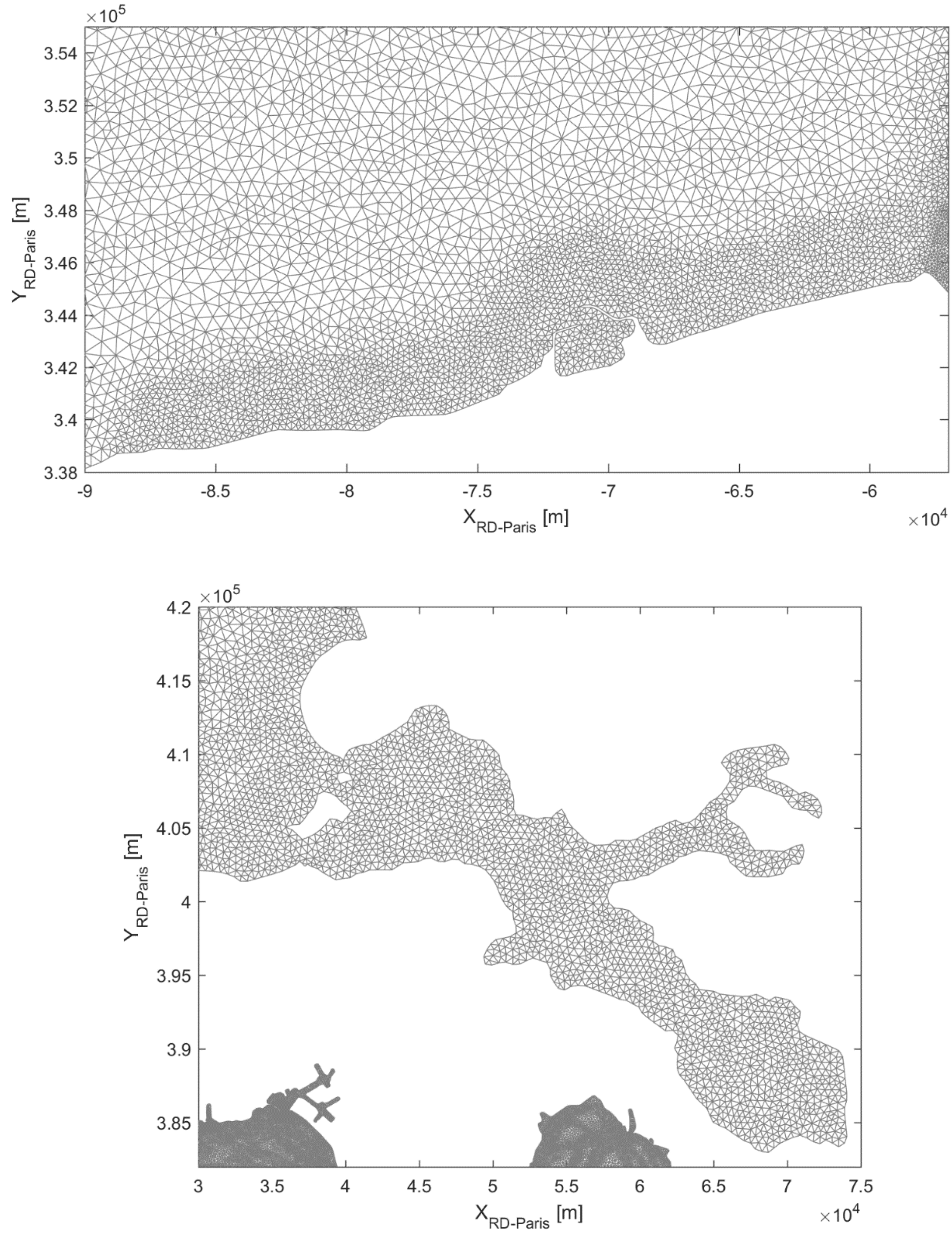

Along the Belgian coastline (from De Panne to Cadzand) the grid is refined up to a size equal to 25m using the so-called *Boundary Layer* size field of GMSH. In this way a gradual (exponential) increase of the element size is applied as the distance from the coastline increases. The selected size ratio between two successive elements determines the 'thickness' of the grid boundary layer. Lower values of the ratio lead to thick boundary layers, i.e. higher resolution for longer distance from the coast. An illustration of the grid formation at the eastern part of the Belgian coast, after the implementation of the *Boundary Layer* technique is shown in Figure 6. For the eastern part of the coast and the Zeebrugge harbour a ratio equal to 1.03 is used, while for the Zwin a slightly smaller value (1.025) is utilized.

Figure 6 – Grid formation at the area around Zeebrugge harbour and the Zwin, at the eastern part of the Belgian coast.

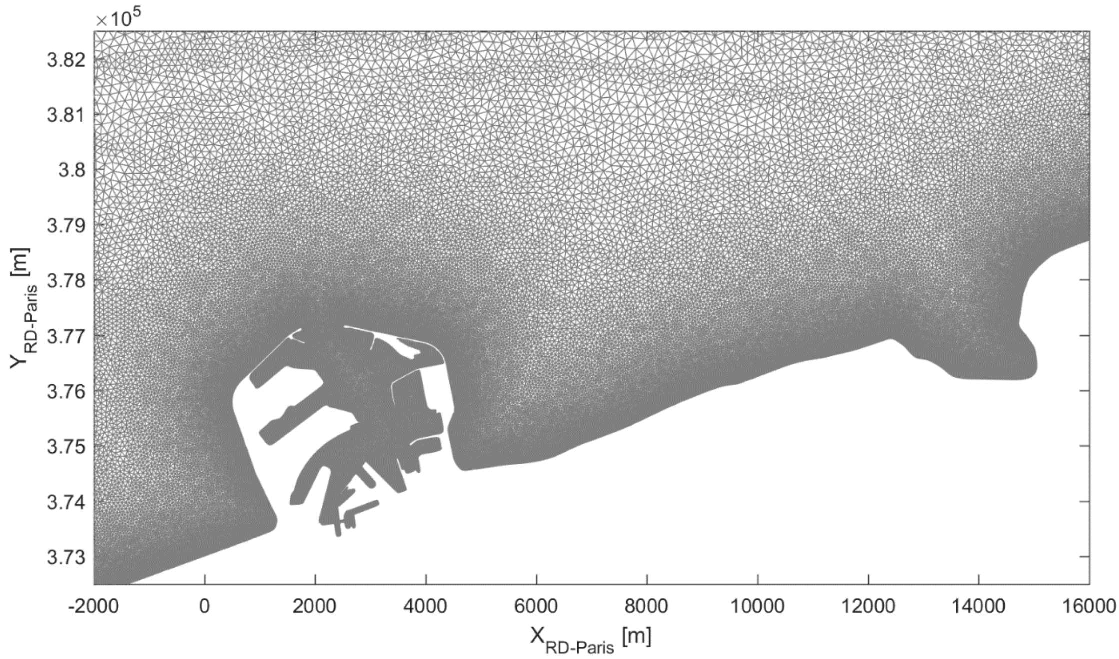

The Boundary Layer technique is utilized for the smooth adaptation of the grid from the fine coastal area to the coarser offshore area (see top Figure 4) and also for the generation of boundary conforming elements in selected locations in the Western Scheldt estuary where the boundaries present intense diversity (see Figure 7). The size ratio in both cases is 1.1. The locations in the Western Scheldt where boundary conforming mesh refinement was performed are: the port and the marina at Breskens, the port of Vlissingen (east entrance included), the port of Terneuzen, and the area in front of Zandvliet lock where two dams are located. The minimum grid size at these lacations is equal to 50 m.

For the schematized (upstream) part of the computational domain a channel mesh is generated using the so-called transfinite algorithm of GMSH (see Figure 8). The channel mesh is preferred rather than the unstructured grid in order to efficiently reduce the number of the elements at this part of the domain, taking into account that the flow is directed parallel to the boundaries of these schematized streams. The necessary input of the transfinite meshing is the number of nodes that will be created on each boundary line. In the specific case, three nodes are considered in the direction transverse to the stream flow, while in the direction of the flow, the distance between successive nodes is set equal to 400m. Note that at the junctions of the streams unstructured grid is utilized.

In the end, the merging of the selected size fields is performed in such a manner that the minimum value of the element size from all the selected fields is selected.

More information on the practical use of GMSH for Telemac models can be found in Appendix 1 and in Kolokythas *et al.* (2018)

Figure 7 – Implementation of the *Boundary Layer* size field for a boundary conforming grid at the coastal structures of Vlissingen and Breskens (green shaded areas).

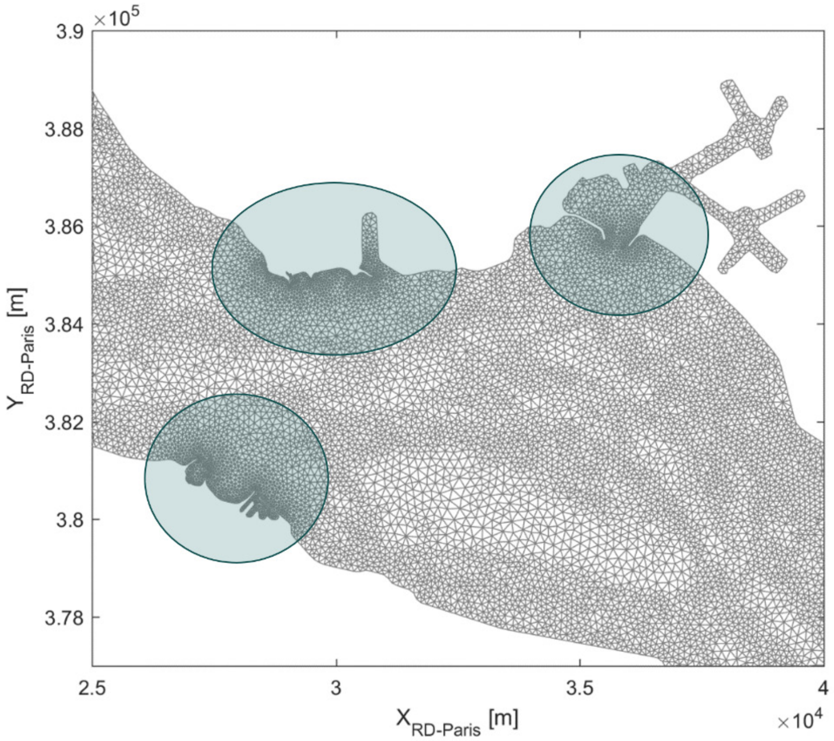

Figure 8 – Grid formation at the schematized (upstream) part of the computational domain, also known as channel mesh.

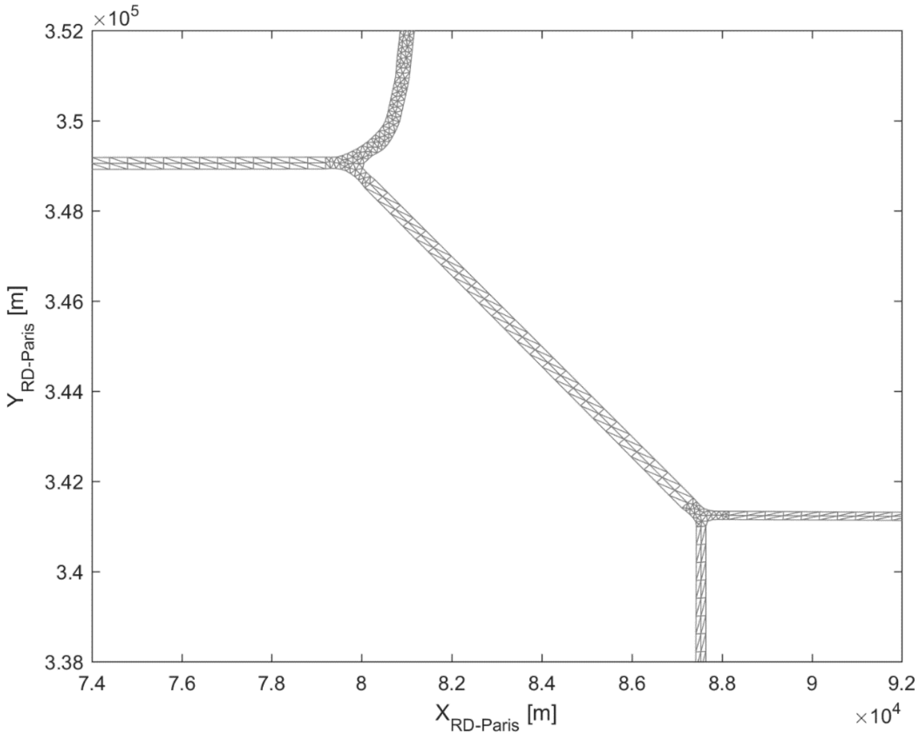

2.1.4 Grid Quality control

The grid quality control is based on the calculation of the following three basic metrics:

- Skewness: determines how close to an ideal shape, i.e. equiangular triangle, a grid cell is. It is defined as:

  $Sk = \max[(\vartheta_{max} - \vartheta_e)/(180 - \vartheta_e), (\vartheta_e - \vartheta_{min})/\vartheta_e]$

  where ϑ_{max} and ϑ_{min} are the maximum and the minimum angles of a cell, respectively, and $\vartheta_e = 60$ is the angle of a equiangular cell. Skewness varies between 0 and 1. According to the definition of skewness, a value of 0 indicates an equilateral cell (best) and a value of 1 indicates a completely degenerated cell (worst). Degenerate cells (slivers) are characterized by nodes that are nearly co-linear. Note that *Sk* values up to 0.95 are considered acceptable (ANSYS inc., 2015).

- Aspect ratio: The aspect ratio of a triangular cell is defined as:

  $AR = 2R_i/R_o$

  where R_i is the radius of the circle inscribed in a triangle and R_o is the radius of the circle circumscribed around the triangle. The aspect ratio varies between 0 and 1. The larger aspect ratio implies the better quality of the triangle and so the aspect ratio of the equilateral triangle is 1.

- Smoothness: is defined as the area ratio of two adjacent cells (same inner face). According to ANSYS inc. (2015) it is recommended that the smoothness remains lower than 2.5 (area of larger cell over the one of the smaller cell). Meshes with smoothness values greater than 5 are of poor quality.

Note that the GMSH software is designed to optimize for these quality parameters taking into account the geometric complexity and the user defined targets without the need for manual interventions.

In Figure 9, the aforementioned quality metrics for the base grid of the Scaldis-Coast model, are presented. On the subfigures of the left column the quality metrics are plotted versus the number of elements, while in the right column versus the cumulative density or else the cumulative percentage (divided by 100) of the elements. The constructed mesh is generally of very good quality as indicated by the skewness distribution (Sk<0.38 for 99.9% of the elements - Sk_{max}= 0.8), the aspect ratio distribution (AR>0.76 for 99.9% of the elements), and the smoothness distribution since 99.9% of the elements presented values lower than 1.94. The maximum values of smoothness metric (close to 7) are observed at the junctions of the schematized part of the domain where channel mesh is connected to unstructured triangle mesh. In total, a very low number of elements (148 out of 493 842 elements) present smoothness over 2.5.

Another metric for the quality of the mesh is the number of the neighbouring nodes around a computational node. In general, large number of neighbouring nodes should be avoided. For the base grid a small number of nodes (less than 2%) has more than 8 neighbours, i.e. 466 nodes (out of 251 607) have 9 neighbours and just 15 nodes have 10 neighbours.

Figure 9 – Quality metrics for the base grid of Scaldis-Coast model.

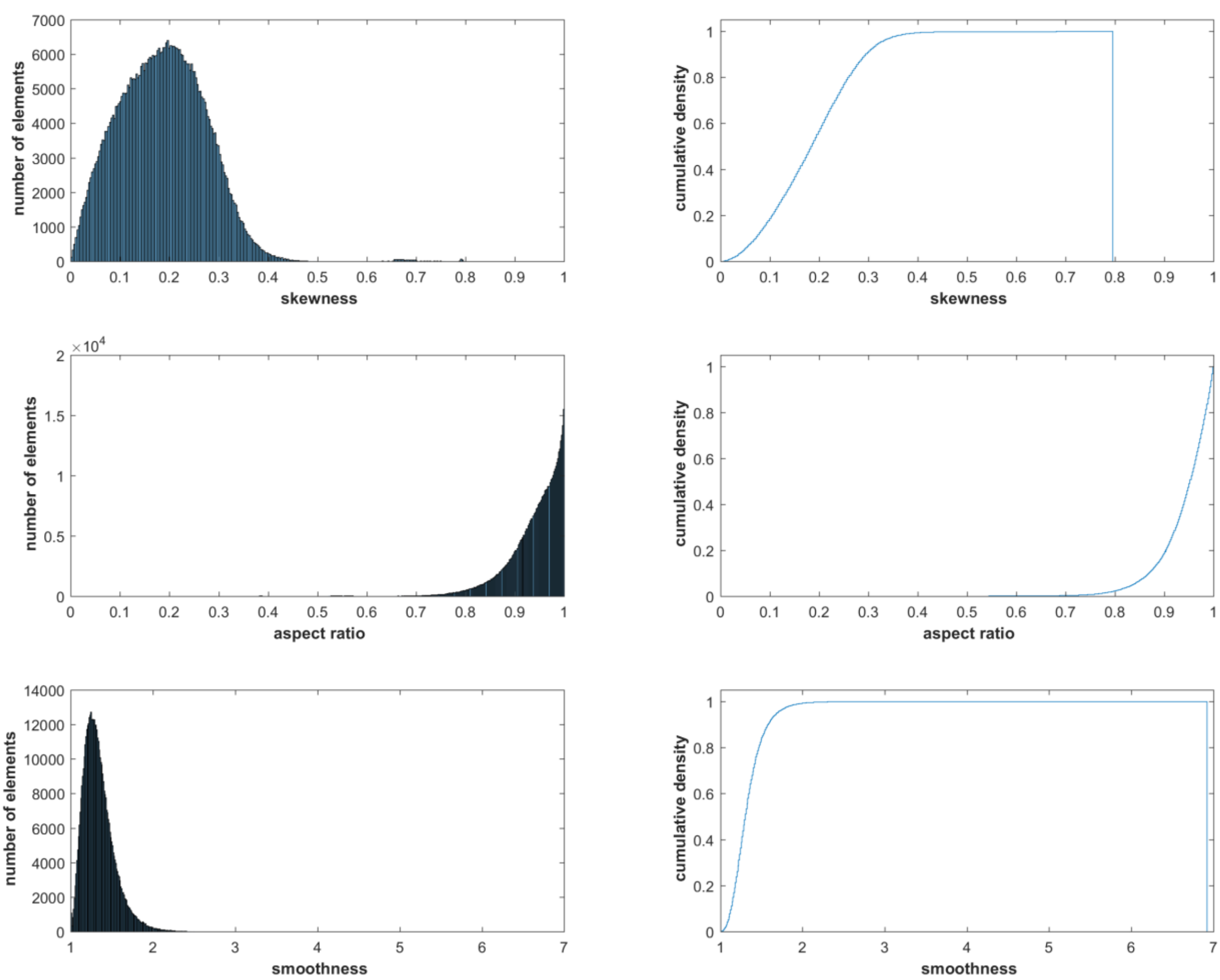

Table 3 – Main characteristics of the base grid of the Scaldis-Coast model.

Parameter	Value
Number of grid points	251 604
Number of elements	493 842 (triangular)
Max. / Min. grid size	750 m / 25 m
Min. /Max. number of (interior) neighbours	4 / 10
Nodes with more than 8 neighbours	466
Elements with angles >120° (<135°)	3
Elements with angles <15°	138
Elements with Smoothness > 2.5	148

2.1.5 Computation time and parallel performance

The scalability of the utilized software, i.e. its ability to present substantially decreasing computational times with increasing number of utilized number of CPUs (cores), is investigated in this section. To this end, five test hydrodynamic simulations, with simulation period of 10 days, were run on 1, 12, 24, 48 and 96 cores (one serial and four parallel simulations). Notice that the efficiency of parallelisation can be dependent on the model settings. For the scalability test de setting as presented later in this report, see Table 8, are used. The time step is set to 10 seconds. This is also the time step of the final setting of the model. See Section 3.2.4 for the motivation of the time step selection.

The computational time versus the number of utilized cores is shown in Figure 10. Two metrics for the evaluation of the parallelization performance are the following:

- Speedup index (S_p), which is defined as the ratio between the computational time of the serial run (1 core) and the computational time of a parallel run.
- Performance (α_p), which is defined as the ratio between the Speedup and the number of the cores (S_p/n_{cpu})

The Speedup and the Performance versus the number of cores are presented in Figure 11. A theoretically perfect parallelization would give S_p values on the black line of the left figure. However, in practice the Speedup values decrease substantially when the number of cores becomes very high (96 cores), due to increased communication between the processors. As for the Performance, it is observed that it decreases linearly for n_{cpu} values greater or equal to 24 cores. Interestingly a local drop for the test run of 12 cores is observed.

Summarizing the findings of the parallelization tests, the suggested number of processors to be used for better performance of TELEMAC software ranges between 24 and 48 CPUs. The CPU time for a full 14-day spring-neap tidal cycle is expected to be between one and two hours, depending on the number of output steps and the occupation of the computational facilities.

Notice that here the performance is investigated for the stand-alone hydrodynamic model only. For the fully coupled morphodynamic model a good speed-up performance was found up to more than one-hundred processors (Kolokythas *et al.*, 2021). In the fully coupled morphodynamic model the TOMAWAC wave propagation model is computationally the most time-consuming module by far. Due to the spectral nature of the model, i.e. many computations per timestep on a nodal base, the parallel efficiency of the wave model is high. Also note that the performance depends on the architecture of the utilized high performance computing system. The performance test described above has been executed on the Flanders Hydraulics high performance cluster (Navier queue), while the morphodynamic model performance test was executed on the KU Leuven Tier-1 supercomputer (VSC[1] - BrEniac cluster).

[1] VSC – Vlaamse Supercomputercenter Centrum (https://www.vscentrum.be/)

Figure 10 – Computational time versus the number of cores utilized for the parallel test runs (Run D18a-d).

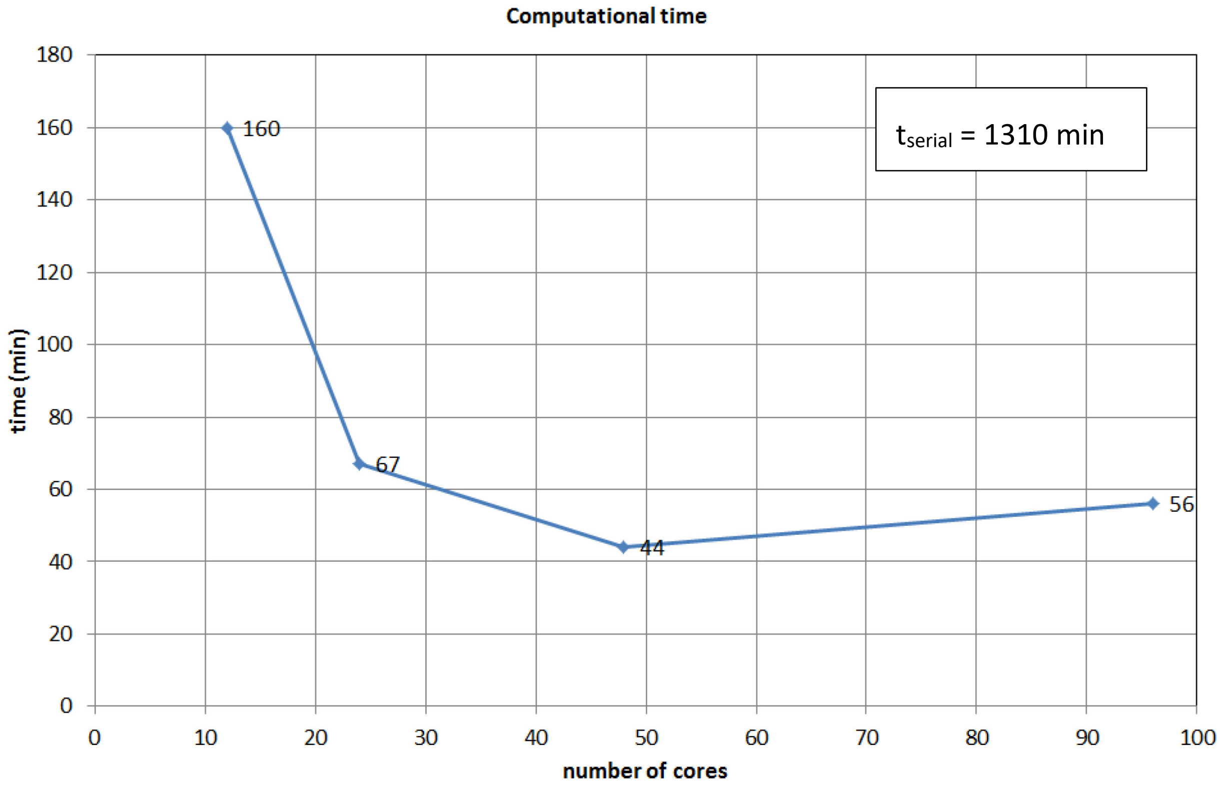

Figure 11 – Speedup (S_p) versus the number of cores (left figure) and Performance(α_p) versus the number of cores utilized for the parallel test runs.

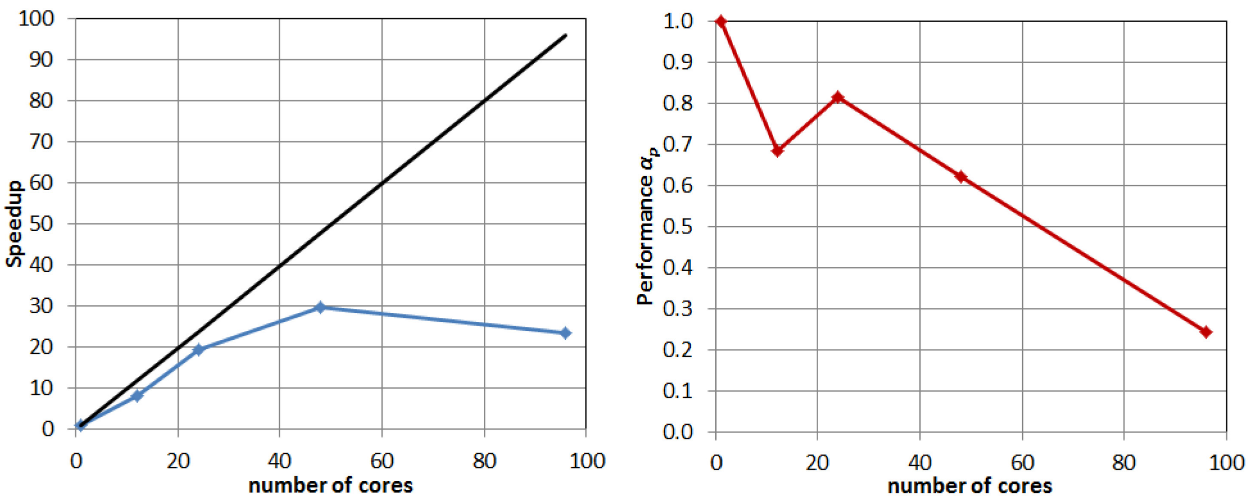

2.1.6 Grid size sensitivity

The sensitivity of the numerical results to the grid size was investigated by performing the same hydrodynamic simulation two times, using the base grid and a grid with the same configuration (as described in §2.1.3), but a higher resolution. The characteristic element size at different regions of the computational domain are depicted in Figure 12. Compared to the base grid, the refined version has about 87 000 nodes more, i.e. the computational grid consists of 338 645 nodes (666 108 triangular elements) with the maximum resolution being equal to 20 m (instead of 25 m in the base grid) and the minimum resolution being 600 m (intead of 750 m). The bathymetry gradient based grid ranges from 100 to 200 m in the high resolution grid (instead of 125 - 225 m), while the resolution in the Eastern Scheldt becomes equal to 400 m (instead of 500 m).

The performance of the two grid versions (base grid and refined one) was evaluated through two basic statistical parameters for the temporal evolution of the water level at selected coastal and estuarine locations. The location of the considered stations on the computational grid are shown in Figure 13. The bias and the RMSE in the water level time-series and velocities for a certain time period (5 days), between identical simulations conducted on the two grid versions are presented in Figure 14 to Figure 17, indicate very good agreement between them. Especially at the stations located at the coastal zone only minor differences are observed at the temporal evolution of the water level and the velocity magnitude. For the upstream stations in the Western Scheldt the maximum differences in the water level bias and the RMSE are limited to 1 cm and 4 cm, respectively. As for the velocity, relatively larger differences are observed at some stations in the Western Scheldt (e.g. maximum difference of 9 cm/s at Walsoorden). It is conjectured that the slightly different position of the closest to the stations computational nodes (due to the different refinement of the two grids) influences more the velocities than the water level. However, the overall outcome can be considered as indicative of independence of the results from the grid resolution and gives a good feedback for the usage of the selected base grid.

As expected, the performance of the refined grid in terms of computational time is not as good as that of the base grid, presenting about 68% higher computational time for the simulation period of 10 days using 32 cores. This increase is two times the increase of the nodes in the refined version, which is about 34%. Although for the refined grid the same time-step of 10 seconds has been used, so same number of time-steps, the computation time increases stronger than the increase in number of cells. This is a common fact in numerical mathematics. By keeping the time-step the same, locally the CFL number might increase, which might relect in a slower convergence rate (higher number of iteration steps) of the iterative numerical matrix solver. However, notice as well that the wall clock time of a single run is only a snapshot in time and depends on the local state, it is the total work load at that time, of the high performance computing system.

Figure 12 – Characteristic element sizes of the refined base grid.

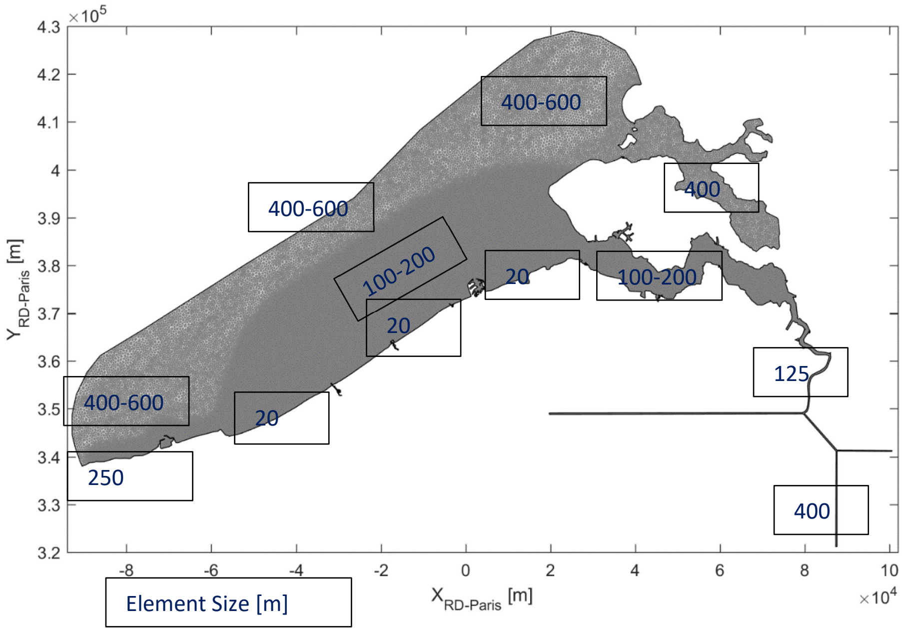

Figure 13 – Stations used for the statistical analysis within grid resolution sensitivity.

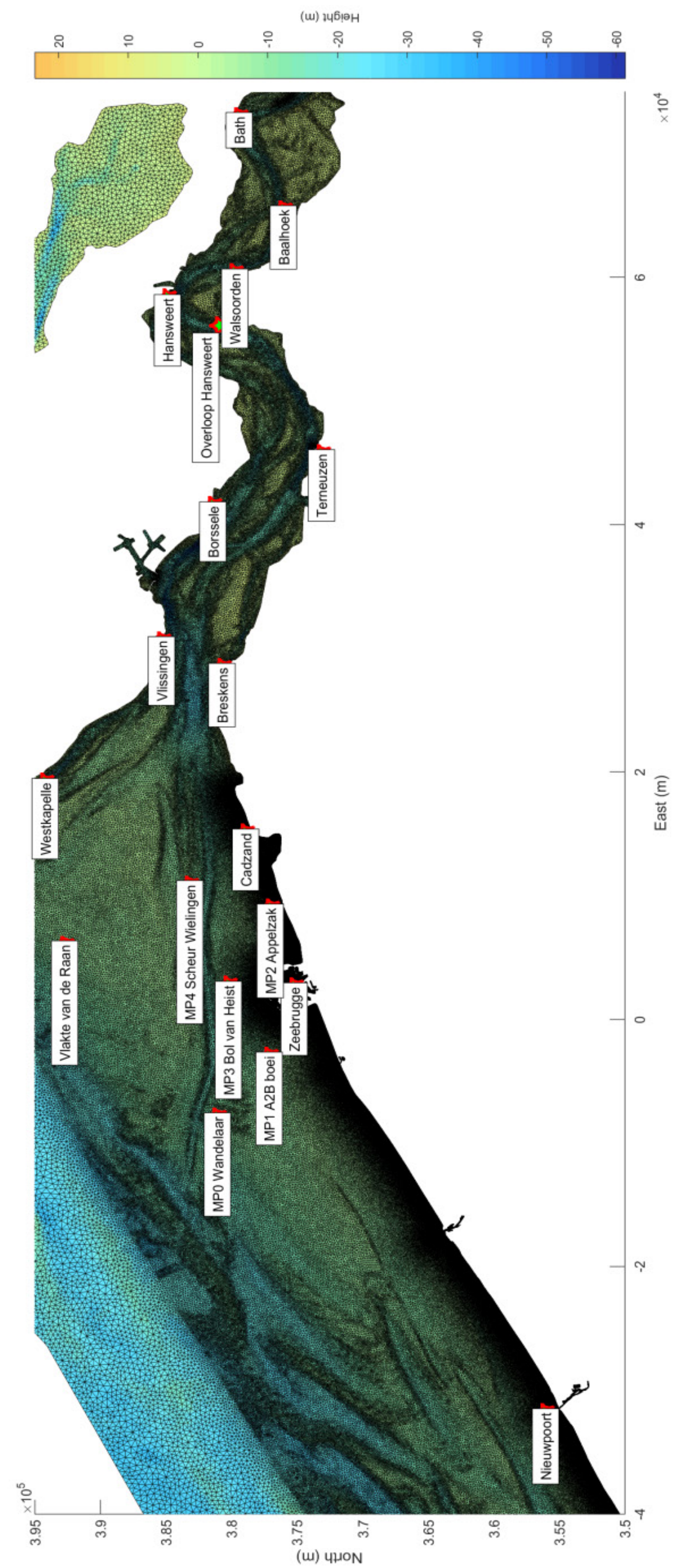

Figure 14 – Bias (top figure) and RMSE (bottom figure) in the complete water level time-series (5 days) between the refined base grid (F01) and the original base grid (D12).

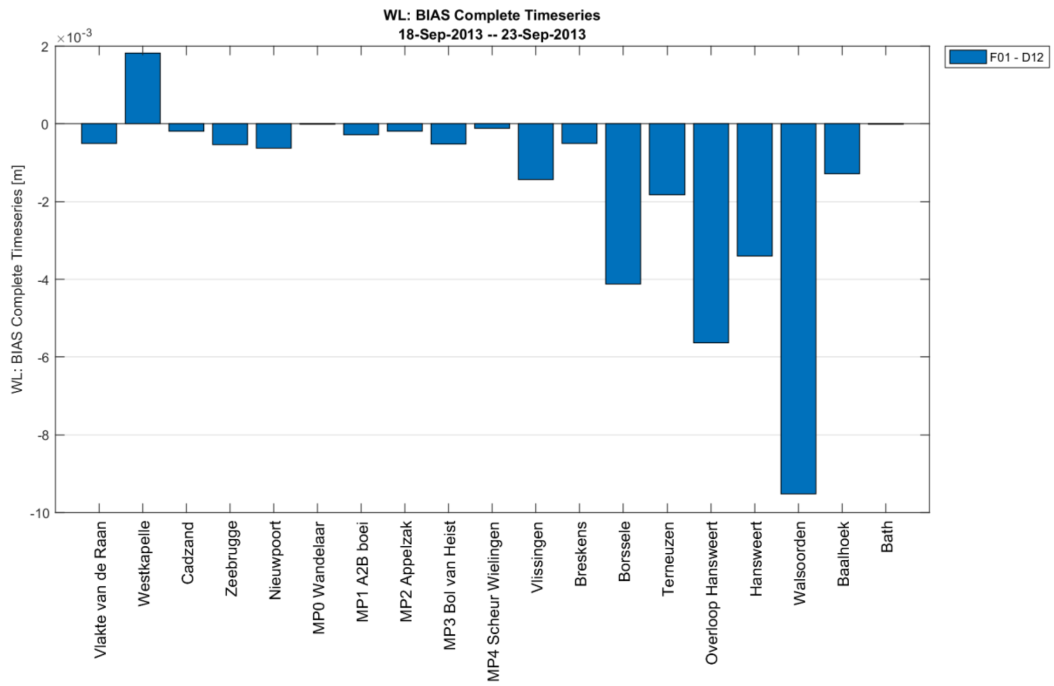

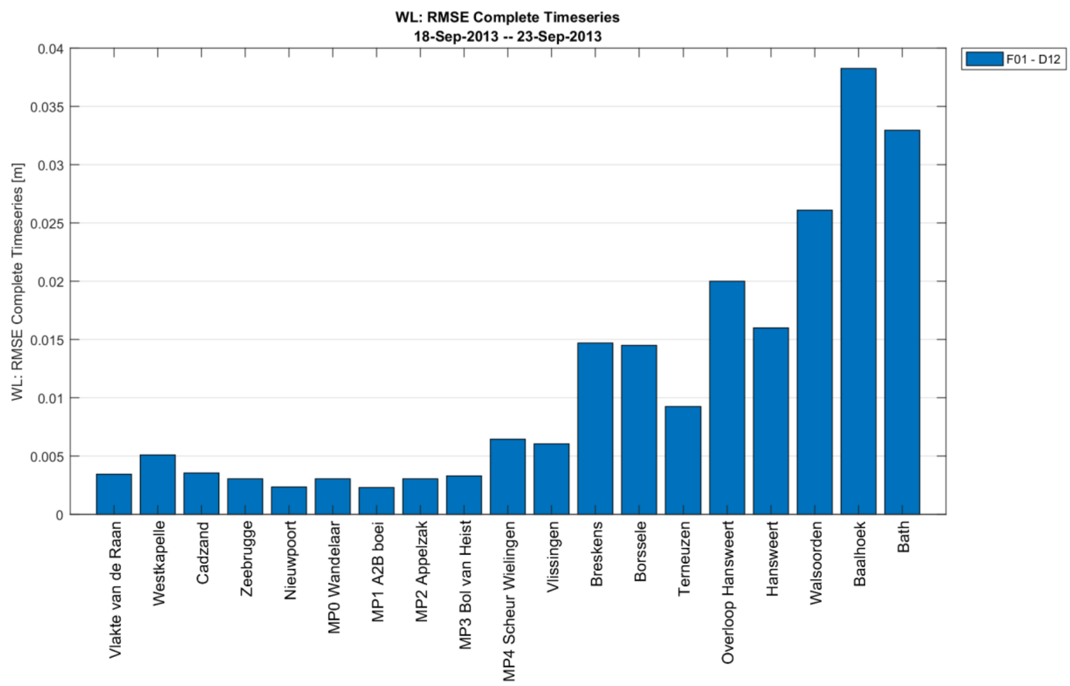

VIMM version TELEMAC
(c)Waterbouwkundig Laboratorium 2018

Figure 15 – Bias of the velocity direction magnitude and direction in the complete water level time-series (5 days) between the refined base grid (F01) and the original base grid (D12)

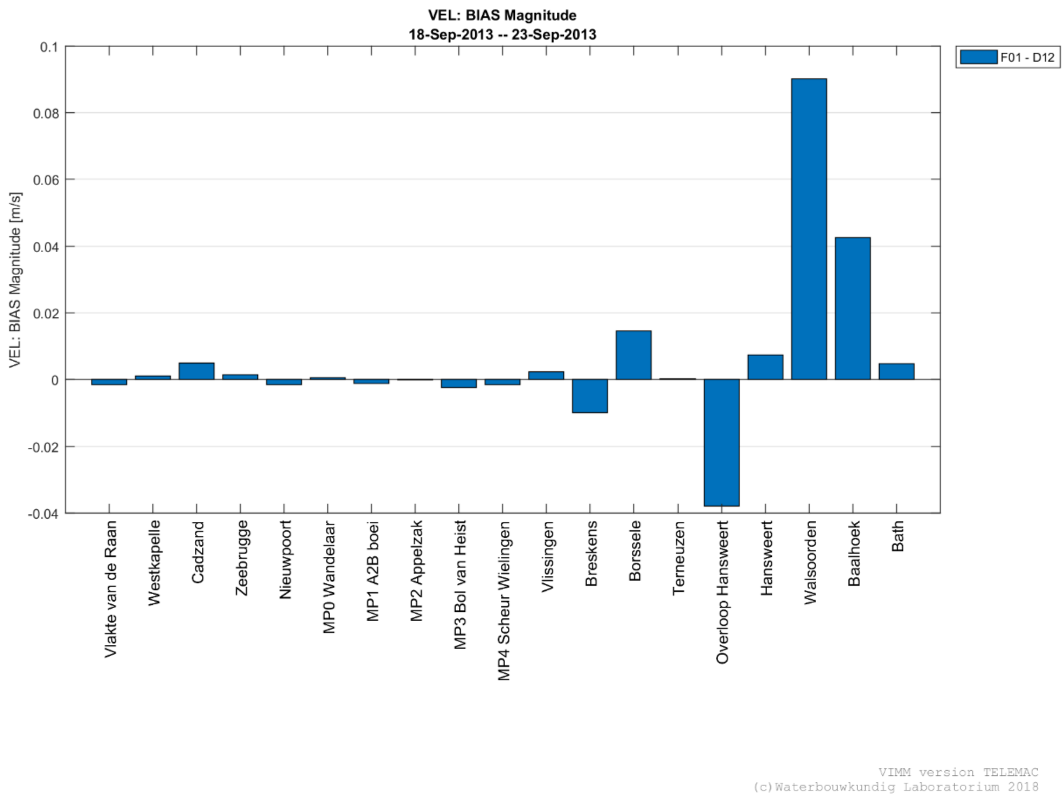

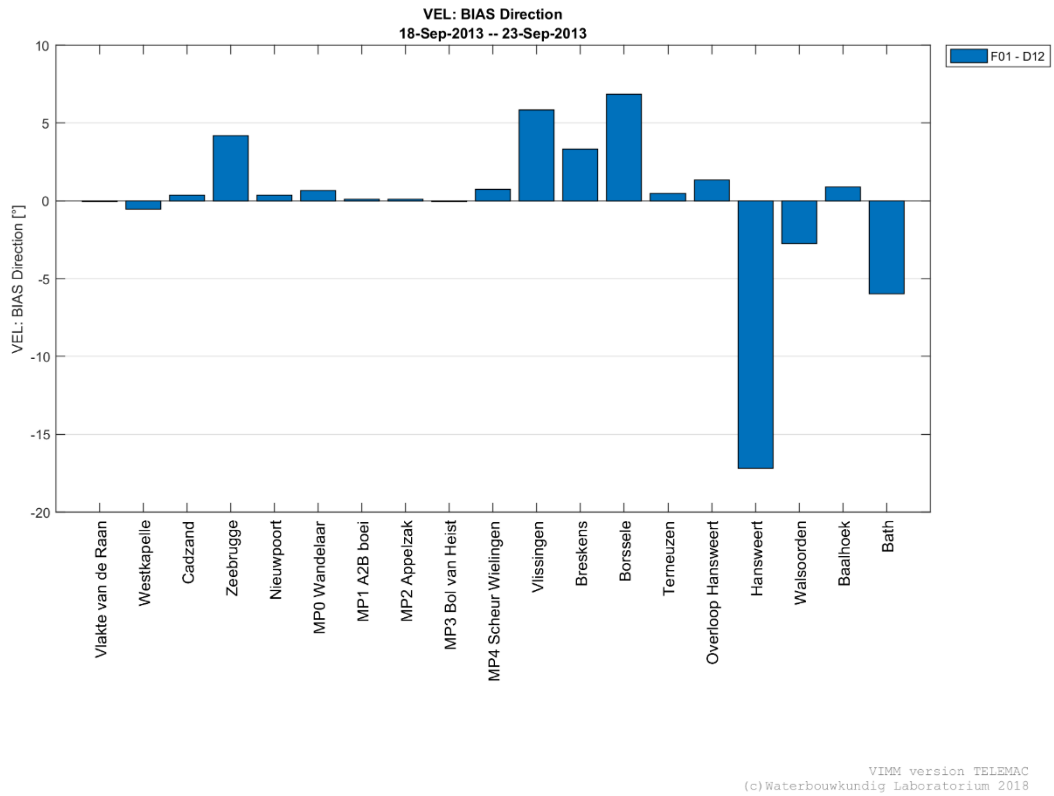

Figure 16 – Root Mean Square Error of the velocity direction magnitude and direction in the complete water level time-series (5 days) between the refined base grid (F01) and the original base grid (D12)

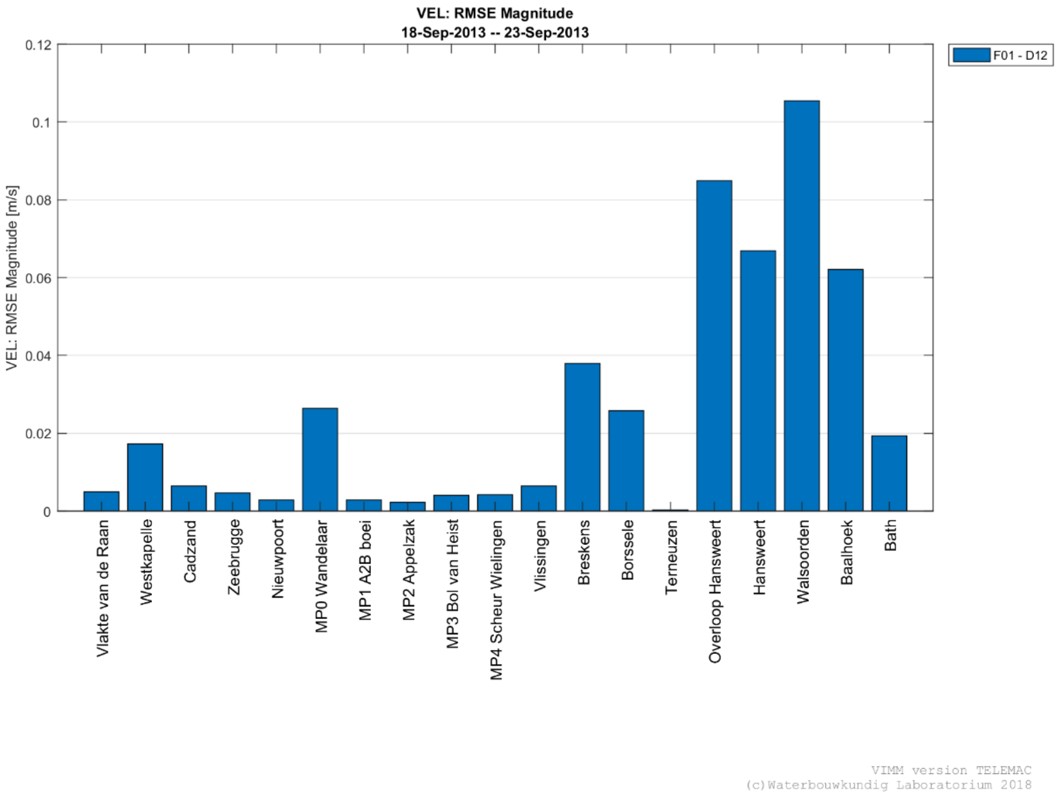

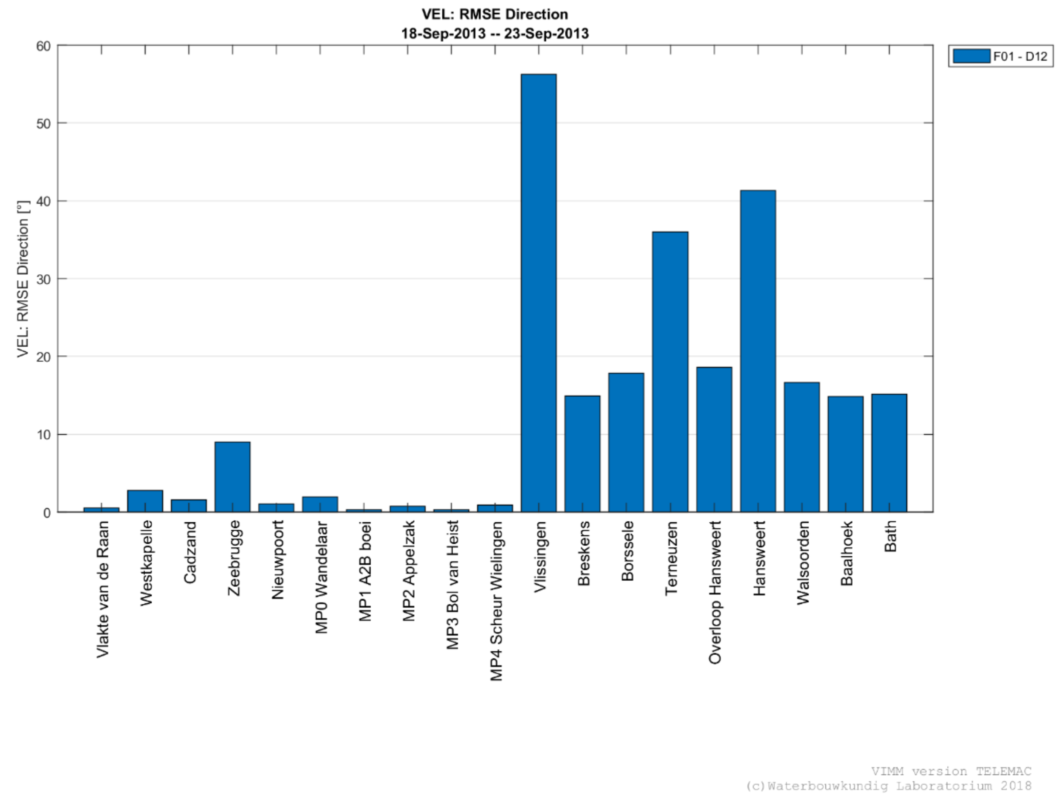

Figure 17 – Mean Absolute error and Relative Mean Absolute Error of the velocity vectors in the complete water level time-series (5 days) between the refined base grid (F01) and the original base grid (D12).

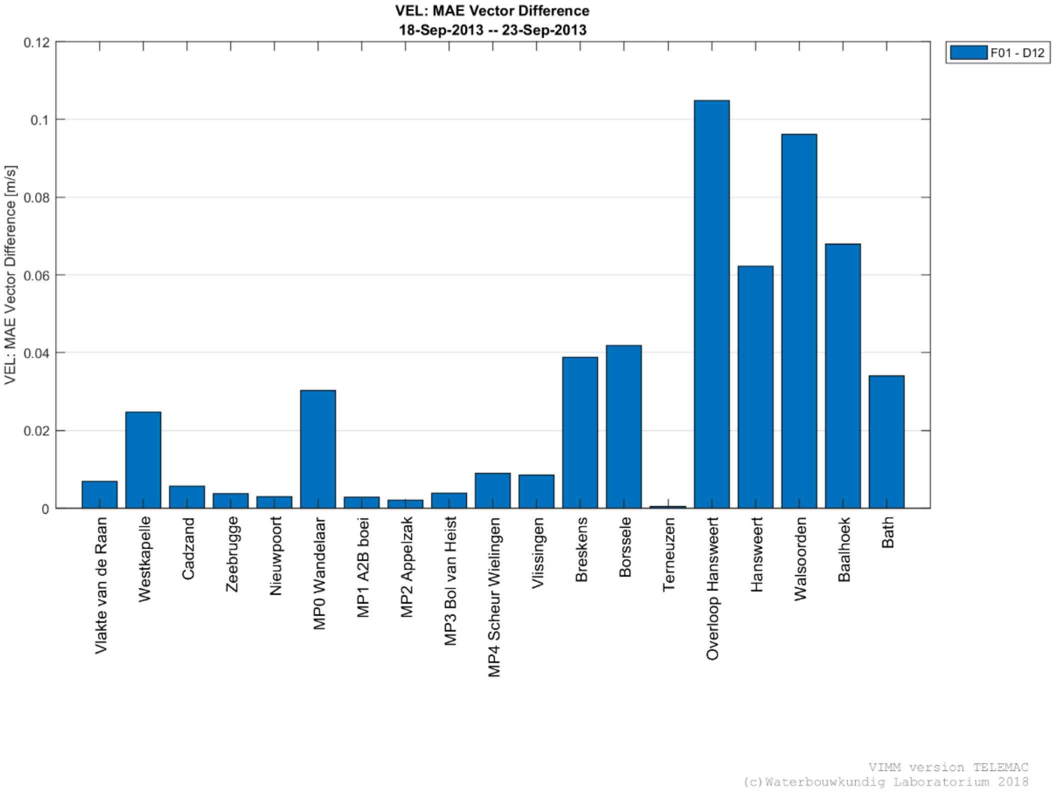

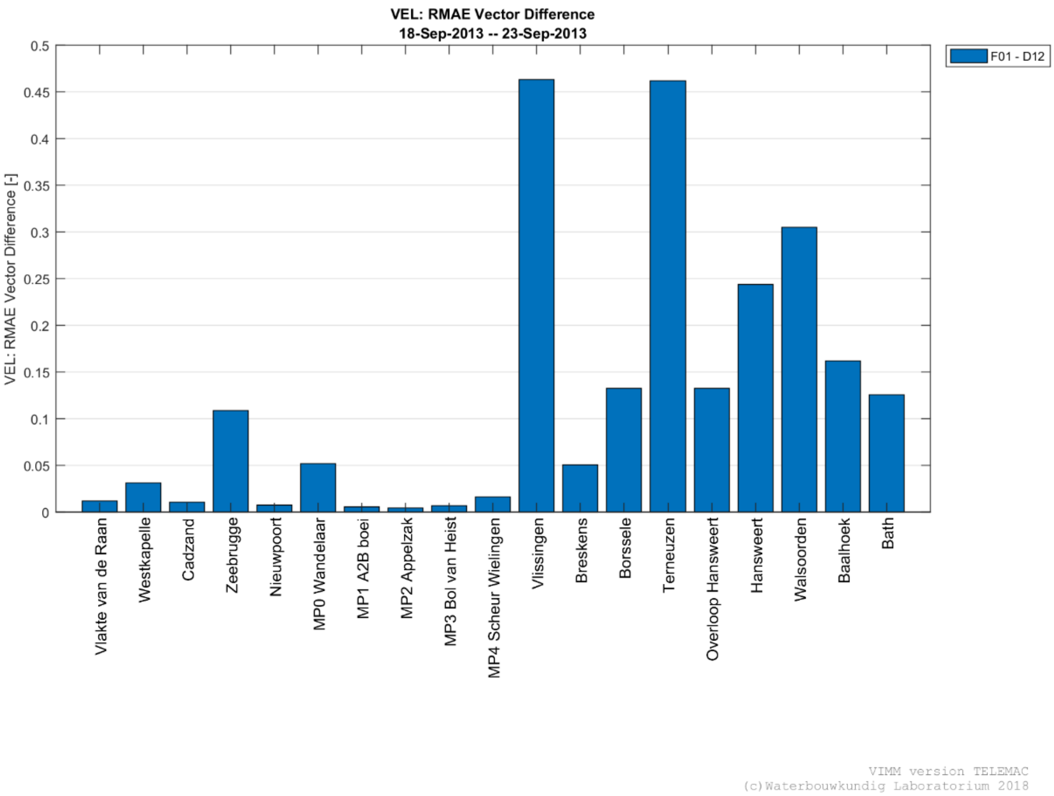

2.1.7 Velocity gradient grid

Taking advantage of the capability of GMSH grid generator to determine the size of the elements based on gradients of scalar variables (most obvious one is the bathymetry), a grid of which the local resolution was determined by the gradients of the maximum flow velocity magnitude was constructed. Hereafter this type of grid will be called as velocity gradient grid. It is expected that the formation of the velocity gradient grid will be similar to the one of the bathymetry gradient grid, since it is expected that at locations with steep bathymetry slopes, also flow velocity gradients will occur.

As in the case of the bathymetry gradient grid, the first step is to feed GMSH with the basic input data, i.e. the maximum velocity magnitude gradients, interpolated on a structured grid through the size field *Structured*. This data was produced by a hydrodynamic simulation using the base grid presented previously. In Figure 18 the resulting maximum velocity (magnitude) gradients[2] during a spring tide utilized for the grid size determination are presented. Obviously, the higher velocity gradients are observed in the Western Scheldt estuary, around Zeebrugge harbour, at the Eastern Scheldt and at the area of the sandbanks of the Belgian continental shelf.

Figure 18 – Maximum gradients of flow velocity magnitude during a spring tidal cycle calculated on the base grid of Scaldis-Coast.

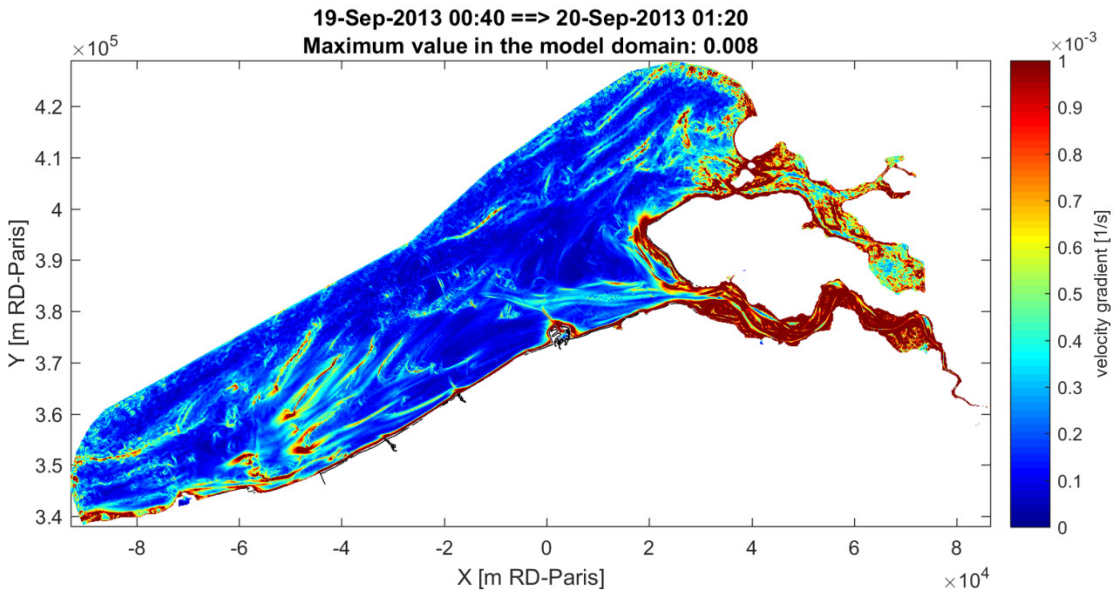

Then the *Gradient* field was combined with a *Threshold* field in order to get a grid with the same size parameters as in the case of the bathymetry gradient grid, i.e. 500-750m offshore and 125-225m at the coastal and estuarine area (for the size parameters see Figure 3). In this case the DistMin and DistMax parameters in the *Gradient* field correspond to the critical velocity gradients that will define the mesh density. The chosen values for this case are:

- for the offshore and coastal area, DistMin=$0.5{\cdot}10^{-3}$ and DistMax=0
- for the Western Scheldt estuary, DistMin=$2{\cdot}10^{-3}$ and DistMax=0

Different critical values are utilized for the two regions, since the velocity gradients at the estuary are much higher than those at the coastal zone.

[2] Magnitude of velocity gradients: $\sqrt{\left(\frac{dU}{dx}\right)^2+\left(\frac{dU}{dy}\right)^2}$ where U is the velocity magnitude (scalar)

Apart from the *Gradient* size field, the rest of the sizing parameters for the configuration of the grid (boundary layer refinement, channel mesh, etc.) remain the same as in the case of the base grid. The resulting grid consists of 244 543 nodes (about 7000 nodes less that the base grid) and 479 649 triangular elements. Typical fragments of the grid covering the same regions that are depicted in Figure 4 (for rough visual comparison), are presented in Figure 19.

Figure 19 – Element size determination based on the local gradient of maximum velocity magnitude by use of GMSH Size Field options (Structured, Gradient, Threshold).
Top figure: Focus on the coastal and offshore area (Nieuwpoort is located at the bottom right corner);
Bottom figure: Focus on part of the Western Scheldt and its mouth.

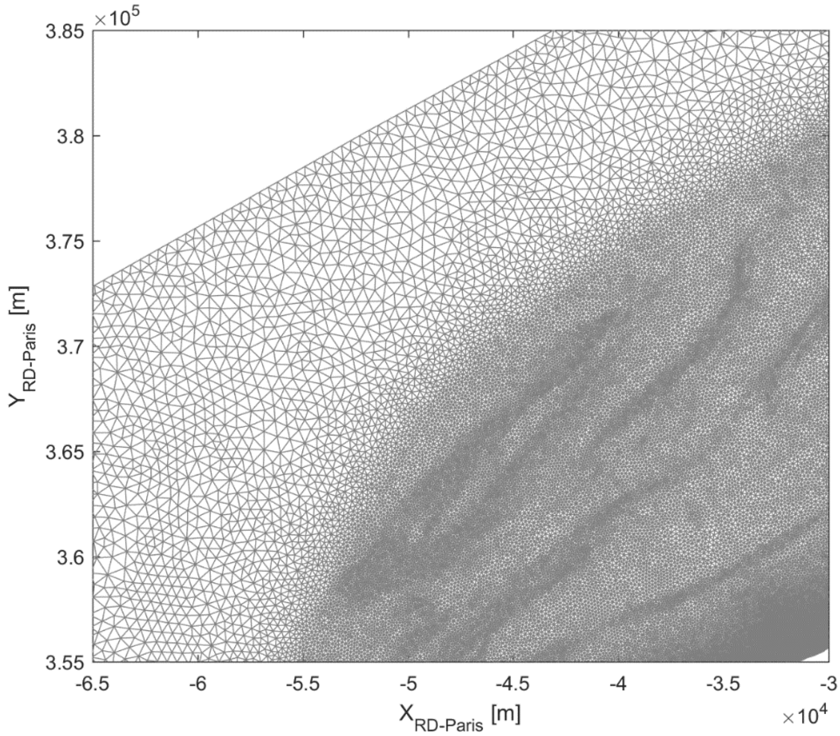

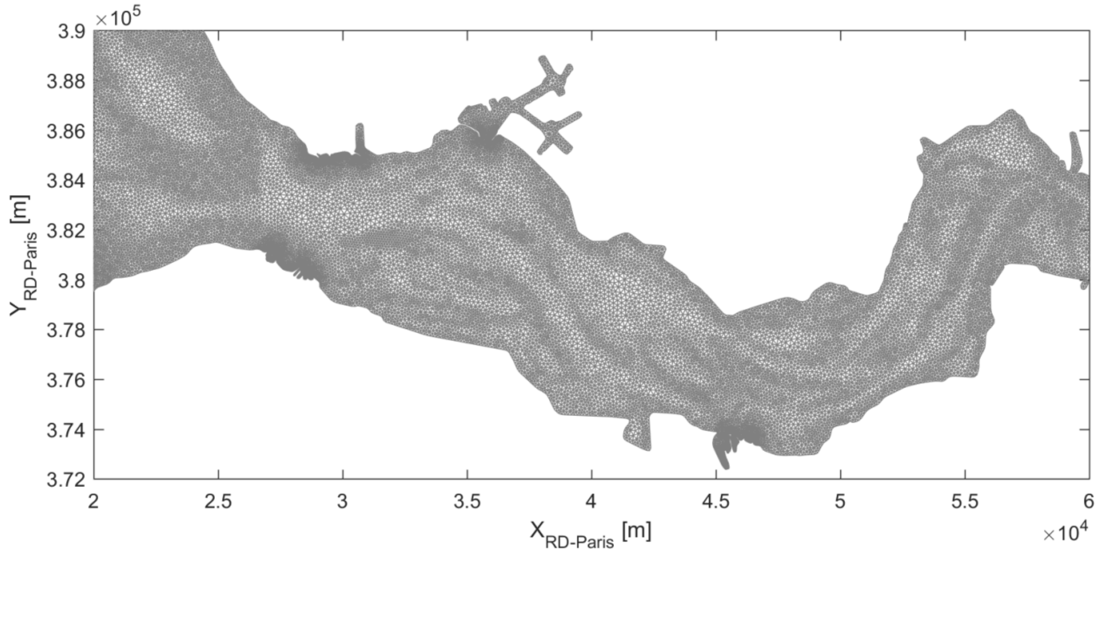

The performance of the velocity gradient grid was evaluated with respect to the bathymetry gradient grid through statistical parameters. The bias and the RMSE in the water level time-series at several locations at the coast and in the estuary for a certain time period (5 days), between identical simulations conducted on the two grid types are presented in Figure 20, indicate very good agreement between them. Especially at the stations located at the coastal zone only minor differences are observed at the temporal evolution of the water level.

Figure 20 – Bias (top figure) and RMSE (bottom figure) in the complete water level time-series (5 days) between the velocity gradient grid (E01) and the bathymetry gradient grid (D10).

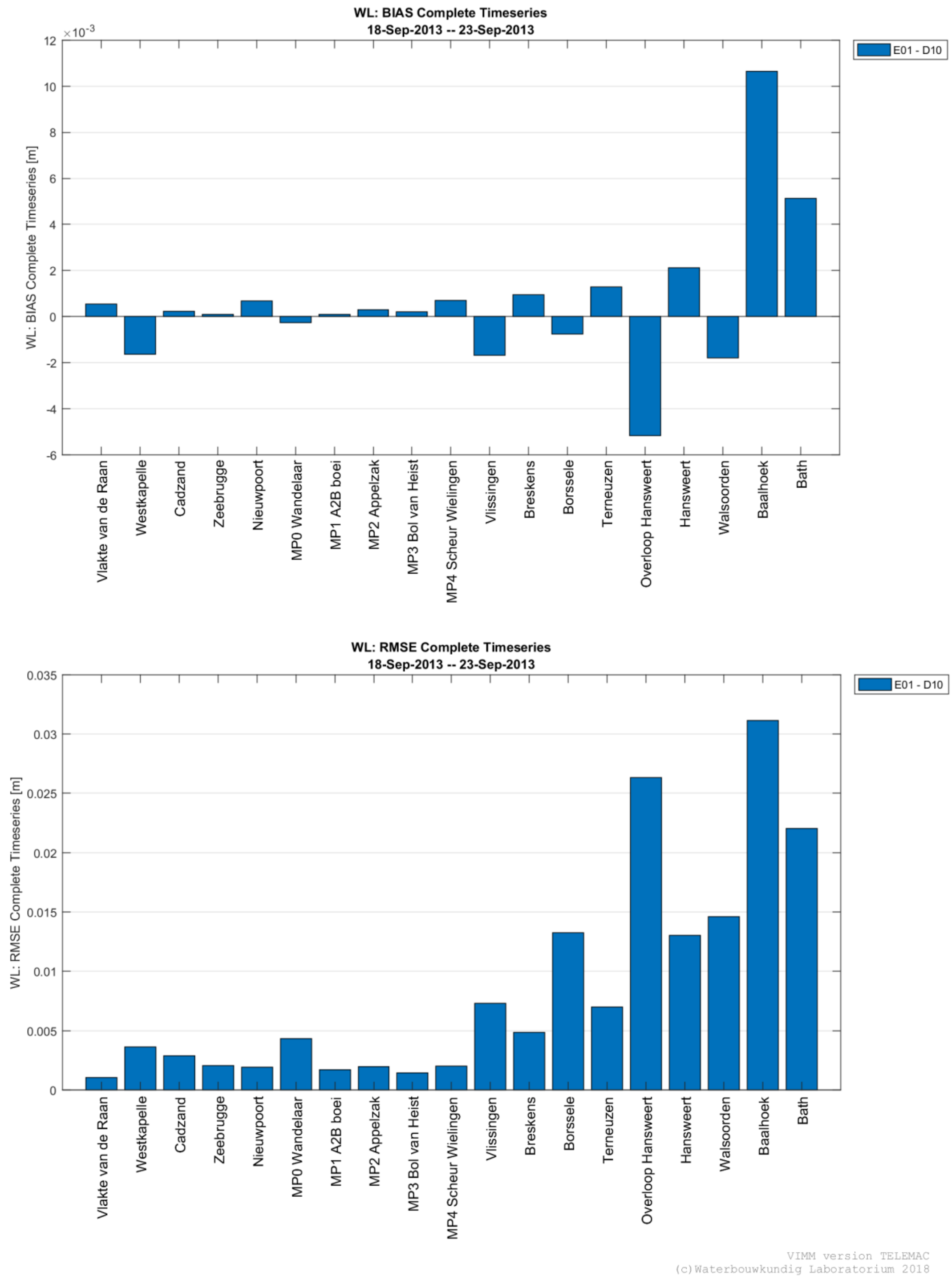

Although the determination of the grid size from the gradients of the maximum velocity magnitude is theoritically the best option, it presents some difficulties in its implementation. For example choosing correctly the critical velocity gradients (DistMin & DistMax) at different regions it is not a trivial task due to the large range of the gradients over the computational domain. Furthermore, in order to acquire the map of the velocity gradients (for the *Structured* size field) a simulation on a reliable grid has to be performed first. On the other hand the determination of the grid size based on the bathymetry slopes is more concrete even though it connects indirectly the grid size with the flow regime. All in all the comparison of the numerical results of the two types of grid has shown that they are in a very good agreement as long as their resolution is comparable. Therefore the bathymetry gradient grid was selected as the base grid of the Scaldis-Coast model.

2.2 Bathymetry

In order to fill bathymetry of the whole model domain, a number of data sources have been applied (Figure 21), and are listed below following the priority order applied to the model.

1) **Lidar data**
   This data was collected by airborne Lidar sensors in 2015, and has a very high resolution 1m x 1m.
   p:\15_068-VlabaKustzone\3_Uitvoering\5_Model Prp\Bathy\unprocessed\Lidar\DHM_kustzone.txt
2) **BCP data**
   It comes from MDK coastal division, and was collected by different measurement campaigns from 2004 to 2016.
   p:\15_068-VlabaKustzone\3_Uitvoering\5_Model Prp\Bathy\unprocessed\BCP_bth_2004-2016_VH_rds_taw_D_meest-recent-beschikbaar-in-2016\BCP_2016_rds_taw.shp
3) **WES data**
   It seems to be delivered by RWS, and is copied from \\wap148613m\GIS\Masterarchief\tob\
   p:\15_068-VlabaKustzone\3_Uitvoering\5_Model Prp\Bathy\unprocessed\WES_tob_2015_RWS_rds_taw_R\ga2015_in_m_taw.tif
4) **BEZ data**
   It comes from Maritime Access, and is copied from \\wap148613m\GIS\Masterarchief\tob\
   p:\15_068-VlabaKustzone\3_Uitvoering\5_Model Prp\Bathy\unprocessed\BEZ_bth_2015_MT_utm31etrs89_taw_R\bez_2015_m\w001001.adf
5) **Vaklodingen data**
   This data is downloaded from Open Earth database, and was measured from 2010 to 2015.
   p:\15_068-VlabaKustzone\3_Uitvoering\5_Model Prp\Bathy\unprocessed\Vaklodingen\SLCT\Part01\Bathy_part01_2015_M02.xyz
   p:\15_068-VlabaKustzone\3_Uitvoering\5_Model Prp\Bathy\unprocessed\Vaklodingen\SLCT\Part02\Bathy_part02_2013_M02.xyz
6) **French data**
   This data is collected by Service hydrographique et océanographique de la Marine (SHOM), and covers the French territory with resolution ≈20 m in the model domain. The original data could be found by
   p:\15_068-VlabaKustzone\2_Input_gegevens\Bathy\FransContinentaalPlat\
7) **Port data for Nieuwpoort, Oostende, Blankenberge and Zeebrugge**
   The data for Nieuwpoort, Oostende and Blankenberge are all provided by *Vlaamse Hydrografie* from *Maritieme Dienstverlening afdeling Kust* (MDK VH). The measurement of Nieuwpoort and Oostende was performed in 2014 and 2015, and the measurement of Blankenberge was done in 2015. Their original reference level is LAT, which can be converted to TAW by adding 0.65 m,

0.50 m and 0.32 m respectively for Nieuwpoort, Oostende and Blankenberge (Smolders *et al.*, 2016).
The bathymetry of Zeebrugge was measured in 2014. The original data could be referred to the aMT GIS database \\wm162458\Data\GISdata\frame\bth\frame_bth_kub_etrs89utm31n.gdb

p:\15_068-VlabaKustzone\3_Uitvoering\5_Model Prp\Bathy\unprocessed\HNP_bth_2014_VH_utm31etrs89_LAT_D°\
p:\15_068-VlabaKustzone\3_Uitvoering\5_Model Prp\Bathy\unprocessed\HNP_bth_2015_VH_utm31etrs89_LAT_D°\
p:\15_068-VlabaKustzone\3_Uitvoering\5_Model Prp\Bathy\unprocessed\HOO_bth_2014_VH_utm31etrs89_LAT_D°\
p:\15_068-VlabaKustzone\3_Uitvoering\5_Model Prp\Bathy\unprocessed\HOO_bth_2015_VH_utm31wgs84_LAT_R°\
p:\15_068-VlabaKustzone\3_Uitvoering\5_Model Prp\Bathy\unprocessed\HBB_bth_2015_VH_utm31etrs89_LAT_D°\
p:\15_068-VlabaKustzone\3_Uitvoering\5_Model Prp\Bathy\unprocessed\Zeebrugge_2014_MT_RD_TAW.xyz

8) **EMODnet data**
This data is available from the public database http://www.emodnet-bathymetry.eu/. The original vertical reference level is LAT, but it is uncertain in which year the data was sampled.
p:\15_068-VlabaKustzone\3_Uitvoering\5_Model Prp\Bathy\unprocessed\EMODnet\B3.xyz
p:\15_068-VlabaKustzone\3_Uitvoering\5_Model Prp\Bathy\unprocessed\EMODnet\C3.xyz

Figure 21 – Overview of the bathymetric data for the model domain:
yellow – 1) Lidar data; red – 2) BCP data; dark green – 3) WES data; light blue – 4) BEZ data;
orange – 5) Vaklodingen data; purple – 6) French data; magenta – 7) Port data;
blue – 8) EMODnet data; green – uniform values for the schematised part of the Scheldt Estuary

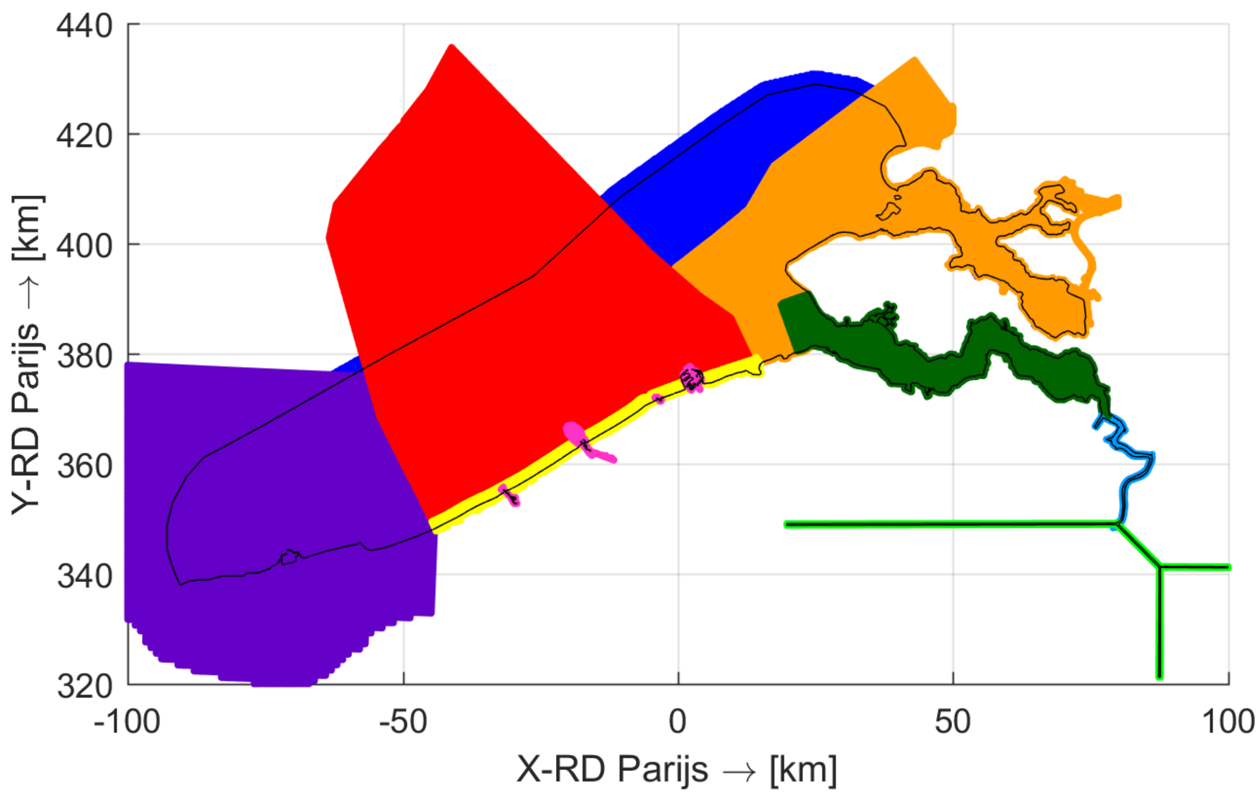

These datasets have been merged and processed to one ascii file (XYZ) with uniform coordinate system (RD Paris), vertical reference level (TAW), which is locally stored at:

p:\15_068-VlabaKustzone\3_Uitvoering\5_Model Prp\Bathy\Struct\Bathy_BENL_EMD_TAW_M12a.xyz

According to the priority order, the dataset with higher priority was firstly kept, and artificial gaps were made between two neighbouring datasets, then an interpolation was performed within these gaps for a smooth transition between two datasets.

Figure 22 – Bathymetry merged from different data sources (vertical datum: TAW)

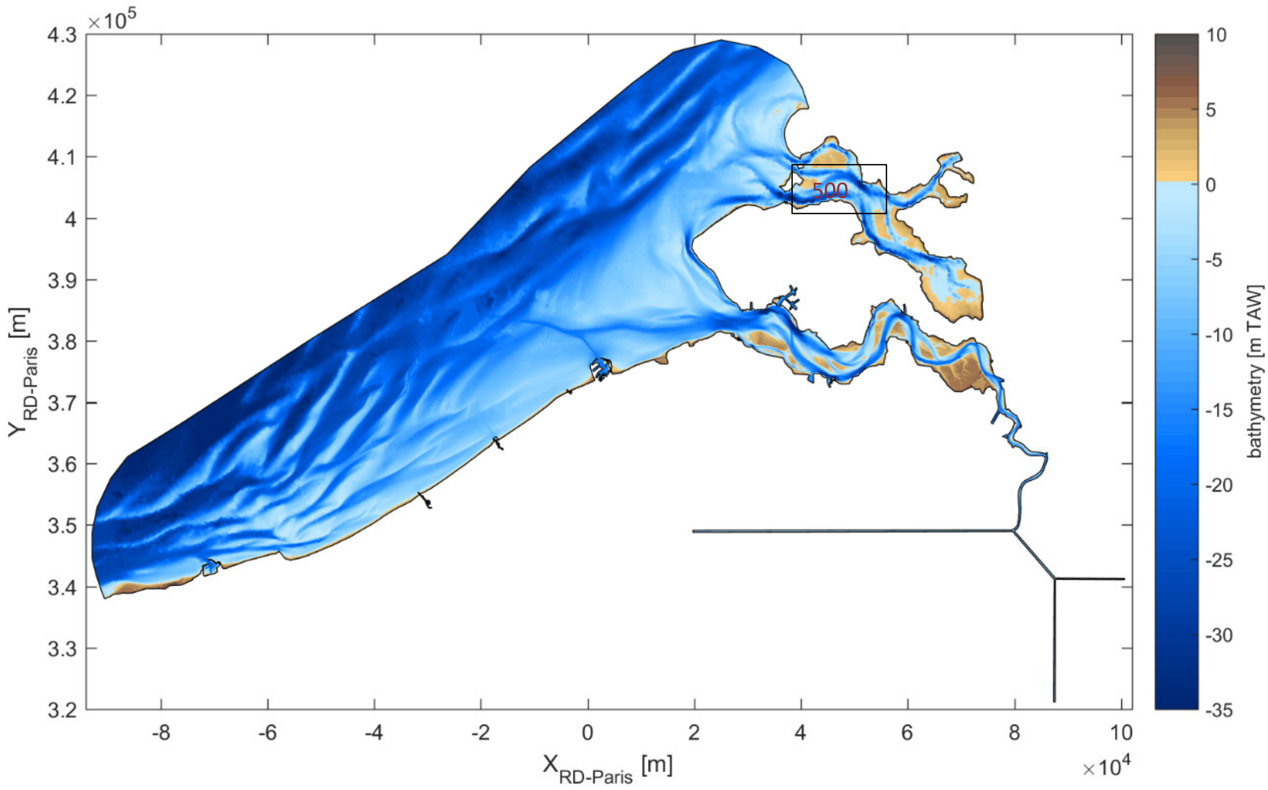

3 Hydrodynamics

3.1 Available measurement data

3.1.1 Water levels

Water level measurements for the years 2013 and 2014, which are used for the calibration/validation of Scaldis-Coast model are available from different sources. Table 4 shows the list of the stations for which validated measured water levels are available for the selected simulation periods. Figure 23 shows the locations of the measurement stations.

Ten minute interval time series of the water level measurements (m NAP, CET) were retrieved from the Hydro Meteo Centrum Zeeland database (HMCZ, www.hmcz.nl) for the stations located in the Netherlands and some Belgian stations. Measured water levels for the coastal Belgian stations were available from the Meetnet Vlaamse banken (www.kustdata.be) for Zeebrugge and Nieuwpoort. For other Belgian coastal stations the data were received from the Afdeling Kust. For the Belgian stations in the Sea Scheldt and Rupel the data (m TAW, UTC) were available from Hydrologisch Informatie Centrum (HIC).

Table 4 – Water level stations used for the calibration/validation of Scaldis-Coast model and their data sources.

	Station	**Data source**
	North Sea	
1	MP0 Wandelaar	Afdeling Kust
2	MP1 A2B boei	
3	MP2 Appelzak	
4	MP3 Bol van Heist	
5	MP4 Scheur Wielingen	
6	Nieuwpoort	www.kustdata.be
7	Oostende	
8	Zeebrugge	
9	Vlakte van de Raan	HMCZ
	Western Scheldt	
10	Westkapelle	HMCZ
11	Cadzand	
12	Vlissingen	
13	Breskens	
14	Borssele	
15	Terneuzen	
16	Overloop van Hansweert	
17	Hansweert	
18	Walsoorden	
19	Baalhoek	
20	Bath	
	Sea Scheldt	
21	Zandvliet	HIC
22	Prosperpolder	HMCZ, HIC
23	Liefkenshoek	
24	Kallo lock	
25	Antwerp	

Figure 23 – Locations of the water level measurement stations on the computational domain of Scaldis-Coast.

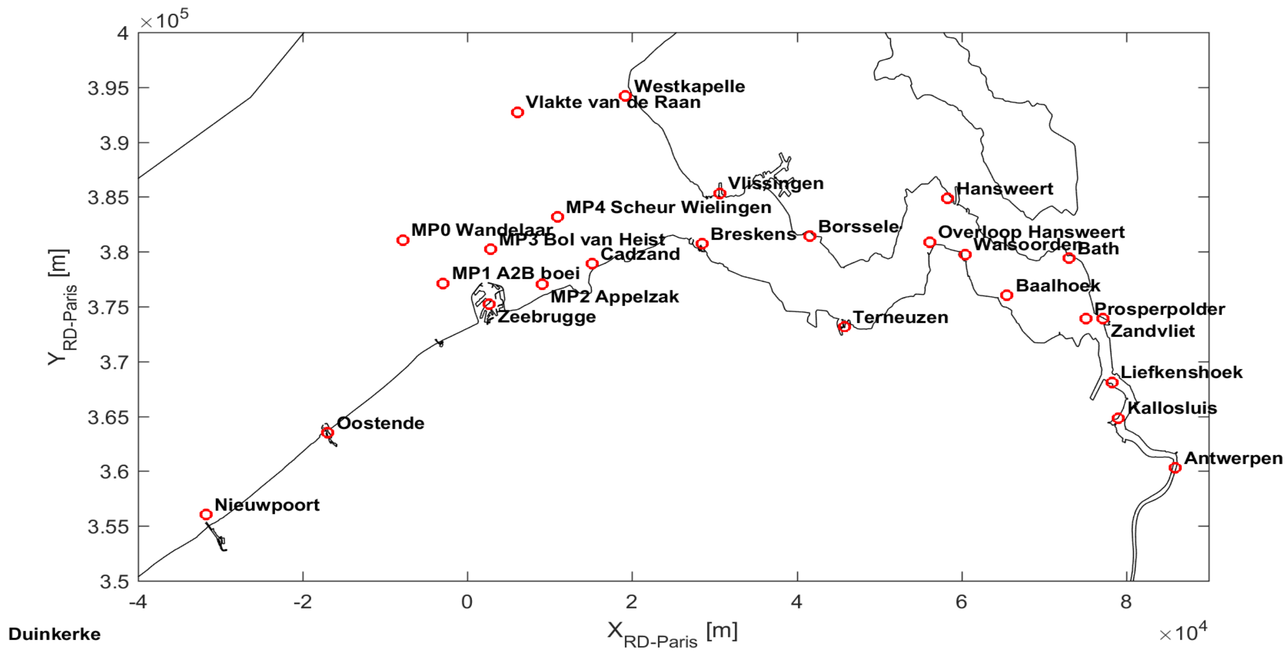

3.1.2 Velocities

Sailed ADCP measurements

The sailed ADCP measurements used for the calibration/validation of the model are located at the area of Zeebrugge harbor and in the Western Scheldt and they are included in Table 5. The locations of the ADCP transects are shown in Figure 24.

Table 5 – Available ADCP measurements used for the validation of Scaldis-Coast model.

Location	Date and time (MET)	Project
North Sea		
Zeebrugge entrance	31/07/2007 05:18 – 17:44	HCBS IMDC 2007
Zeebrugge entrance	07/08/2007 04:22 – 15:42	HCBS IMDC 2007
ZB Pas van het Zand	01/08/2007 05:45 – 18:34	HCBS IMDC 2007
ZB Wiel	03/08/2007 07:37 – 19:49	HCBS IMDC 2007
ZB Scheur	02/08/2007 06:45 – 18:47	HCBS IMDC 2007
Western Scheldt		
R7 Everingen	05/07/2011 05:05 – 17:55	MONEOS
R7 Terneuzen	06/07/2011 05:34 – 18:14	MONEOS
R6 Middelgat	08/05/2012 05:58 – 18:55	MONEOS
R6 Gat van Ossenisse	09/05/2012 04:57 – 17:50	MONEOS
Waarde	23/03/2006 09:07 – 20:55	HCBS IMDC 2006 March
Waarde	28/09/2006 06:52 – 19:53	HCBS IMDC 2006 September
R5 Schaar van Waarde	24/04/2013 05:35 – 18:28	MONEOS
R5 Zuidergat	25/04/2013 06:18 – 19:12	MONEOS

Figure 24 – Locations of the ADCP sailed transects (red lines) in the North Sea (top figure) and in the Western Scheldt estuary (bottom figure).

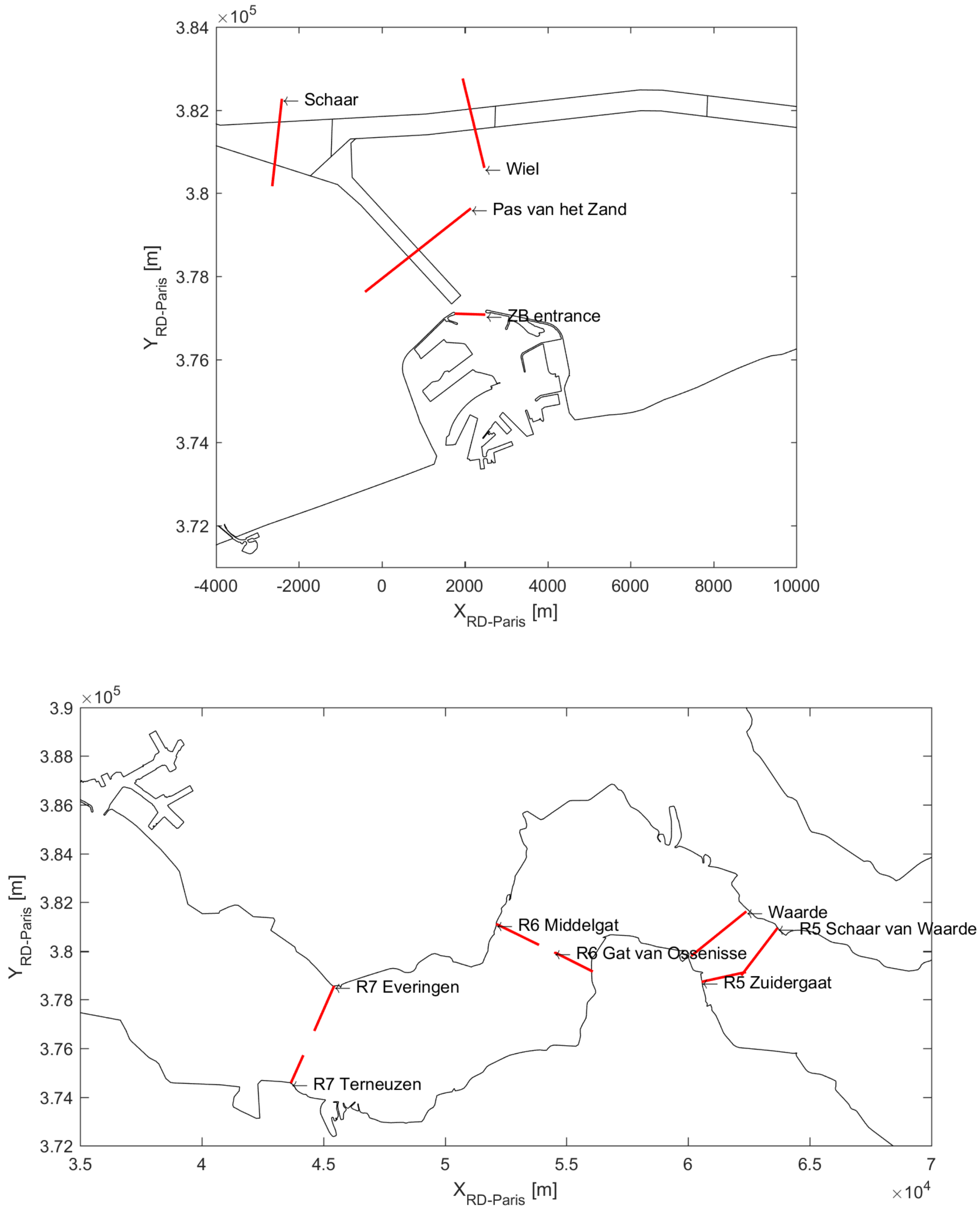

Stationary velocity measurements

Stationary velocity measurements from 2013 are available at four locations in deep water and at two locations in shallow water (see Table 6). From 2014, measurements from two locations at deep water are used for the validation of the model (Table 6). The locations of the velocity measurement stations are shown in Figure 25.

Table 6 – Stationary velocity measurements used for the validation of Scaldis-Coast model.

Location	Height
Deep water	
MP0 Wandelaar (2013 – 2014)	Profile averaged from 2.5 m to 10 m below the surface
MP3 Bol van Heist (2013 – 2014)	Profile averaged from 2.5 m to 10 m below the surface
MP4 Bol van Knokke (2013 – 2014)	Profile averaged from 2.5 m to 10 m below the surface
WZ-buoy (BMM) (2013)	Profile averaged up to 3 m above the bottom
Geul van de Walvisstaart – GvW 1 (2014)	Depth-averaged
Geul van de Walvisstaart – GvW 2 (2014)	Depth-averaged
Shallow water	
Hooge Platen West (HPW MP101) (2013)	Depth-averaged
Hooge Platen West (HPW MP205) (2013)	Depth-averaged

Figure 25 – Locations of the stationary velocity measurements on the computational domain of Scaldis-Coast.

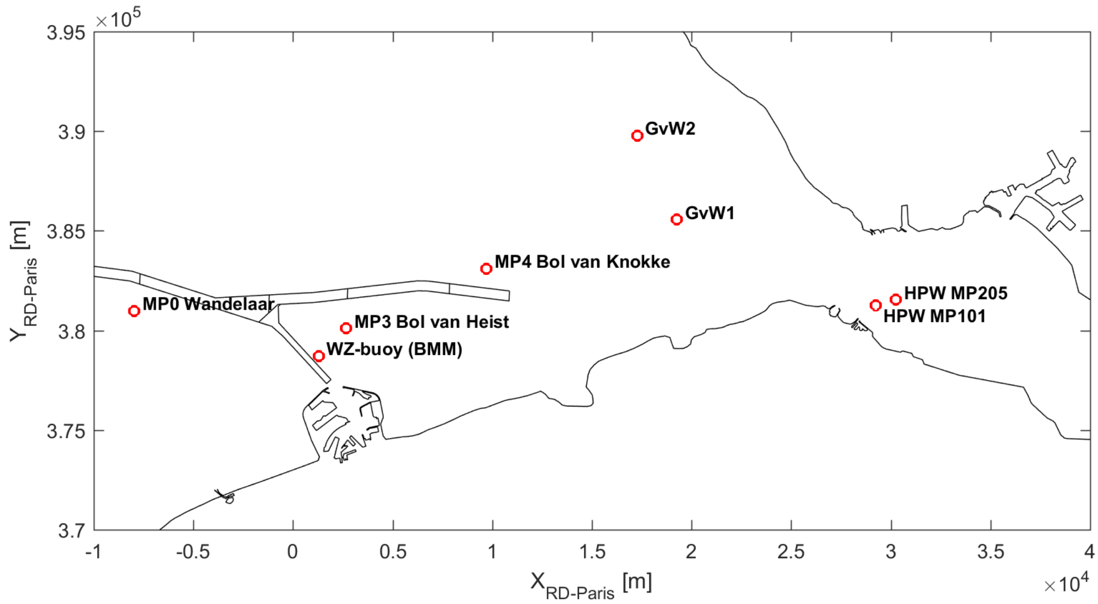

3.1.3 Flow discharges

There are 8 upstream boundaries where flow discharges have to be introduced in the model. The daily averaged measured discharges at the Upper Sea Scheldt for Melle, Dender, Zenne, Dijle, Kleine Nete, Grote Nete and the channel Ghent – Terneuzen, are imposed properly at the schematized boundaries of the model as upstream boundary conditions. Due to the schematized upstream boundaries the discharges of Zenne and Dijle and those of Grote and Kleine Nete are imposed at the same location of the boundaries. For the channel of Bath, hourly discharge measurements were available. Note that the small negative values observed in this time series were set equal to zero in order to prevent possible instabilities. Since all the other upstream discharges were daily averaged, before their introduction in the model they were hourly interpolated, so that all discharge boundaries could be imposed in the model as hourly discharge time series. The time series of the tributary and channel discharges for the considered calibration and validation periods are presented in Figure 26 and Figure 27 as they were imposed in the model.

Figure 26 – Time series of the flow discharges in the Scheldt river in 2013, as imposed in the Scaldis-Coast model.

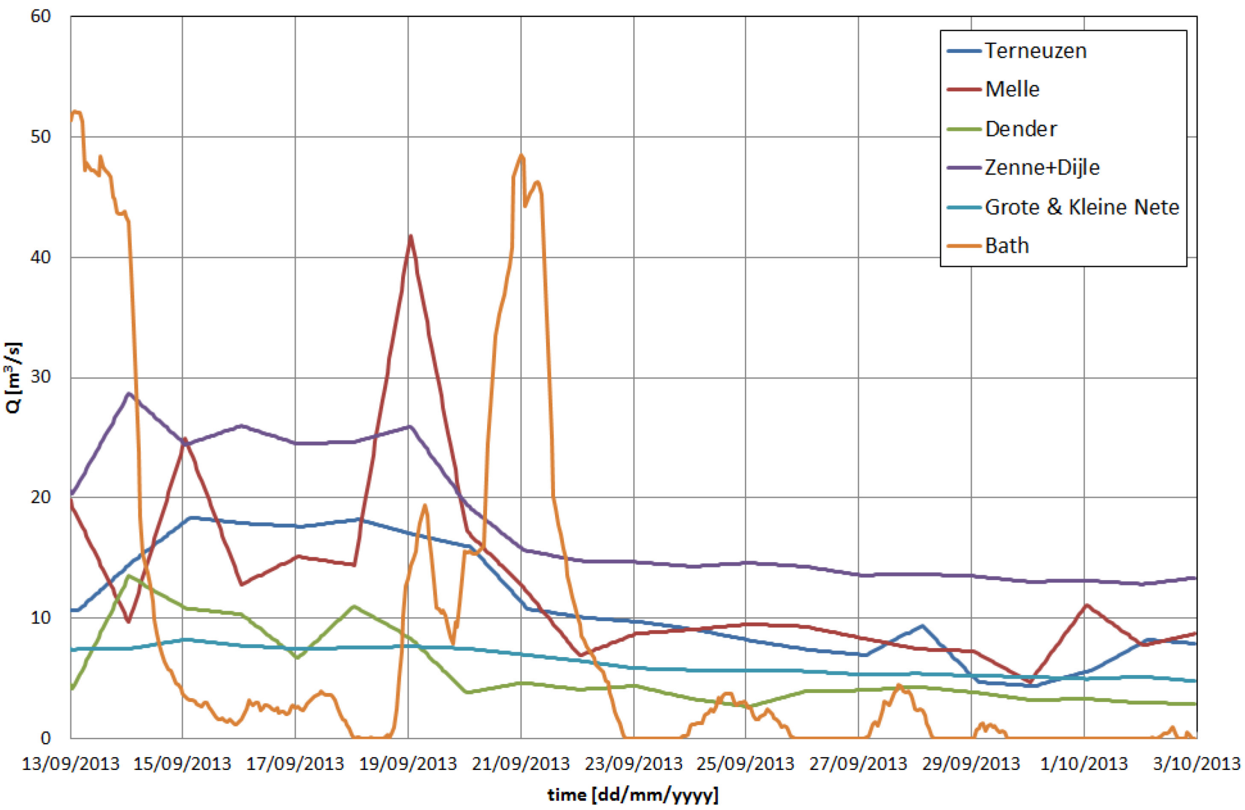

Figure 27 – Time series of the flow discharges in the Scheldt river in 2014, as imposed in the Scaldis-Coast model.

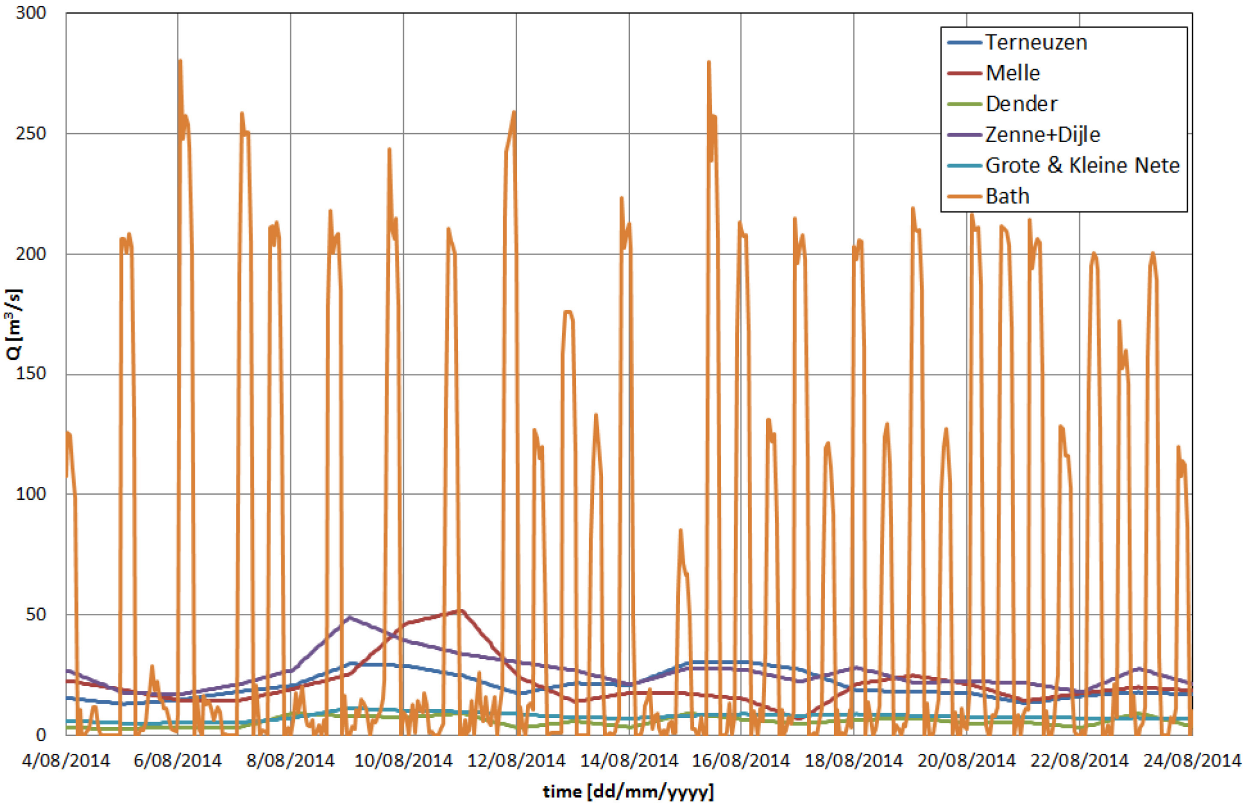

3.1.4 Wind data

Wind measurements are available at Vlakte van de Raan with a time interval of 10 minutes, which are used to force the Scaldis-Coast model. In Figure 28 and Figure 30 the time series of the wind magnitude and direction are plotted for the considered calibration and validation periods of the model. In Figure 29 and Figure 31 the wind roses for the aforementioned periods are also shown for better representation of the wind climate. It is shown that the wind conditions for the selected calibration period (in 2013) are in general moderate with wind velocities less than 10 m/s, except for a few time windows where the speed reaches values up to 14 m/s. Wind direction presents diversity but mainly East, and West winds are observed. For the selected validation period (in 2014) higher wind velocities up to 19 m/s are observed, while the wind blows mainly from the West-Southwest direction.

In Figure 32, the long term wind climate at the Belgian coast is illustrated through the wind rose of the 11-year period from 2007 to 2017. It is shown that the prevailing winds blow from Southwest and their magnitude can reach values higher than 20 m/s. Taking this observation into account, the wind conditions during the validation period (2014) could be characterized as more representative of the long term wind climate.

Figure 28 – Wind magnitude and direction time series at Vlakte van de Raan during the calibration period (2013).

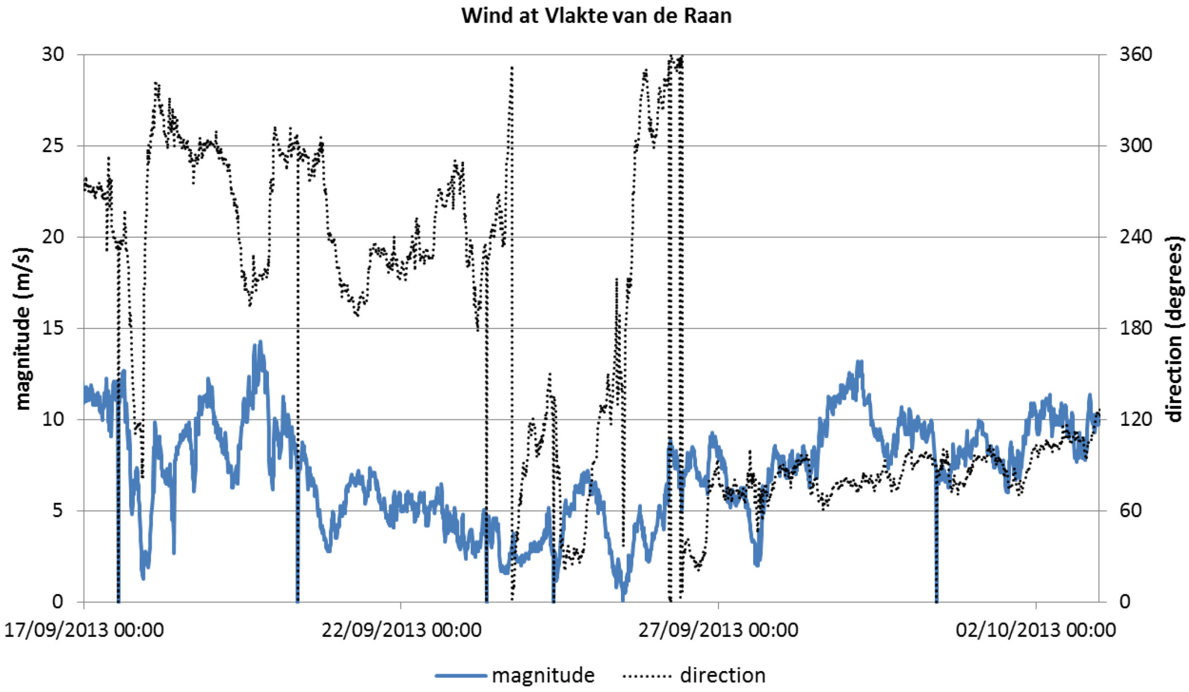

Figure 29 – Wind rose at Vlakte van de Raan during the calibration period (2013).

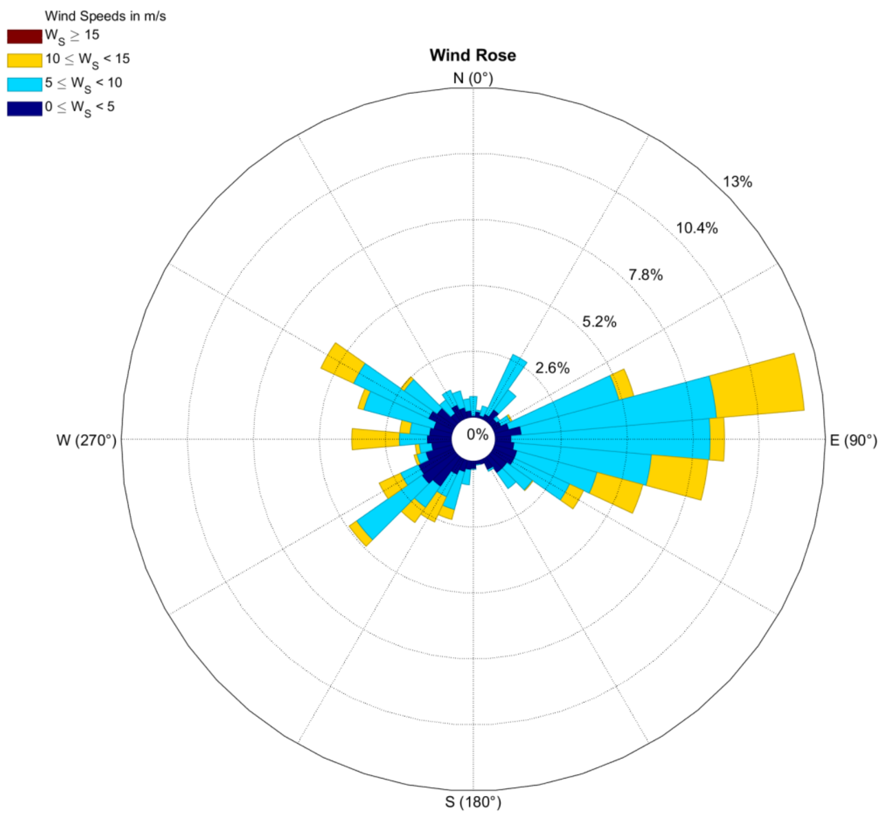

Figure 30 – Wind magnitude and direction time series at Vlakte van de Raan during the validation period (2014).

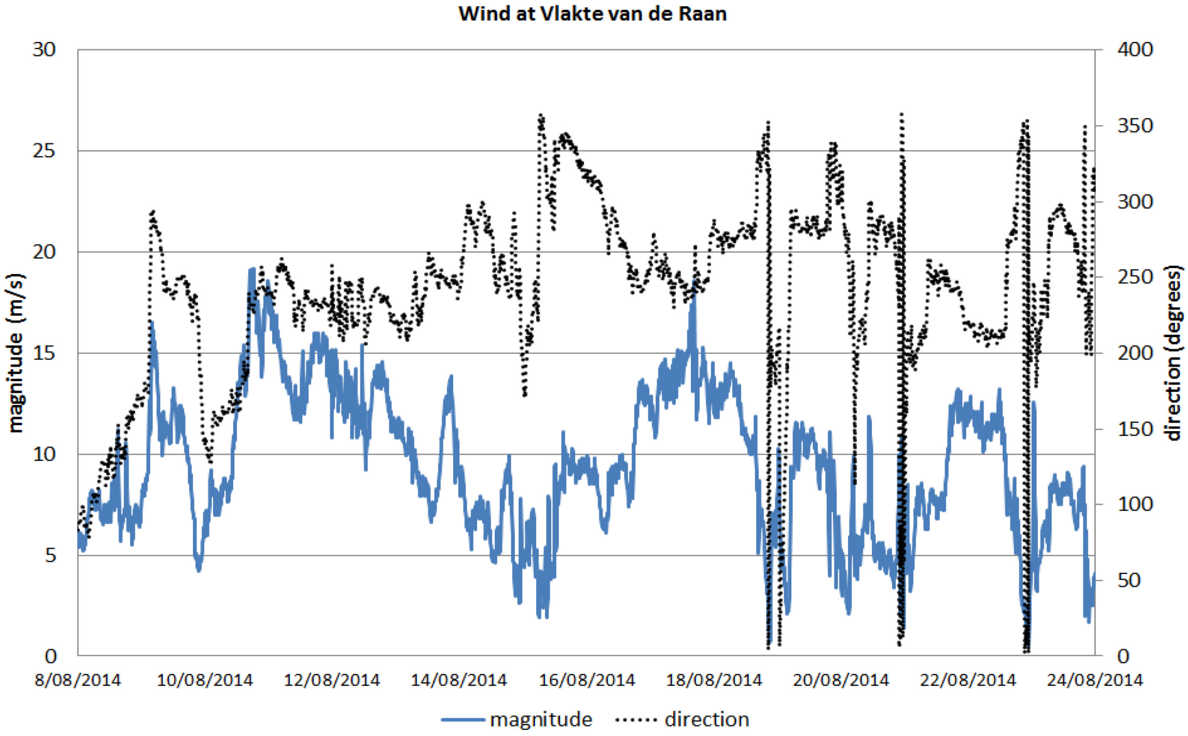

Figure 31 – Wind rose at Vlakte van de Raan during the validation period (2014).

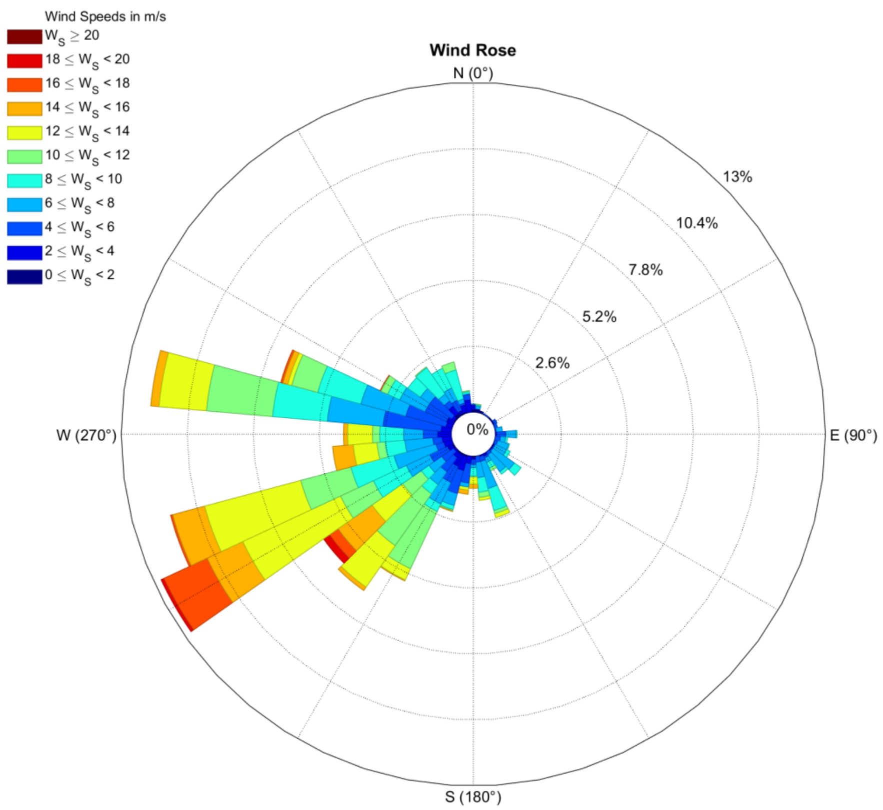

Figure 32 – Wind rose at Vlakte van de Raan for the 11-year period 2007-2017.

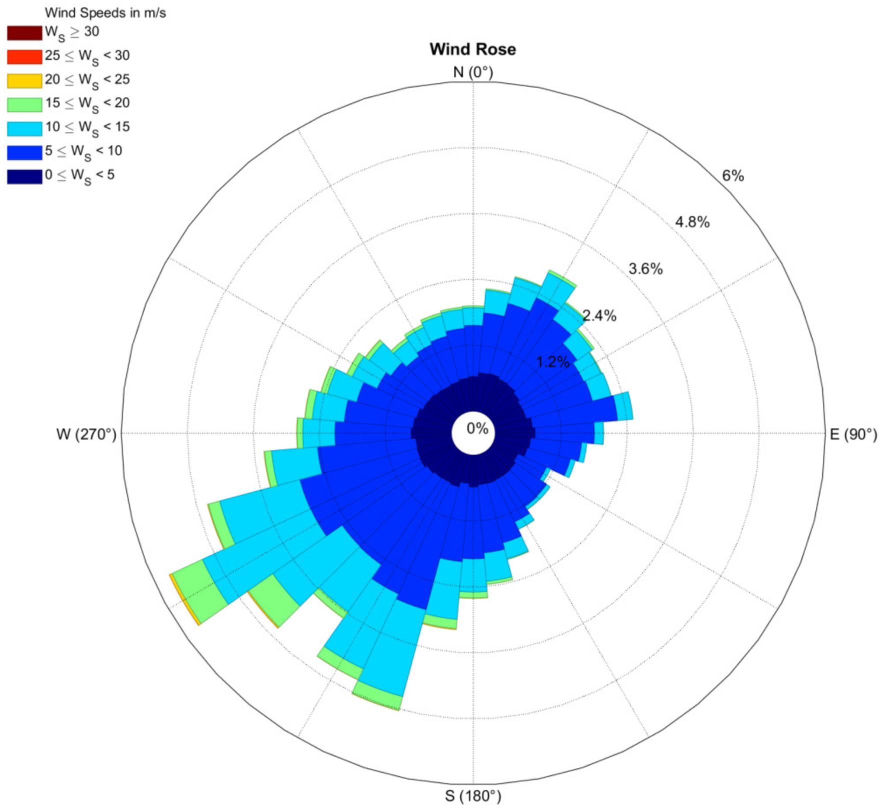

3.2 The Scaldis-Coast model

The Scaldis-Coast hydrodynamic simulations are performed by means of TELEMAC2D software (Hervouet, 2007), which solves the shallow water equations (Saint-Venant) on unstructured triangular meshes using the finite element method. The utilized software version has the acronym v7p2r2. TELEMAC software is capable of performing computations on adaptive meshes that incorporate a broad range of element sizes (from kilometres to a few meters) making it suitable for complex geometries like in our study area. It also allows for efficient parallel computing of high scalability, carrying out ‘heavy’ computations in reasonable computational times. For the analysis of the results conducted in the framework of the calibration/validation of the model presented in this section, the VIMM toolbox was utilized. Extended results can be found in: P:\15_068-VlabaKustzone\3_Uitvoering\6_Model Psp\HydrodynamicSimulationsT2D_CPK\Calibration.

3.2.1 Model grid & bathymetry

Detailed presentation of the computational grid and the bathymetric data has been done in Chapter 2. The choice of the dimensions of the computational domain is justified in detail in section 5.2 in Smolders *et al.* (2016).

3.2.2 Forcing of the model

Offshore boundary conditions

The offshore boundary conditions of the Scaldis-Coast model come from the regional ZUNOv3 model of the southern North Sea through nesting. Specifically, the nesting procedure consists of numerical simulations conducted in two levels: First a continental shelf model (CSM) is run in order to provide the boundary conditions of the second-level nested model (ZUNO), which includes the southern North Sea and the Channel. The description, the detailed model settings and the validation of CSM and ZUNO models are reported in Maximova *et al.* (2016). The models include meteorological forcing.

A correction of the harmonic components is calculated based on the comparison of the harmonic components of the ZUNO results and measurements for a period of 1 year (Maximova *et al.*, 2016). The correction is based on the average differences in harmonic components (ZUNO vs. measurements) found for several stations in the Belgian and Dutch Coastal zone for the M2, M4, S2 phases and the Z0 component (see Table 7Table 7). After decomposition and correction, the water level signal is re-synthesized in order an unbiased time series to be applied at the boundary of Scaldis-Coast model.

The model is forced by 10-minute time series of the water level and velocities calculated by ZUNOv3 model. The subroutine bord.f of TELEMAC was modified properly to allocate water level and velocity values for each boundary node separately.

Table 7 – Correction of harmonic components of water level variation.

Harmonic component	Correction
Phase M2	+4°
Phase M4	-6°
Phase S2	+7°
Z0	-16 cm

Upstream boundary conditions

Flow discharges from 8 upstream tributaries and channels are introduced at model in the manner described in section 3.1.3 of the present report.

Wind forcing

Wind time series presented in section 3.1.4 is imposed uniformly on the computational domain through the subroutine meteo.f.

3.2.3 Simulation period

The model ran for two simulation periods of 20 days each, i.e. for a period in 2013 (13/09/2013 to 03/10/2013) and for a second one in 2014 (04/08/2014 to 24/08/2014). The model's calibration-validation presented in sections 3.2.6 and 3.2.7 is based on the statistical analysis of the results for the period from 17/09/2013 to 03/10/2013 (a full spring-neap tidal cycle). The simulation of the second period (2014) is used for an additional validation of the model making use of the available stationary velocity measurements of this period.

The first simulation period which is used for the calibration-validation of the model was selected to be identical to the one used for the calibration of the existing Scaldis model (Smolders *et al.*, 2016). In this way the performance of Scaldis-Coast can be directly compared to the existing Scaldis model. As mentioned in section 3.1.4, the meteorological conditions were rather moderate for the specific period.

The selection of both the simulation periods was done based on the analysis of the comparable tides for the available ADCP measurements and on the availability of stationary velocity measurements at the North Sea.

3.2.4 Model settings

The most important model settings are copied from the Scaldis model (Smolders *et al.*, 2016). They are included in Table 8.

Table 8 – Main settings of the Scaldis-Coast model.

Parameter	Value
Time step	10 s
Initial conditions	Constant elevation (1 m TAW)
Version of TELEMAC	TELEMAC V2P2R2
Wind / Coefficient of wind influence	On / $0.565 \cdot 10^{-6}$
Coriolis / coefficient value	YES / $1.13522 \cdot 10^{-4}$ s^{-1}
Salt transport	Off
Roughness formula	Manning
Bed roughness value	varying roughness distribution (see Figure 33)
Option for treatment of tidal flats	1: equations solved everywhere with correction on tidal flats
Treatment of negative depths	2: flux control
Free surface gradient compatibility	0.9
Horizontal turbulence model	4: Smagorinski
Velocity Diffusivity	10^{-6} (default)
Scheme for advection of velocities	1: method of characteristics
Scheme for advection of depth	5: conservative scheme
Scheme for diffusion of velocities	1: implicit (1 is default; 0 cancels the diffusion)
Solver	3: Conjugate gradient on normal equation (default)
SUPG Option	2;0
Mass-Lumping on H / Velocity	1 / 0
Treatment of the linear system	2 (wave equation)

The bed roughness coefficient (according to Manning's law) distribution over the computational domain of Scaldis-Coast is presented in Figure 33. In the main part of the domain the coefficient is constant and equal to 0.022 $m^{1/3}$/s. Upstream of the Western Scheldt and in the Low Sea Scheldt is reduces to values equal to 0.012 $m^{1/3}$/s following the findings of the calibration of the Scaldis model reported in Smolders *et al.* (2016). In the schematized upstream part an increased coefficient is considered taking into account the findings of the calibration of the Zeebrugge model (IMDC, 2015). Sensitivity test results about bed roughness in Scaldis-Coast model are presented in the following section.

Figure 33 – Bed roughness coefficient (Manning) distribution (test D18) on the computational domain of Scaldis-Coast model.

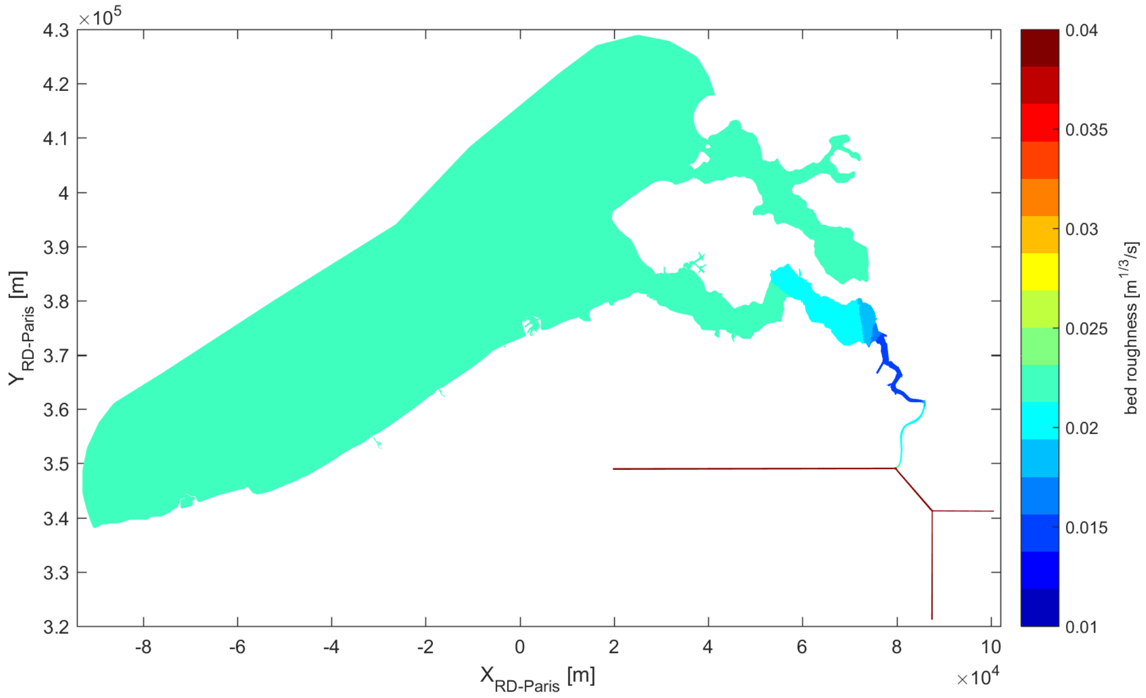

3.2.5 Time step sensitivity

The sensitivity of the numerical results to the selected time step was investigated by repeating the hydrodynamic simulation of 2013 utilizing three different time steps as shown in the following table:

Table 9 – Time step sensitivity tests.

Test	time step (s)
D10	10
D15	5
D16	20

The comparison of the results of these tests are illustrated better by means of statistical error parameters such as the RMSE in the water level and the velocity time series of the simulation period. Test D10 was used as reference, the time step of which is finally selected for the calibration/validation of the model. In Figure 34 and Figure 35 the RMSE between the two time step tests of 5 s and 20 s (D15 & D16) and the reference (finally selected) test of 10 s (D10) for the selected water level stations and the stationary velocity locations, are shown respectively. In general, the differences between the tests are very small, namely in the order of magnitude of 10^{-3} m and m/s, respectively. This means that a time step of 20 s would also lead into similar results as the reference run, at least at the presented areas of interest where the grid is of relatively high resolution. However due to the relatively low computational time of the hydrodynamic simulations it is chosen to keep the time step equal to 10 s.

Figure 34 – RMSE in the water level time-series (5 days) between the two time step tests of 5 s and 20 s (D15 & D16) and the reference (finally selected) test of 10 s (D10) at selected stations in the computational domain.

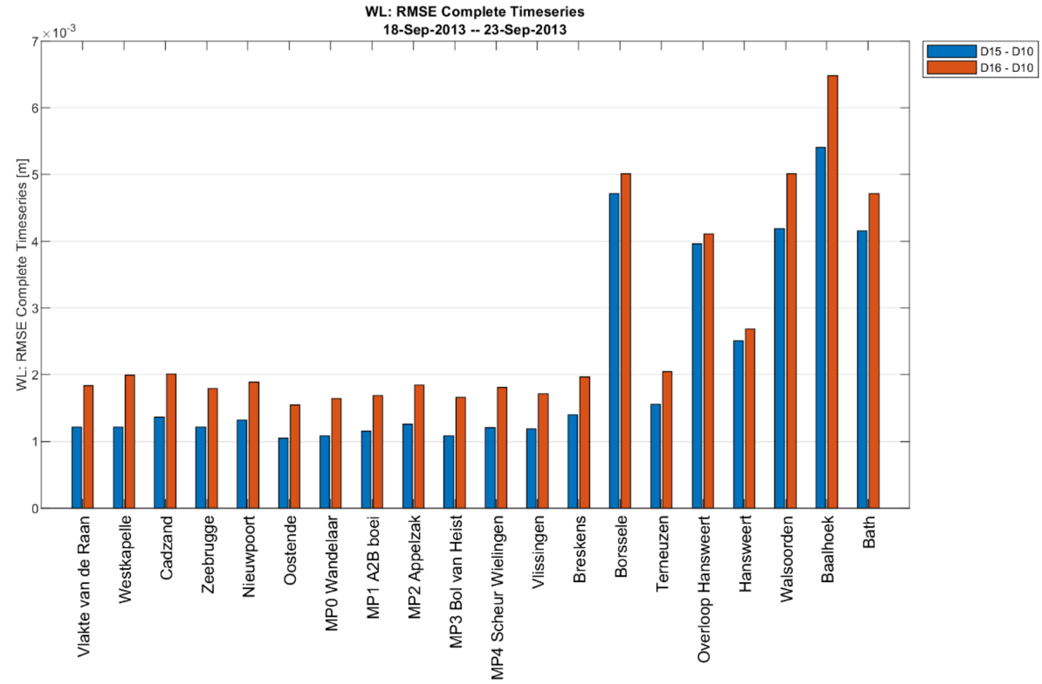

Figure 35 – RMSE in the velocity magnitude time-series (5 days) between the two time step tests of 5 s and 20 s (D15 & D16) and the reference (finally selected) test of 10 s (D10) at selected stations in the computational domain.

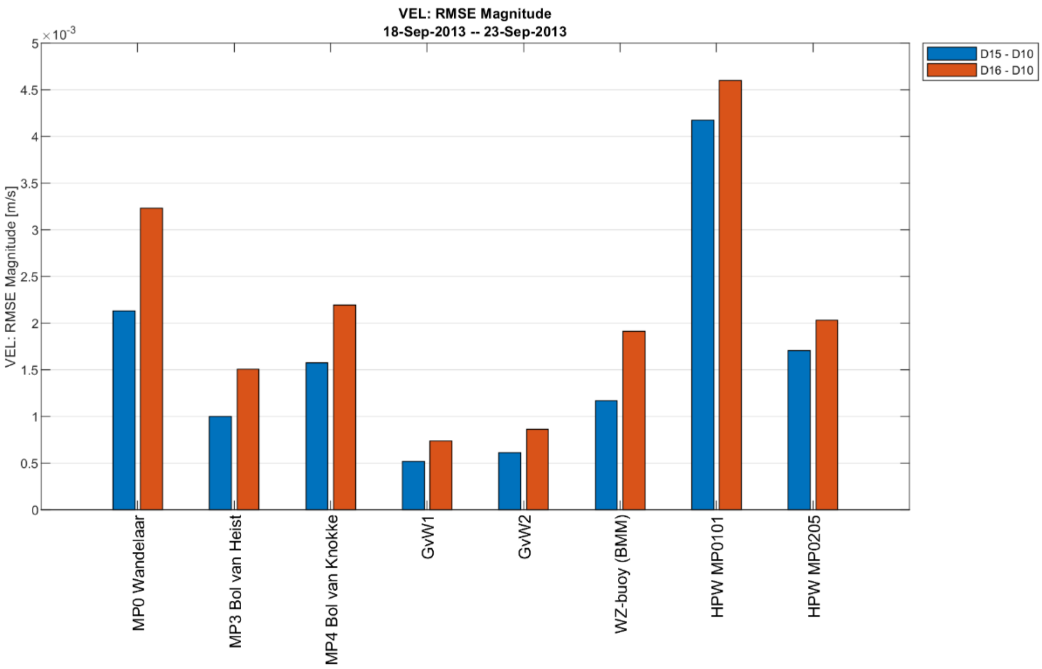

3.2.6 Bed roughness sensitivity

The selected bed roughness distribution presented in Figure 33 resulted from a number of test simulations. The main idea in defining the bed roughness field was to keep it as uniform as possible, since the model is intended to be extended so that it can be used for morphological calculations. On the other hand, features of the calibrated Scaldis and the Zeebrugge models should also be taken into account. For the aforementioned reasons it was decided to start with considering a uniform bed roughness coefficient equal to 0.02 $m^{1/3}/s$ everywhere in the computational domain, except for the upstream schematized part where an increased value equal to 0.04 $m^{1/3}/s$. This distribution resembled more the one of the Zeebrugge model (IMDC, 2015) and was tested in simulation test D19.

The finally selected distribution adds to previous one the considerations of the calibrated Scaldis model for bed roughness in a simplified way, i.e., a bit increased Manning coefficient for the main part of the domain (0.022 $m^{1/3}/s$) and a reduced one at the downstream of the Western Scheldt and in the Lower Sea Scheldt (up to 0.012 $m^{1/3}/s$) was implemented (test D18 – see Figure 33). In Figure 36 the RMSE in the water level time-series at the selected measurement locations for the 16 last days of the simulation period, between the two aforementioned bed roughness tests (D19 and D18) and the measurements, are presented. It was found that the two sensitivity tests lead to comparable results at the coastal stations, while test D18 with the varying Manning coefficient at the Western Scheldt and the Lower Sea Scheldt gives substantially better predictions at these locations compared to test D19. Note that the RMSE values at the stations in Western Scheldt (from Vlissingen to Bath) are always lower than 0.2 m for test D18. For the Lower Sea Scheldt stations RMSE becomes higher, but this is a known effect of the upstream schematized part on the results.

Figure 36 – RMSE in the complete water level time-series (16 days) between the two bed roughness distribution tests (D19: incipient and D18: finally selected) and the measured values at the selected stations in the domain.

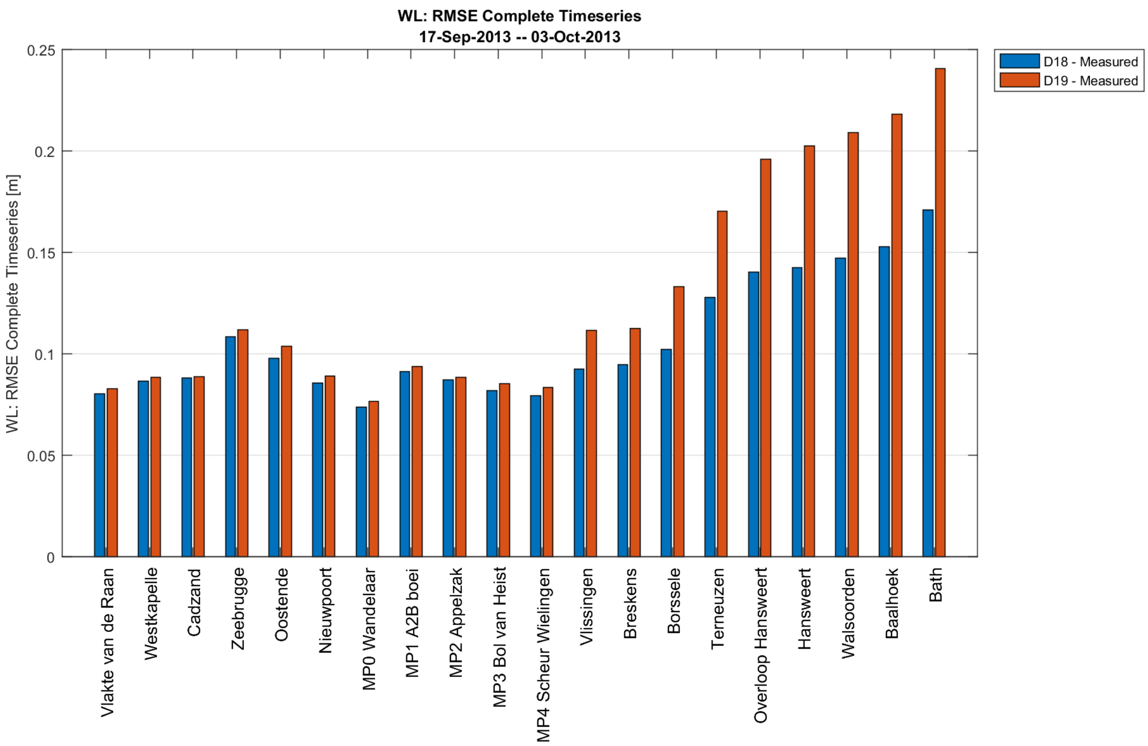

In Figure 37 the RMSE in the velocity magnitude (top figure) and direction (bottom figure) time-series between the two bed roughness distribution tests (D19 and D18) and the measurements, are presented. As in the case of water levels, the results for velocities at the coastal stations and the HPW station at the mouth of Scheldt are comparable. Although the selected bed roughness distribution (D18) performs slightly worse at the area around Zeebrugge harbour (stations MP0, MP3 and MP4), the difference of 2 cm/s is considered negligible. Moreover, the performance of D18 in the estuary is much better than that of D19. This difference in velocities is attributed to the slight difference in the utilized Manning's coefficient at the coast (n_{D18} = 0.022 $m^{1/3}$/s and n_{D19} = 0.02 $m^{1/3}$/s).

More tests with other bed roughness distributions with local or extended modifications compared to the presented tests were conducted as well. Tests included the consideration of both Manning's and Nikurades's laws. The aim was to reduce the bottom friction using lower values for the Manning's coefficient, *n*, (or Nikuradse's k_s) in order to improve the prediction of the peak flood velocities at specific locations around the port of Zeebrugge. However, the tests revealed that even with extensive lower roughness coefficient (n = 0.018 $m^{1/3}$/s) the impact on the peak flood velocities at the specific locations was limited: up to 10 to 15 cm/s. Therefore, it was decided to keep the more convenient value of 0.022 $m^{1/3}$/s. It was decided to not spatially vary the roughness coefficients within the domain of interest, i.e. the coastal zone. A spatially varying roughness constant for calibrating currents, can lead to unnatural morphodynamic behaviour. The extra roughness sensitivity tests are added to Appendix 3.

Figure 37 – RMSE in the velocity magnitude (top figure) and direction (bottom figure) time-series between the two bed roughness distribution tests (D19: incipient and D18: finally selected) and the measured values at the selected stations in the domain. Note that time-series of 16 days [17/09-03/10/2013] were used for all stations except for HPW where 6 days were available [17-23/09].

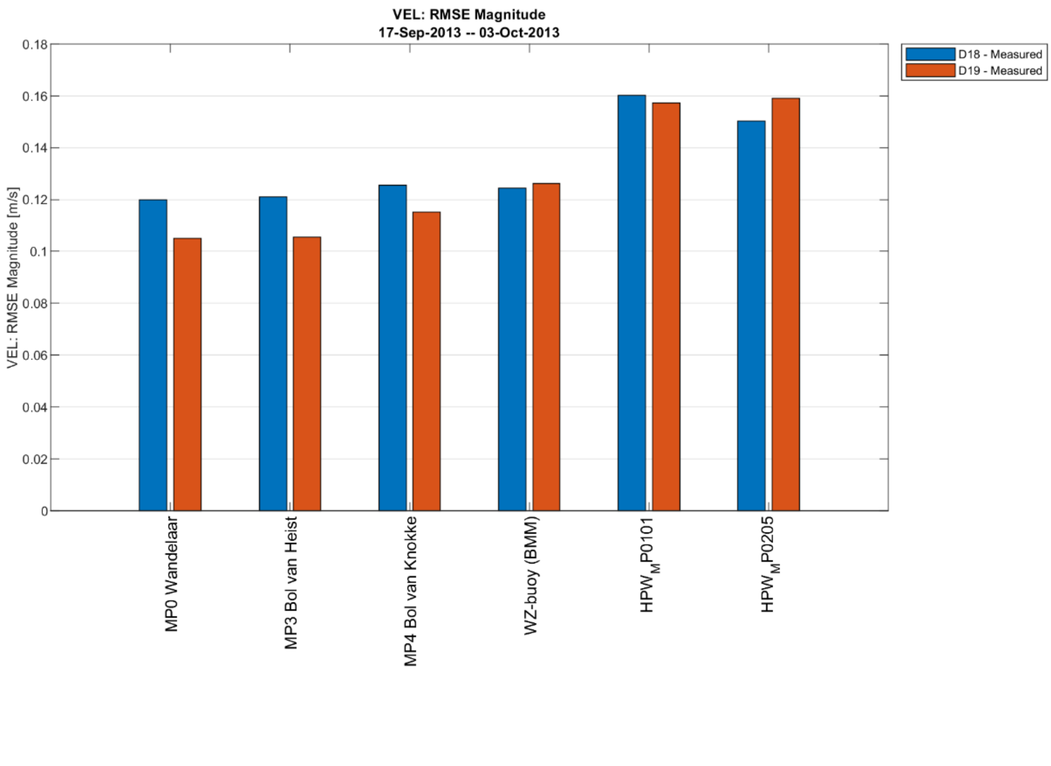

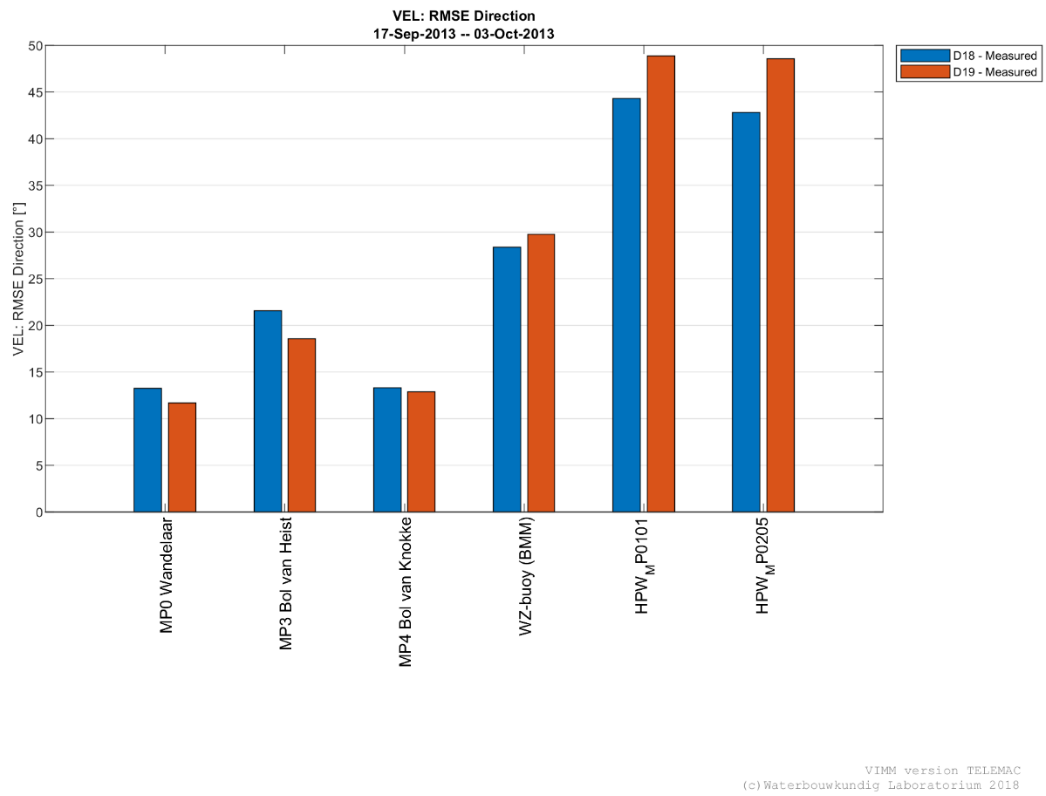

3.2.7 Model validation

The model is validated by comparison of the numerically predicted water levels and velocities against measured water levels, stationary velocities and velocities along transects (ADCP sailed) at several locations at the coast and the Western Scheldt estuary. The available measurement data used for the model validation were presented in section 3.1. The statistical analysis of the results presented in this section is performed for the period from 17/09/2013 to 03/10/2013 (a full spring-neap tidal cycle).

Water levels

The main statistical parameters (Bias, RMSE and RMSE0) of the water level time series at selected North Sea and Western Scheldt stations are presented in Table 10. The total RMSE increases from 9 cm in the North Sea to 13 cm in the Western Scheldt. The absolute value of the bias of water levels is equal or lower than 5 cm at most stations. RMSE0, which corresponds to the bias corrected RMSE, determines in a sense the tidal range/shape. Due to the small biases the total RMSE0 remains close to RMSE. In general the performance of the model in capturing the variation of water level is very good especially at the coastal stations. Figure 38 shows the RMSE0 of the complete water level time series (last column of Table 10) for all the considered stations. The definition of the aforementioned statistical parameters utilized for the validation of the model are given in Appendix 2.

Table 10 – Main statistical parameters for the water level time series (2013) at selected North sea and Western Scheldt stations.

Station	Complete Time Series (16 days)		
	BIAS TS	RMSE TS	RMSE_0 TS
	[m]	[m]	[m]
North Sea			
Vlakte van de Raan	0.01	0.08	0.08
Westkapelle	0.02	0.09	0.08
Cadzand	0.03	0.09	0.08
Zeebrugge	-0.07	0.11	0.08
Oostende	-0.05	0.10	0.09
Nieuwpoort	-0.01	0.09	0.09
MP0 Wandelaar	0.01	0.07	0.07
MP1 A2B boei	-0.05	0.09	0.08
MP2 Appelzak	0.03	0.09	0.08
MP3 Bol van Heist	0.02	0.08	0.08
MP4 Scheur Wielingen	0.02	0.08	0.08
Total	**0.00**	**0.09**	**0.08**
Western Scheldt			
Vlissingen	0.02	0.09	0.09
Breskens	0.00	0.09	0.09
Borssele	0.00	0.10	0.10
Terneuzen	-0.03	0.13	0.12
Overloop Hansweert	-0.07	0.14	0.12
Hansweert	-0.05	0.14	0.13
Walsoorden	-0.06	0.15	0.14
Baalhoek	-0.06	0.15	0.14
Bath	-0.05	0.17	0.16
Total	**-0.03**	**0.13**	**0.12**

Figure 38 – RMSE0 in the complete water level time-series (16 days) between the modelled by Scaldis-Coast and the measured values at the selected stations in the domain.

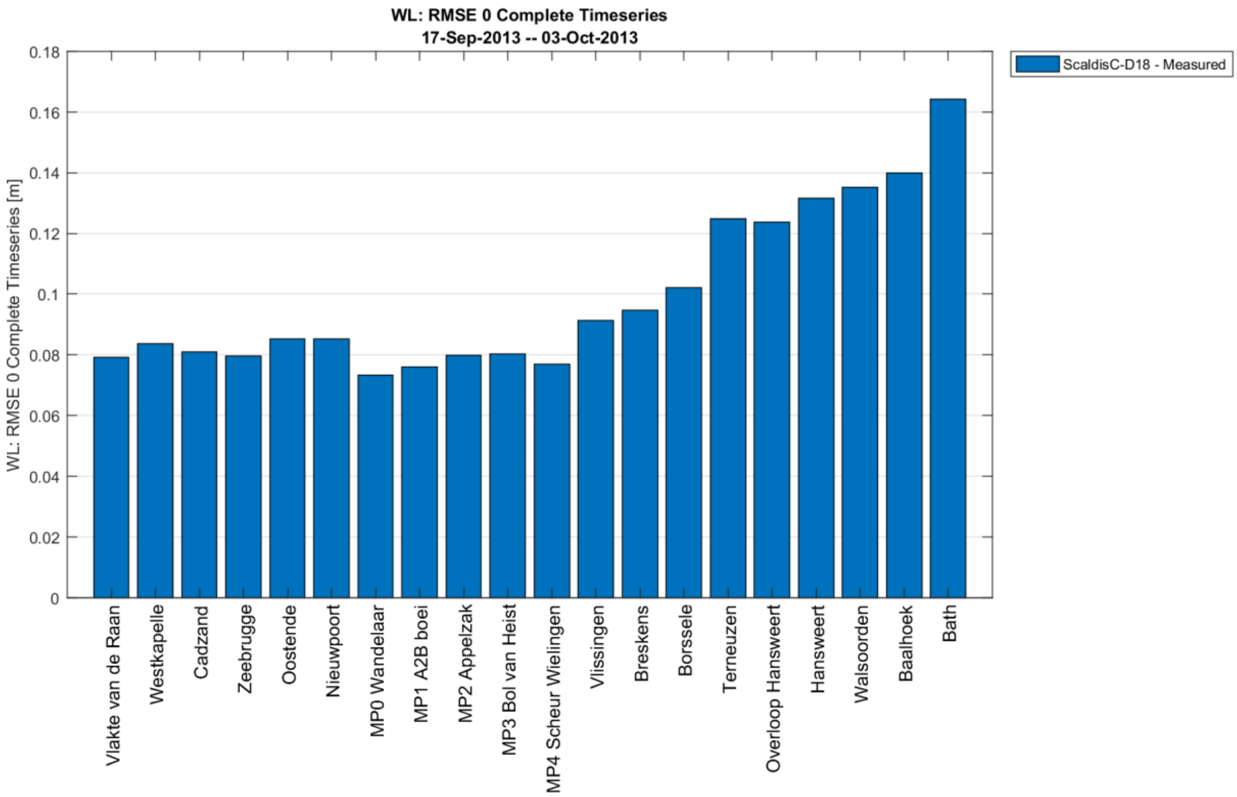

The amplitude of the most important harmonic constituents of the tide, i.e. the M2 and the S2 constituents, as predicted by Scaldis-Coast at the considered stations are plotted against the measured ones, and they are shown in Figure 39. Obviously, the M2 constituent presents the highest amplitude, contributing the most (of all the other constituents) in the determination of the tidal amplitude. In general Figure 39 shows that the numerical predictions agree very well with the values resulting from the measurements. For both M2 and S2 constituents, the agreement is better for the coastal stations than for the stations in Western Scheldt.

The comparison between the numerical and the measured phase of the harmonic constituents M2 and S2 constituents for all the considered stations is presented in Figure 40. The behaviour of the numerically predicted M2 phase is similar to that of the M2 amplitude, i.e. very good agreement at North Sea stations and less good for the Western Scheldt ones. The S2 phase predicted by the model is in general in very good agreement with the measured one for all the stations in the domain.

Figure 39 – Comparison between the numerical and the measured amplitude of the M2 tidal constituent (top figure) and the S2 constituent (bottom figure) at the considered locations.

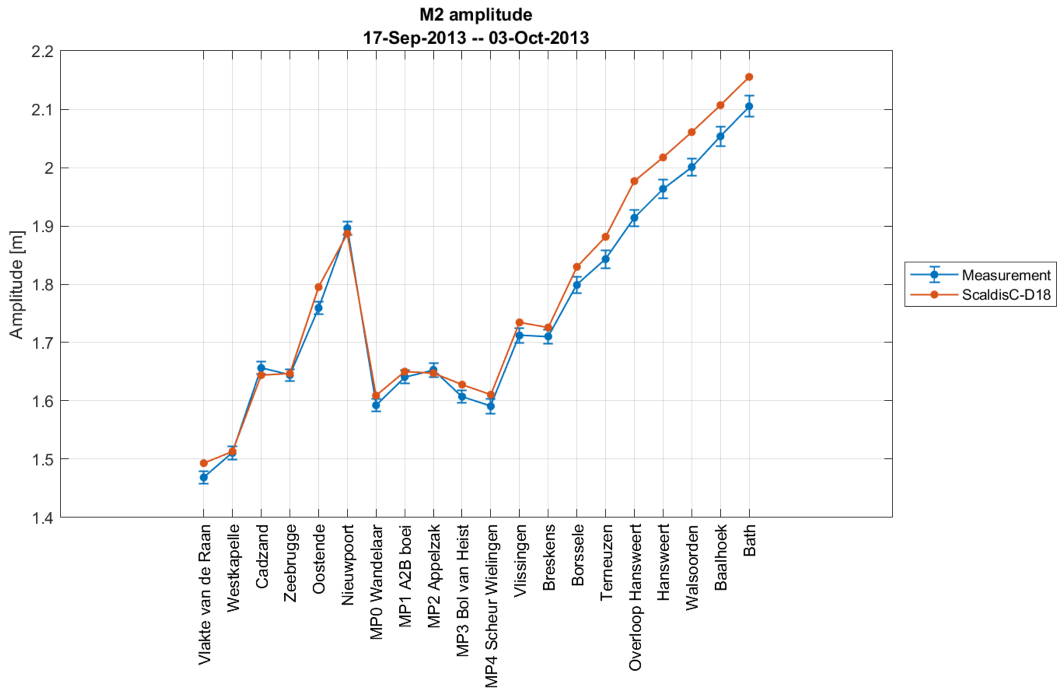

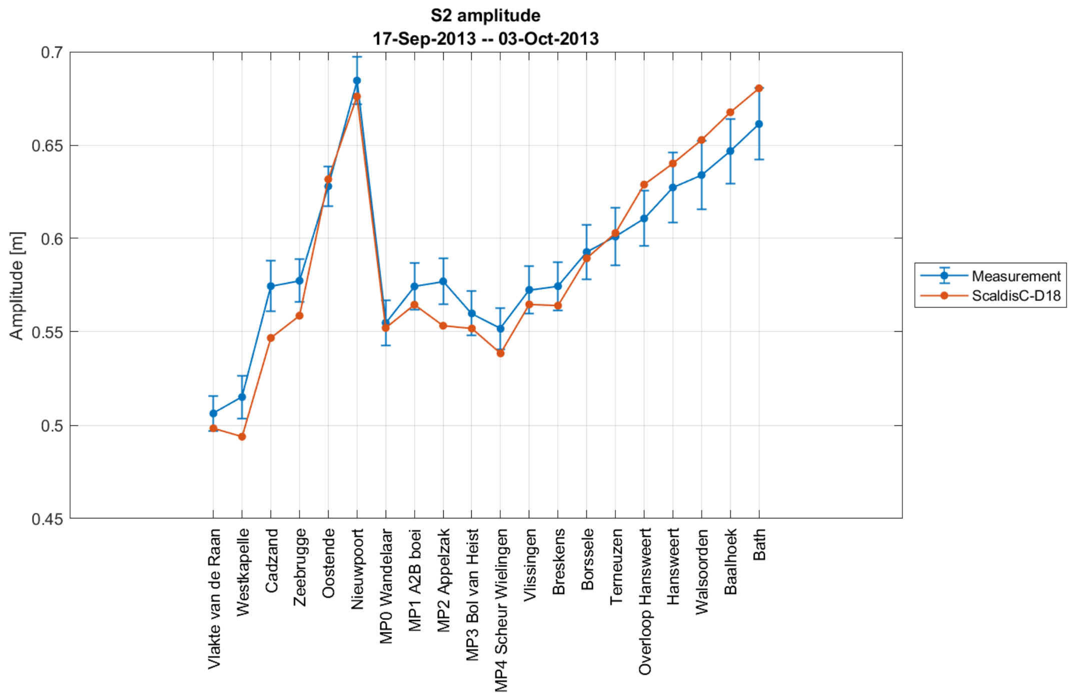

Figure 40 – Comparison between the numerical and the measured amplitude of the M2 tidal phase (top figure) and the S2 phase (bottom figure) at the considered locations.

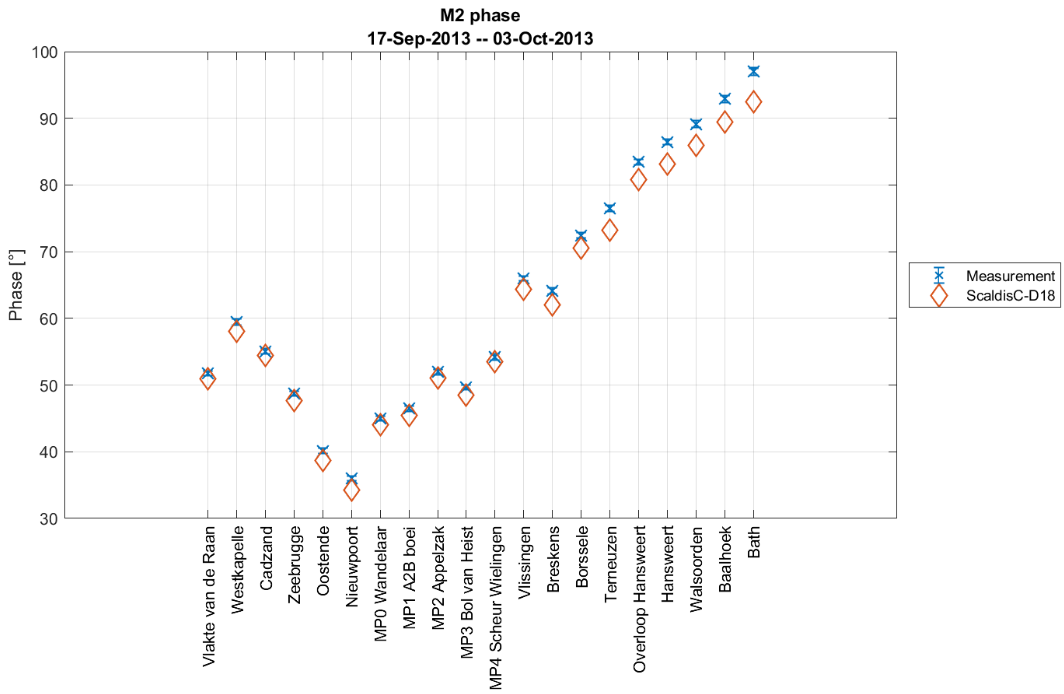

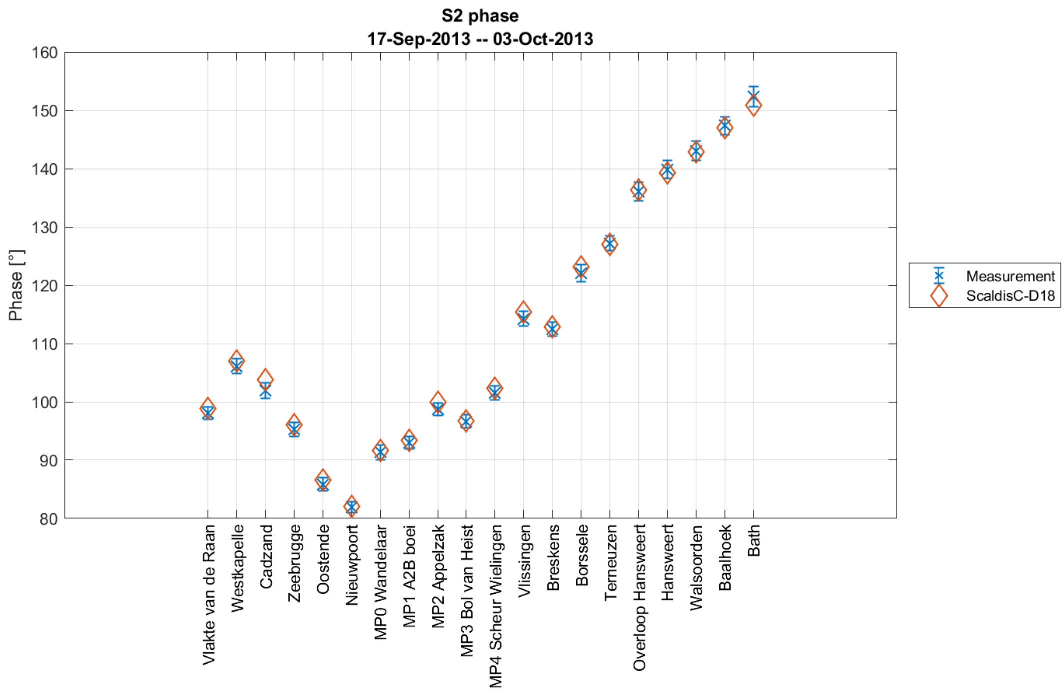

VIMM version TELEMAC
(c)Waterbouwkundig Laboratorium 2018

Velocities along transects

The depth-averaged velocities predicted by Scaldis-Coast are compared to depth-averaged velocities from ADCP (sailed) measurements, which were conducted during 13-hour campaigns at several transects mentioned in Table 5 of section 3.1.2). The calculated error statistics, i.e. the RMSE of velocity magnitude and the RMAE (Relative Mean Absolute Error), are utilized for the model qualification as shown in Table 11 and Table 12. The definition of RMAE and of all the other statistical parameters utilized for the validation of the model are given in Appendix 2. Note that the RMAE includes both the magnitude and direction errors. It is used as a qualification parameter in this study, following the work that has been done by Sutherland *et al.* (2004). On the other hand, the RMSE is sorted using a palette of different colours with an interval of 0.1 m/s, for a clearer representation of the deviation between the predictions and the measurements.

Table 11 – Model qualification based on RMSE of magnitude.

Model qualification	RMSE [m/s]
	<0.1
	0.1-0.2
	0.2-0.3
	>0.3
	-

Table 12 – Model qualification based on RMAE (Sutherland *et al.*, 2004).

Model qualification		RMAE [-]
Excellent		<0.2
Good		0.2-0.4
Reasonable/fair		0.4-0.7
Poor		0.7-1.0
Bad		>1.0
Not Applicable		-

The RMSE and the RMAE parameters for the (13-hour) time series of velocities along the considered ADCP transects, i.e. 4 transects in the North Sea and 7 transects in The Western Scheldt (see Figure 24), are presented in Table 13. It is found that the model performs good for the majority of the considered transects. Looking at each transect separately, the model is better in predicting the velocity field in the North Sea than in the Western Scheldt, even though the average RMAE parameters for the two areas are the same. This is because an increased RMAE value is calculated at the transect in the entrance of Zeebrugge harbour, where in general low velocities and recirculation areas are observed. Currently, the capturing of the flow dynamics at the entrance or in the Zeebrugge harbour is out of scope for the Scaldis-Coast model. Note also that the average RMSE for the North Sea stations is considerably lower than that of the Western Scheldt stations.

In Figure 41 and Figure 42, snapshots of the numerically predicted velocity field and the measured velocities along the transects ‘Pas van het Zand’ and ‘R7 Everingen’ during maximum flood and maximum ebb flow, are shown respectively. There is also shown a comparison between the magnitude and the direction of instantaneous velocities along the aforementioned transects. For the ‘Pas van het Zand’ transect a small underestimation of the maximum ebb flow velocity is observed, but the velocity magnitude and direction is well predicted for the flood phase. The corresponding results for ‘R7 Everingen’ transect are reasonably good for both tidal phases.

Table 13 – RMSE and RMAE quality parameters for the 13-hour time series of velocities along the considered ADCP sailed transects.

ADCP transect	RMSE Magnitude [m/s]	RMAE [-]
North Sea		
Zeebrugge entrance (Aug)	0.13	0.78
ZB Pas van het Zand	0.18	0.32
ZB Wiel	0.10	0.16
ZB Scheur	0.09	0.19
AVERAGE	**0.13**	**0.36**
Western Scheldt		
R7 Everingen	0.16	0.35
R7 Terneuzen	0.18	0.35
R6 Middelgat	0.19	0.37
R6 Gat van Ossenisse	0.17	0.28
Waarde (Sep)	0.16	0.47
R5 Schaar van Waarde	0.13	0.29
R5 Zuidergat	0.20	0.36
AVERAGE	**0.17**	**0.35**

Figure 41 – Snapshots of the numerically predicted velocity field (red vectors) and the measured velocities along transect 'Pas van het Zand' (black vectors) during maximum flood (left figure) and maximum ebb flow (right figure).
Figures below show the comparison between the magnitude and the direction of instantaneous velocities along the transect for the same instant.

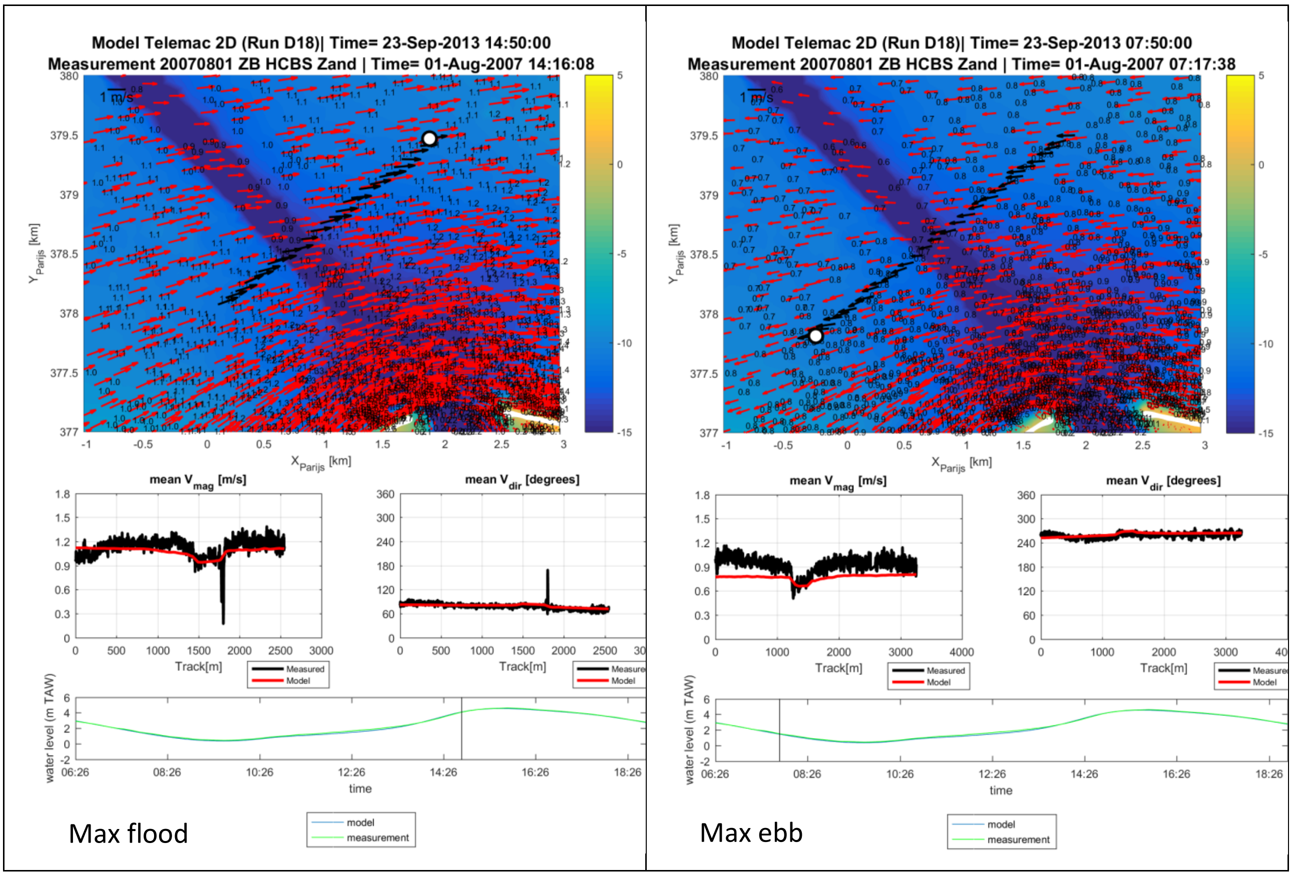

Figure 42 – Snapshots of the numerically predicted velocity field (red vectors) and the measured velocities along transect 'R7 Everingen' (black vectors) during maximum flood (left figure) and maximum ebb flow (right figure).
Figures below show the comparison between the magnitude and the direction of instantaneous velocities along the transect for the same instant.

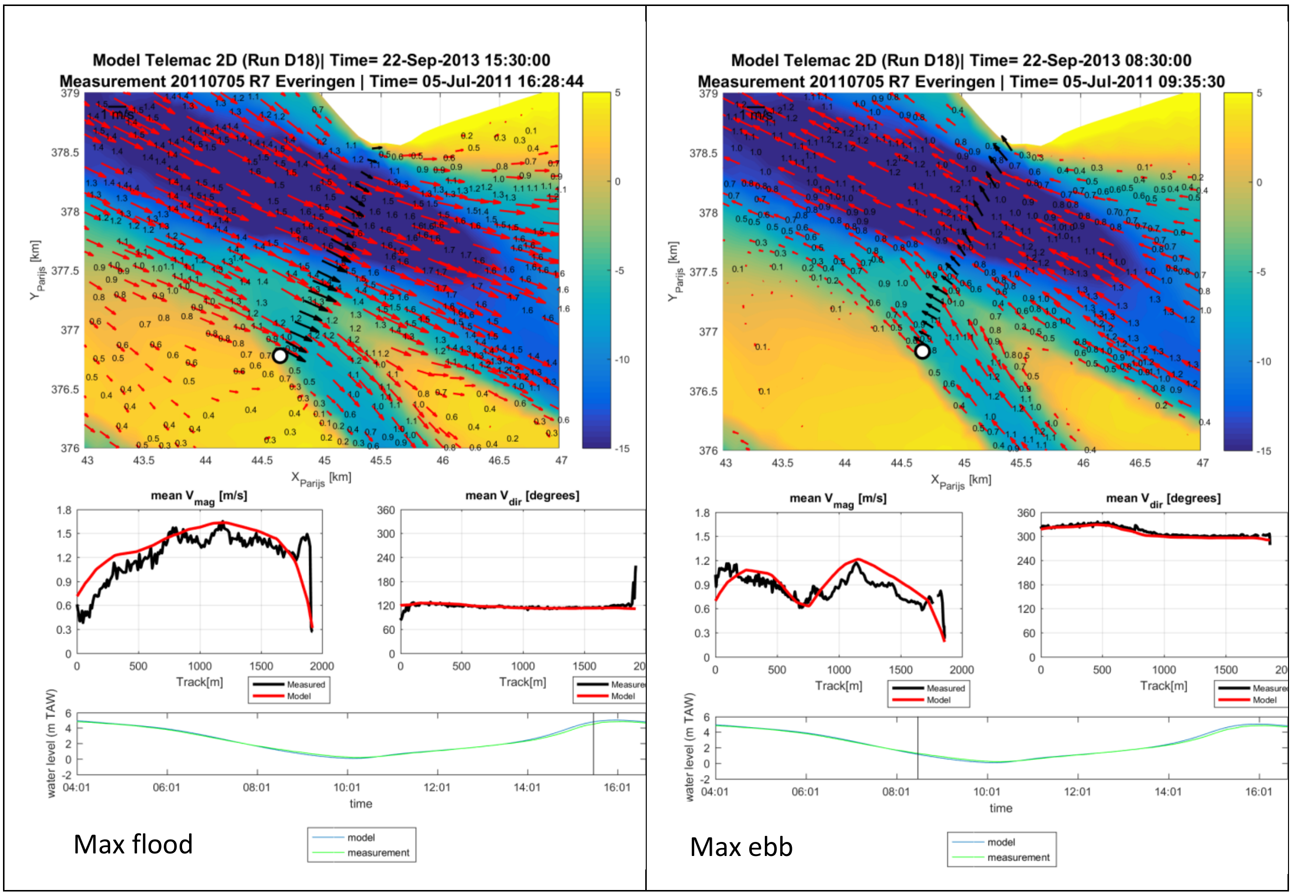

The reasonable agreement among the numerically predicted maximum velocity magnitudes and directions and the corresponding measured ones at the navigational channels of Zeebrugge harbour can also be observed in Figure 43 and Figure 44, which correspond to transects 'Scheur' and 'Wiel', respectively.

Figure 43 – Comparison between the numerically predicted magnitude and direction of instantaneous velocities (red lines) and the corresponding measured ones (black lines) along the transect 'Scheur' during maximum flood [19/09/2013 12:00] (left figure) and maximum ebb flow [19/09/2013 06:00] (right figure).

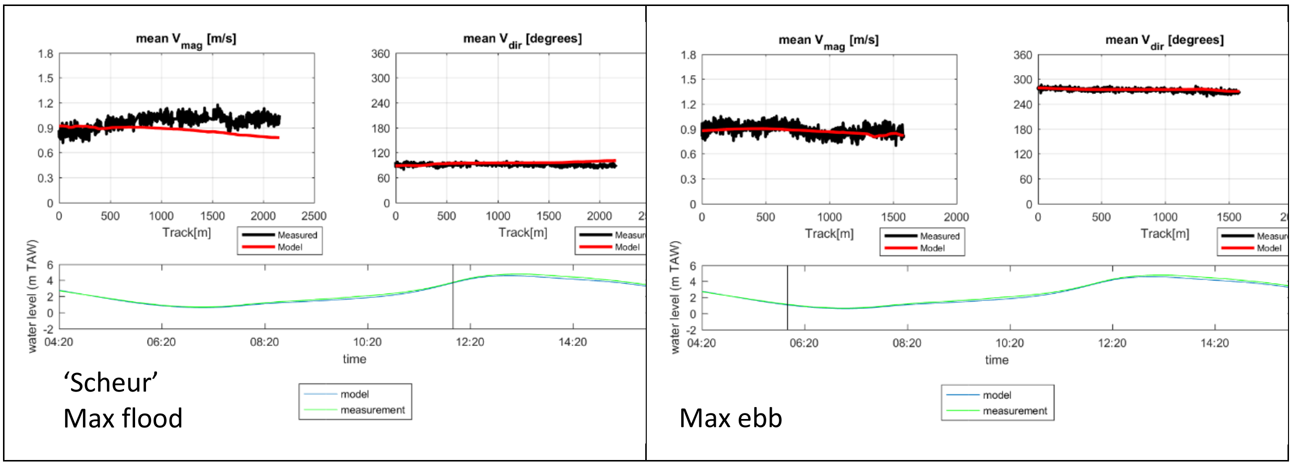

Figure 44 – Comparison between the numerically predicted magnitude and direction of instantaneous velocities (red lines) and the corresponding measured ones (black lines) along the transect 'Wiel' during maximum flood [23/09/2013 15:20] (left figure) and maximum ebb flow [23/09/2013 09:10] (right figure).

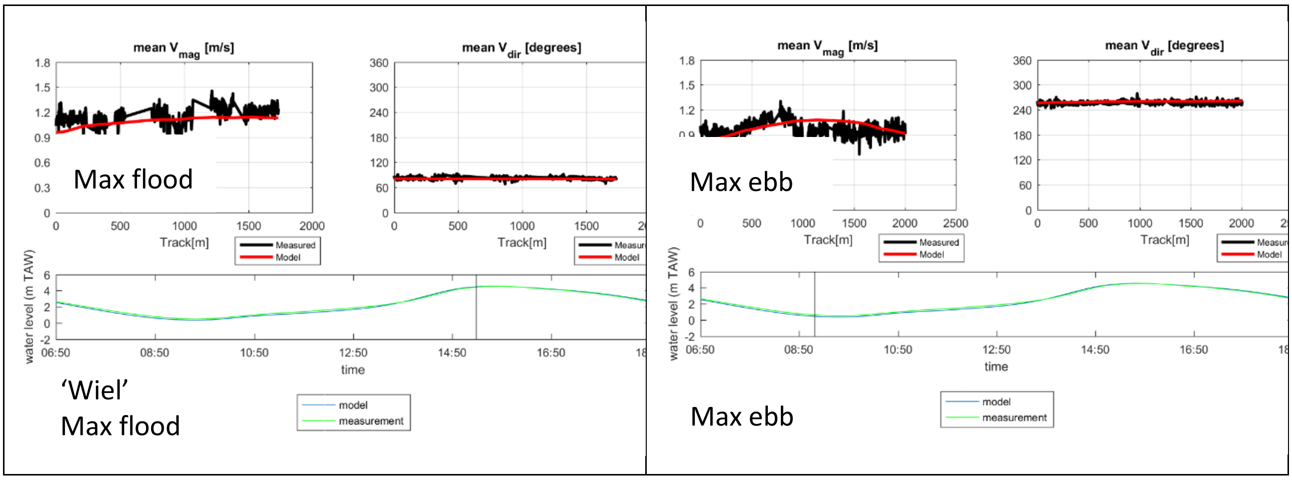

Stationary velocity measurements

The depth-averaged velocities from Scaldis-Coast are compared with the stationary velocity measurements from 2013 (see Table 6) at the locations shown in Figure 25, i.e. at Wandelaar, Bol van Knokke, Bol van Heist, WZ buoy and at Hooge Platen West. Note that the velocities at the three first locations resulted from depth averaging of the 3 middle bins of the current profiler (bins 2, 3 and 4) ranging from 2.5 m to 10 m below the water surface. At WZ buoy, velocity profile is averaged within a distance of about 3 m from the bottom and at Hooge Platen West depth averaged velocities are used for the comparison.

Figure 45 to Figure 47 show the time series of velocity magnitude and direction for a period of 5 days (18-09-2013 and 23-09-2013) at the aforementioned locations. The statistical parameters MAE (Mean Absolute Error) and RMAE of the velocity vector, the bias and the RMSE of the velocity magnitude and direction were calculated in order to evaluate the model accuracy (see Table 14). The Scaldis-Coast performs good in predicting the stationary velocities in the majority of the locations, except for WZ buoy where the predictions are characterized as reasonable. In addition, the RMSE of velocity magnitude is in general up to 0.15 m/s.

Observing the comparison of the modelled and measured velocity time series Figure 45 to Figure 47, it can be noticed that in some stations (e.g. Wandellar and Bol van Knokke) the peak velocity is underestimated. However, it has to be taken into account discrepancies like this can be observed when comparing modelled depth-averaged velocities with stationary velocity measurements. In addition to this, this kind of comparison can be challenging because the point velocity is very sensitive to the local bathymetry, which therefore requires fine mesh, good quality of bathymetry and accurate representation of the location in the model.

Figure 45 – Magnitude and direction of the measured and modelled velocity time series at Wandelaar (top figure) and at Bol van Heist (bottom figure). Measured velocities at both stations come from averaging from 2.5 m to 10 m below water surface.

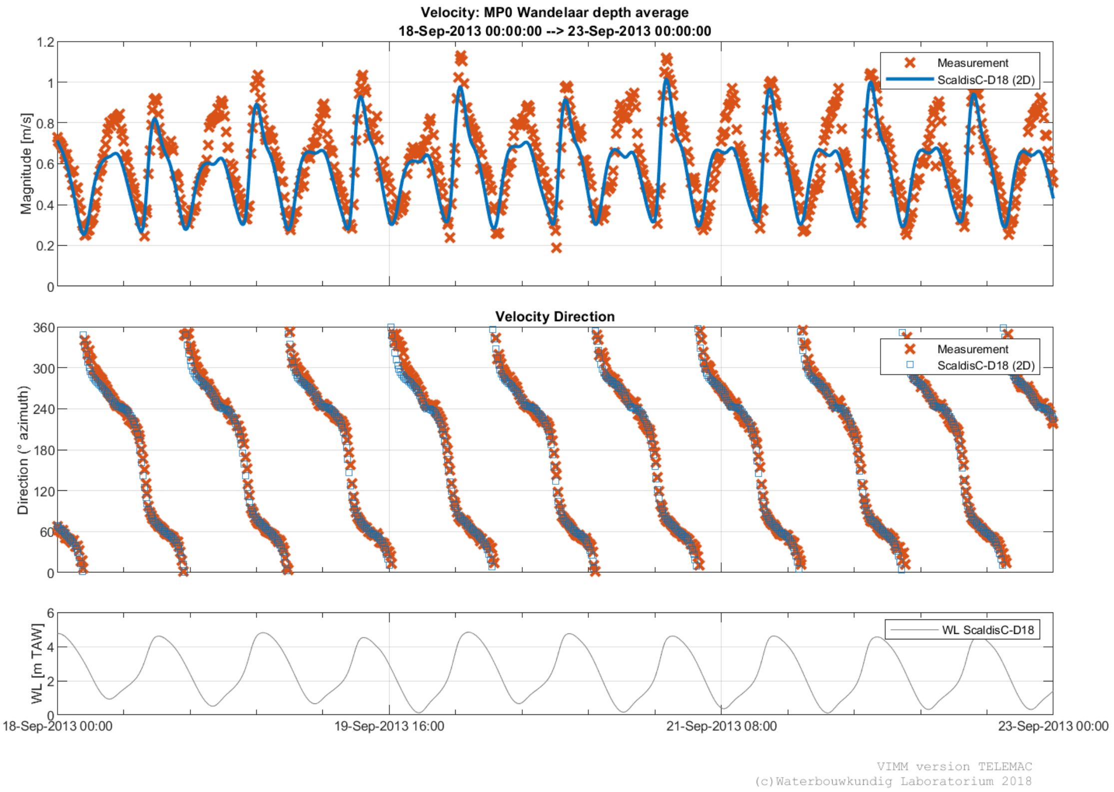

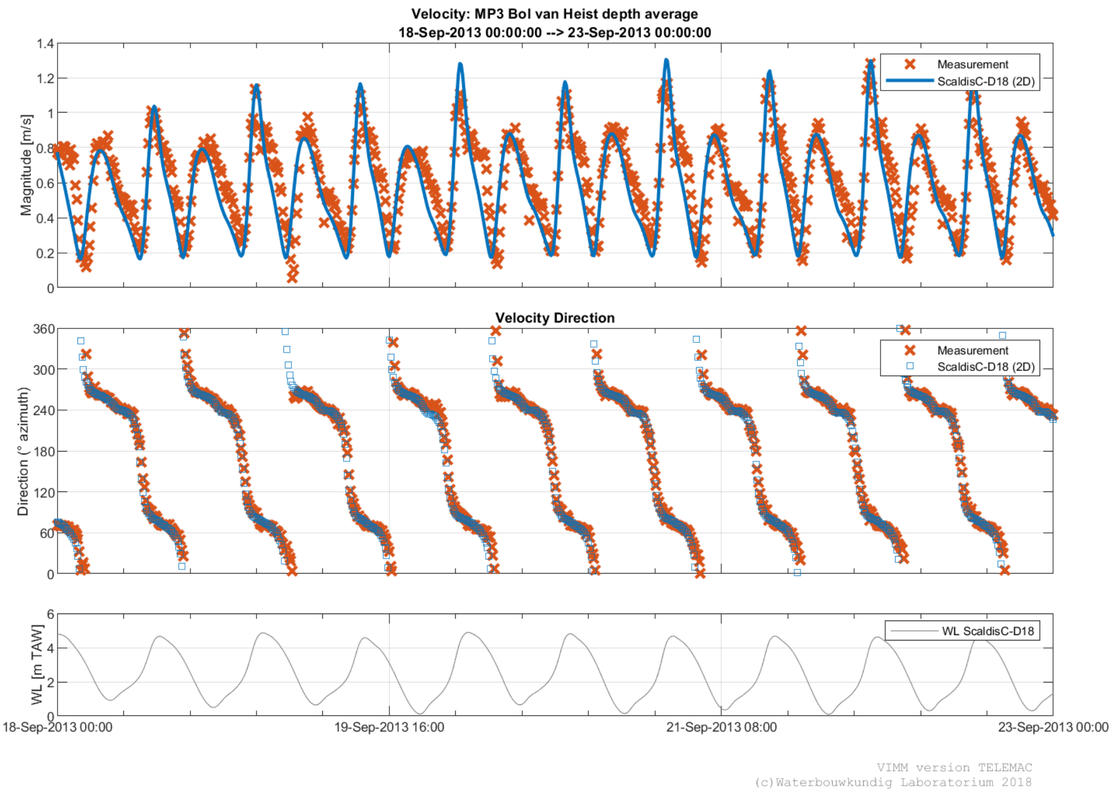

Figure 46 – Magnitude and direction of the measured and modelled velocity time series at Bol van Knokke (top figure) and at WZ buoy (bottom figure).
Bol van Knokke: Depth-averaged measurements from 2.5 m to 10 m below water surface;
WZ buoy: profile-averaging up to 3.0 m from the bottom.

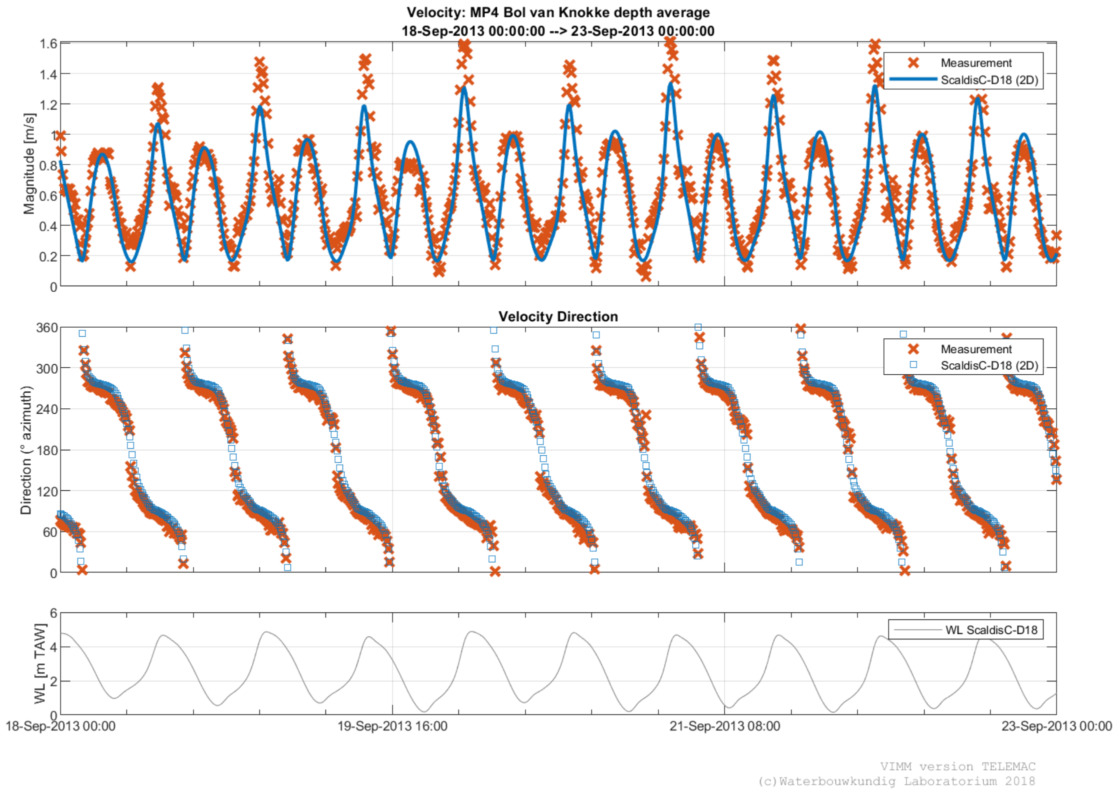

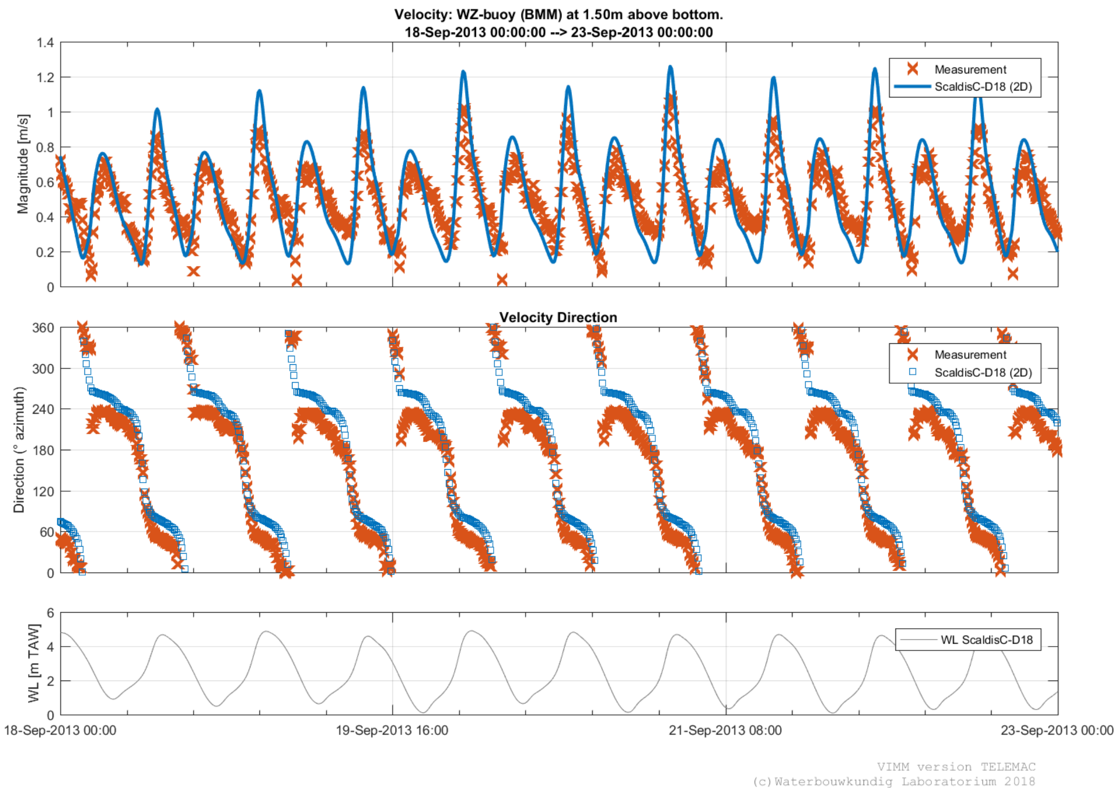

Figure 47 – Magnitude and direction of the measured (depth-averaged) and modelled velocity time series at HPW MP101 (top figure) and at HPW MP205 (bottom figure).

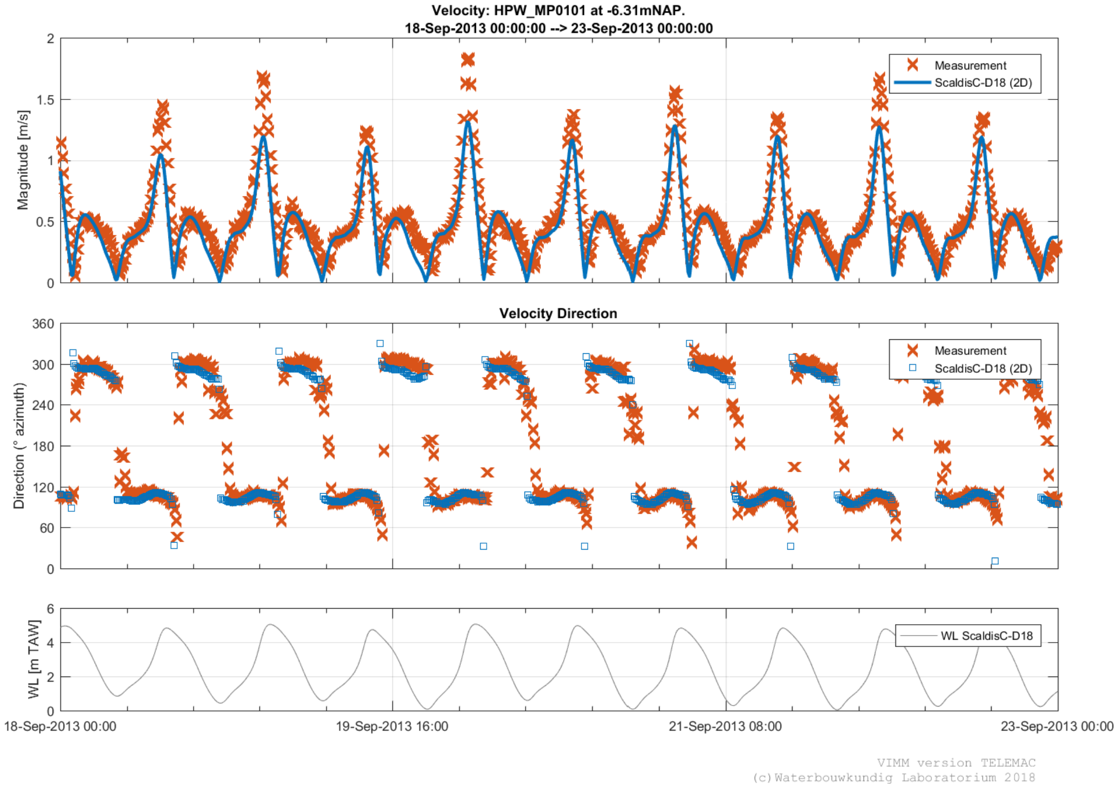

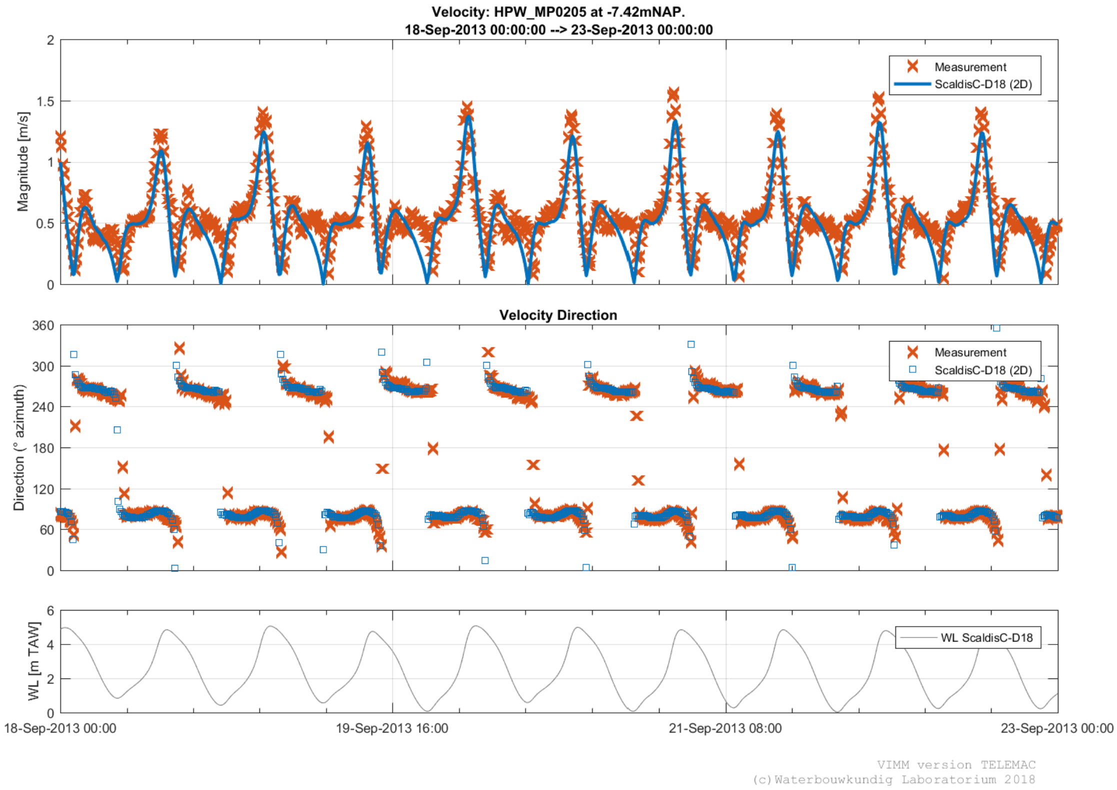

Table 14 – Statistical parameters for the stationary velocities.
Color scaling indicates the quality of the numerical results according to Table 11 and Table 12.

Location	Analysis vector		Magnitude		Direction	
	MAE TS [m/s]	RMAE TS [-]	BIAS TS [m/s]	RMSE TS [m/s]	BIAS TS [°]	RMSE TS [°]
MP0 Wandelaar	0.11	0.22	-0.03	0.10	-6.4	12.9
MP3 Bol van Heist	0.13	0.25	-0.02	0.12	-11.2	20.7
MP4 Bol van Knokke	0.11	0.21	-0.03	0.10	3.8	12.7
WZ-buoy (BMM)	0.22	0.55	0.04	0.12	21.4	28.4
HPW_MP0101	0.17	0.32	-0.07	0.16	-14.0	44.3
HPW_MP0205	0.14	0.25	-0.05	0.15	-5.4	42.8
AVERAGE	0.15	0.30	-0.03	0.13	-2.0	27.0

3.2.8 Model validation for simulation period 2

The statistical analysis of the results presented in this section is performed for the period from 08/08/2014 to 24/08/2014 (a full spring-neap tidal cycle).

Water levels

The main statistical parameters (Bias, RMSE and RMSE0) of the water level time series at selected North sea and Western Scheldt stations are presented in Table 15. The total RMSE increases from 11 cm in the North Sea to 15 cm in the Western Scheldt. The absolute value of the bias of water levels is equal or lower than 10 cm at all the selected stations. In the last column of Table 15, the RMSE0 values from the analysis of the year 2013 (presented in the previous section), are shown for direct comparison with the corresponding of 2014 simulation. It is observed that RMSE0 values of 2014 simulation are increased 2 to 3 cm at most of the stations. Nevertheless, the performance of is still good especially at the coastal stations. Figure 38 shows the RMSE0 of the complete water level time series (last column of Table 10) for all the considered stations.

Table 15 – Main statistical parameters for the water level time series (2014) for North sea and Western Scheldt stations.

Station	Complete Time Series (16 days)			
	BIAS TS	RMSE TS	RMSE_0 TS	RMSE_0 TS (2013)
	[m]	[m]	[m]	[m]
North Sea				
Vlakte van de Raan	0.02	0.11	0.11	0.08
Westkapelle	0.03	0.12	0.11	0.08
Cadzand	0.06	0.12	0.11	0.08
Zeebrugge	-0.05	0.12	0.11	0.08
Oostende	0.00	0.12	0.12	0.09
Nieuwpoort	0.04	0.12	0.12	0.09
MP0 Wandelaar	0.09	0.14	0.11	0.07
MP1 A2B boei	0.03	0.11	0.11	0.08
MP3 Bol van Heist	0.08	0.14	0.11	0.08
MP4 Scheur Wielingen	0.02	0.11	0.11	0.08
Total	**0.03**	**0.12**	**0.11**	**0.08**
Western Scheldt				
Vlissingen	0.02	0.12	0.12	0.09
Breskens	0.02	0.12	0.12	0.09
Borssele	0.00	0.13	0.13	0.10
Terneuzen	-0.03	0.14	0.14	0.12
Overloop Hansweert	-0.07	0.16	0.15	0.12
Hansweert	-0.06	0.17	0.15	0.13
Walsoorden	-0.07	0.17	0.16	0.14
Baalhoek	-0.07	0.18	0.16	0.14
Bath	-0.06	0.19	0.18	0.16
Total	**-0.04**	**0.15**	**0.15**	**0.12**

Figure 48 – RMSE0 in the complete water level time-series of 2014 simulation (16 days) between the modelled by Scaldis-Coast and the measured values at the selected stations in the domain.

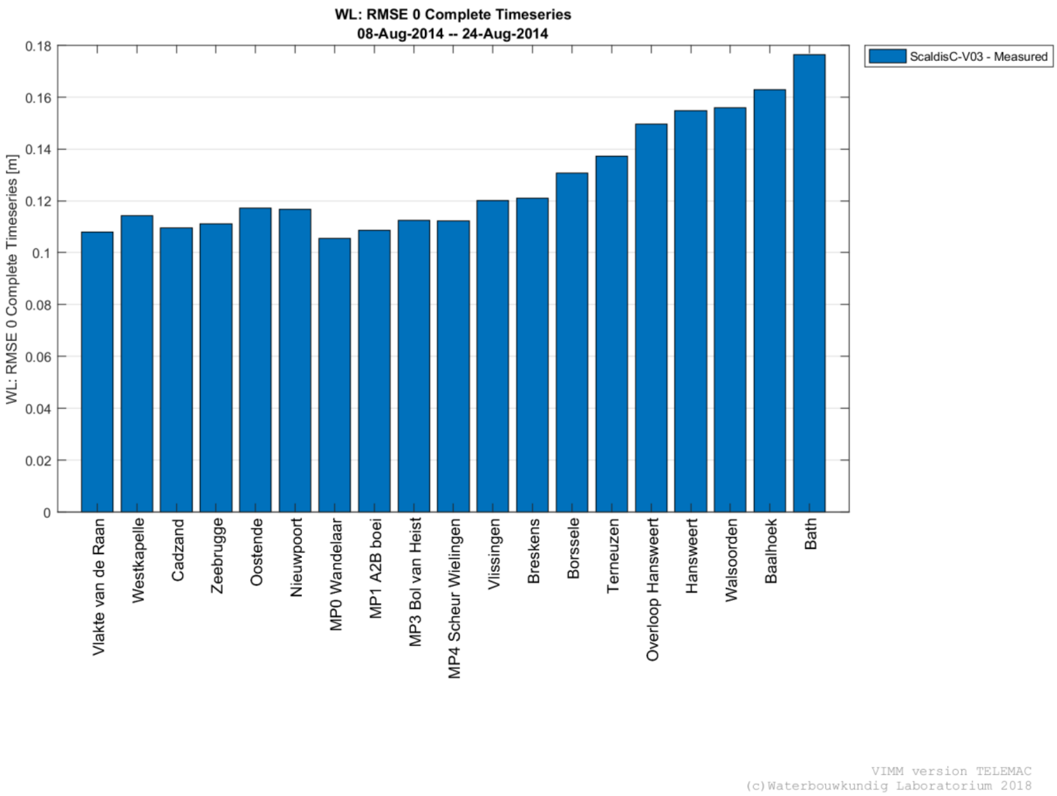

Velocities along transects

The depth-averaged velocities predicted by Scaldis-Coast are compared to depth-averaged velocities from ADCP (sailed) measurements, in the same manner as presented in the previous section for the simulation period of the year 2013. This means that the calculated error statistics, i.e. the RMSE of velocity magnitude and the RMAE are utilized for the model qualification as shown in Table 11 and Table 12.

The RMSE and the RMAE parameters for the (13-hour) time series of velocities along the considered ADCP transects, i.e. 4 transects in the North Sea and 7 transects in The Western Scheldt (see Figure 24), are presented in Table 16. It is found that the model performs good for the majority of the considered transects. Looking at each transect separately, the model is better in predicting the velocity field in the North Sea than in the Western Scheldt, even though the average RMAE parameters for the two areas are almost the same. This is due to the increased RMAE value at the transect in the entrance of Zeebrugge, issue that was discussed previously. Compared to the resulting average RMAE and RMSE values for the simulation period 2013 (see Table 13), the current ones are only slightly increased. The average RMSE for the North Sea stations is considerably lower than that of the Western Scheldt stations. Notice that the simulation time is not identical to the measurement time. The comparison is between two tides that are closely resembling but not the same (comparable tide approach)

Table 16 – Comparison of RMSE and RMAE for the complete time series (2014) of velocities along the considered ADCP transects.

ADCP sailed transect	RMSE Magnitude [m/s]	RMAE [-]
North Sea		
Zeebrugge entrance (Aug)	0.09	0.60
ZB Pas van het Zand	0.21	0.39
ZB Wiel	0.12	0.19
ZB Scheur	0.10	0.22
AVERAGE	**0.13**	**0.35**
Western Scheldt		
R7 Everingen	0.18	0.35
R7 Terneuzen	0.22	0.37
R6 Middelgat	0.19	0.39
R6 Gat van Ossenisse	0.20	0.31
Waarde (Sep)	0.15	0.40
R5 Schaar van Waarde	0.16	0.32
R5 Zuidergat	0.24	0.47
AVERAGE	**0.19**	**0.37**

Stationary velocities

The depth-averaged velocities from Scaldis-Coast are compared with five stationary velocity measurements from 2014 (see Table 6) at the locations shown in Figure 25, (Wandelaar, Bol van Knokke, Bol van Heist, Geul van de Walvisstaart). Note that the velocities at the Wandelaar, Bol van Knokke, Bol van Heist stations resulted from depth averaging of the 3 middle bins of the current profiler (bins 2, 3 and 4) ranging from 2.5 m to 10 m below the water surface. The rest correspond to depth averaged velocities over the whole water column.

Figure 49, Figure 50 and Figure 51 show the time series of velocity magnitude and direction for a period of 9 days (09-08-2014 and 18-08-2014) at the aforementioned locations. The statistical parameters MAE and RMAE of the velocity vector, the bias and the RMSE of the velocity magnitude and direction were used in order to evaluate the model accuracy (see Table 17). The Scaldis-Coast performs good in predicting the stationary velocities in the considered locations. In addition, the RMSE of velocity magnitude is around 0.10 m/s for three locations and around 0.20 m/s for the other two. However, the peak flood velocities seem to be underestimated. Moreover, the measured velocities at Wandelaar station during ebb phase (see Figure 50) present unusual behaviour (very low peak velocities). It is conjectured that the either the local wind conditions or other unwanted factors affected the measurements at those periods. As expected this fact has a negative impact on the comparison through the statistical parameters increasing the value of the error.

Figure 49 – Magnitude and direction of the measured (depth-averaged) and modelled velocity time series at GvW1 (top figure) and at GvW2 (bottom figure).

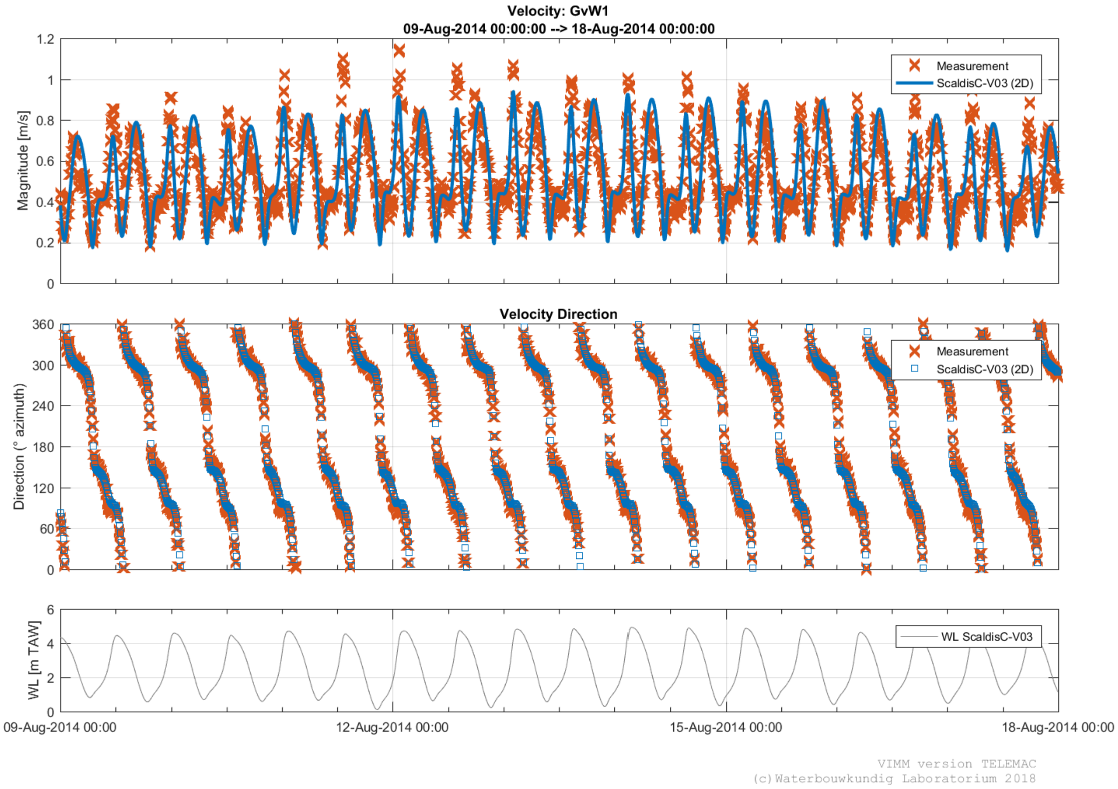

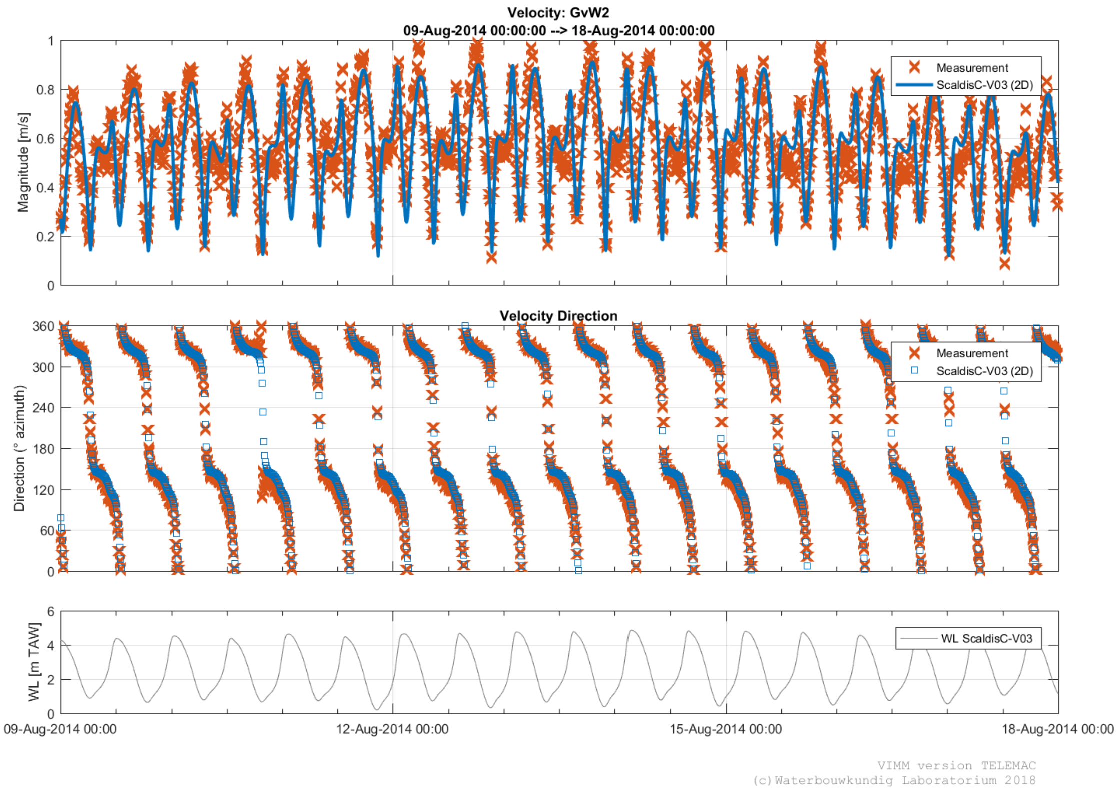

Figure 50 – Magnitude and direction of the measured and modelled velocity time series at Wandelaar (top figure) and at Bol van Heist (bottom figure). Measured velocities at both stations come from averaging from 2.5 m to 10 m below water surface.

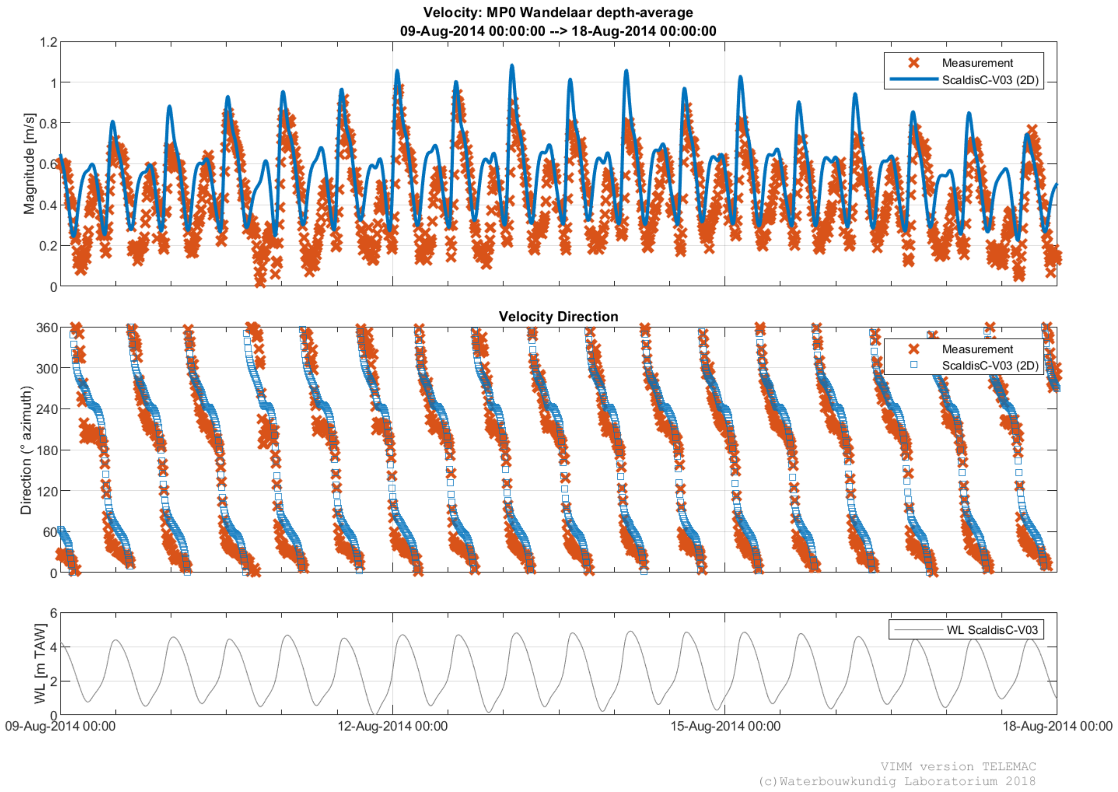

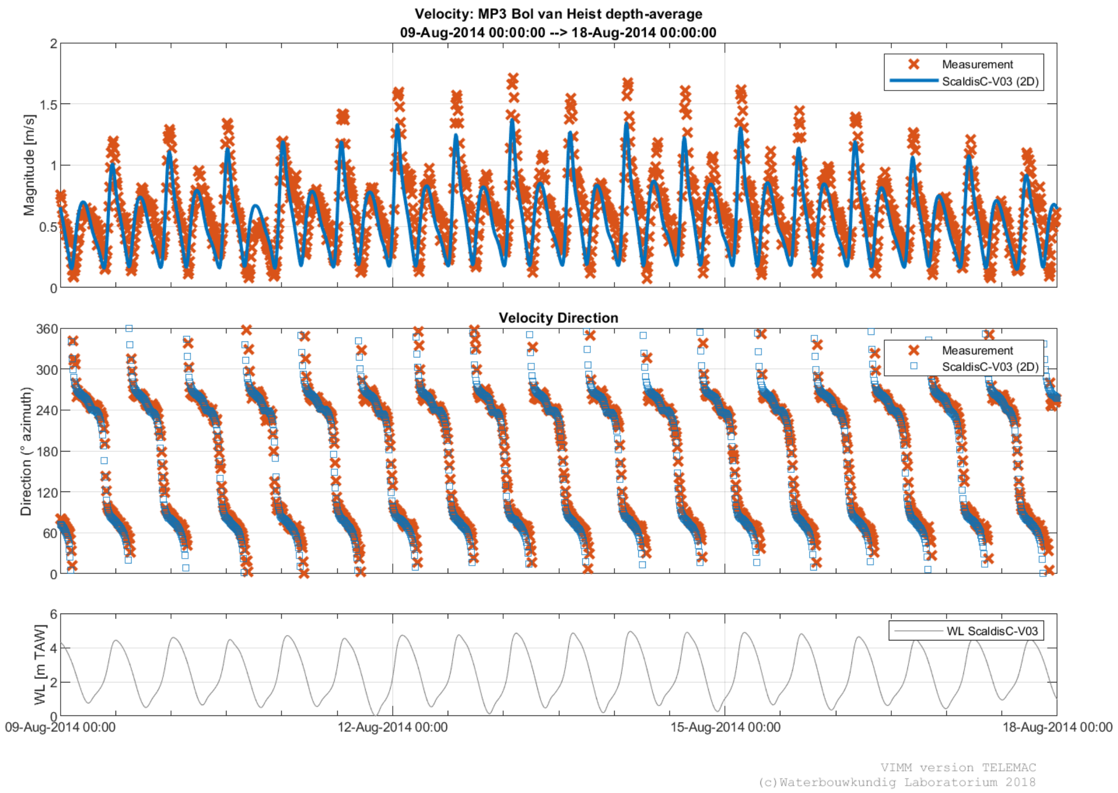

Figure 51 – Magnitude and direction of the measured and modelled velocity time series at Bol van Knokke. Depth-averaged measurements from 2.5 m to 10 m below water surface.

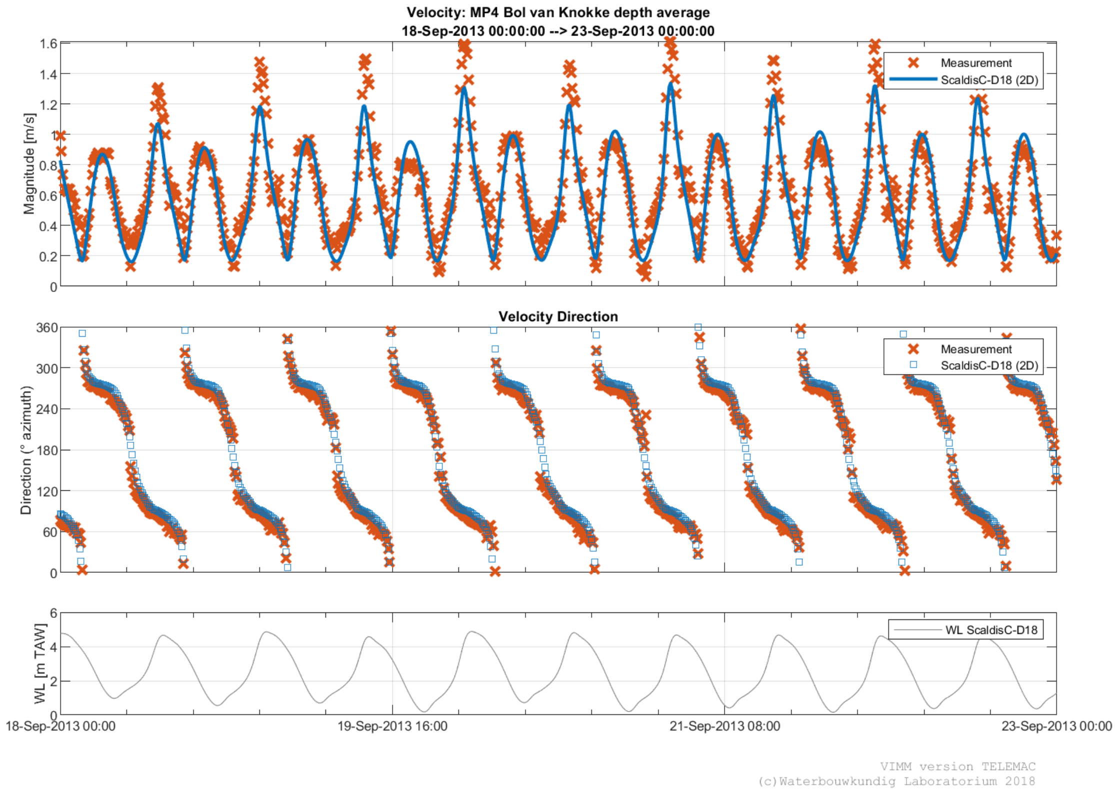

Table 17 – Statistical parameters for the stationary velocities (2014). Color scaling according to Table 11 and Table 12.

Location	Analysis vector		Magnitude		Direction	
	MAE TS [m/s]	RMAE TS [-]	BIAS TS [m/s]	RMSE TS [m/s]	BIAS TS [°]	RMSE TS [°]
Geul van Walvischstaart 1	0.11	0.21	0.00	0.10	1.4	11.0
Geul van Walvischstaart 2	0.10	0.18	0.01	0.08	3.9	12.0
MP0 Wandelaar	0.29	0.69	0.13	0.21	11.5	27.0
MP3 Bol van Heist	0.21	0.34	-0.07	0.19	-13.8	27.0
MP4 Bol van Knokke	0.11	0.19	0.01	0.11	-2.2	11.5
AVERAGE	0.17	0.32	0.02	0.14	0.17	17.7

4 Conclusions

The results from the simulations performed for the calibration and validation of the Scaldis-Coast hydrodynamic TELEMAC2D model were presented.

The calibration of the model was based on sensitivity tests for the tuning of the bed roughness coefficient (Manning's law). The selected bed roughness distribution is a compilation of different values, i.e., a constant coefficient equal to 0.022 $m^{1/3}/s$ in the main (coastal) part of the domain, decreased values downstream of the Western Scheldt and in the Low Sea Scheldt (reduces to values equal to 0.012 $m^{1/3}/s$) and an increased value at the upstream schematized part of the model (0.04 $m^{1/3}/s$).

The model was validated against measured water levels, stationary velocities and velocities along transects (ADCP sailed) at several locations at the coast and the Western Scheldt estuary. Two simulations periods were selected for the validation of the model, i.e. 20 days in September-October 2013 and 20 days in August 2014, based on the analysis of the comparable tides for the available ADCP measurements and on the availability of stationary velocity measurements at the North Sea.

The qualification of the model was based on calculated error statistics, such as the unbiased RMSE of the water level, the RMSE of velocity magnitude and the RMAE (Relative Mean Absolute Error) of the velocity vector. The performance of Scaldis-Coast is found to be good at the Belgian coast but also in The Western Scheldt. The Scaldis-Coast performs good in predicting the stationary velocities in the considered locations, presenting RMSE of velocity magnitude is in general around 0.15 m/s. However, the peak flood velocities seem to be underestimated in some of the considered locations.

The final version of the Scaldis-Coast TELEMAC2D hydrodynamic model is archived in the Flanders Haudraulics Research SVN repository:

https://wl-subversion.vlaanderen.be/!/#repoSpNumMod/view/head/TELEMAC/Scaldis-Kust/15_068%20Complex%20Model%20Kustvisie%202021/1_2D_HYDRODYNAMICS

References

ANSYS inc. (2015). Introduction to ANSYS Meshing: Mesh quality & advanced topics, Lecture7.

De Maerschalck, B.; Renders, D.; Vanlede, J.; Gourgue, O.; Willems, M.; Verwaest, T.; Mostaert, F. (2016). Modellering Vlaamse Baaien: deelrapport 1. Hydrodynamische modellering scenario's Oostkust. Versie 5.0. *WL Rapporten*, 15_068_1. Waterbouwkundig Laboratorium/Afdeling Maritieme Toegang: Antwerpen

Geuzaine, C.; Remacle, J.-F. (2009). Gmsh: a three-dimensional finite element mesh generator with built-in pre-and post-processing facilities. *Int. J. Numer. Methods Eng. 79(11)*. ISBN 1097-0207 *0*: 1309–1331. doi:10.1002/nme.2579

Gourgue, O.; Vanlede, J.; Chen, M. (2015). Pre- and post-processing unstructured grids for estuary and coastal sea models with the PUG Matlab toolbox, ***in***: (2015). *INTERCOH2015: 13th International Conference on Cohesive Sediment Transport Processes. Leuven, Belgium, 7-11 September 2015*. *VLIZ Special Publication*, 74. Flanders Marine Institute (VLIZ): Ostend. ISBN 978-94-920430-8-5. pp.170–171

IMDC. (2015). Analyse impact havenuitbreiding Zeebrugge op baggerwerken vaargeulen Noordzee en voorhaven Zeebrugge - Leveren van ondersteunend numeriek scenario- onderzoek, Telemac Zeebrugge model - Set-up, calibration and validation, I/RA/11401/13.072/JUD: Antwerp. 216 pp.

Kolokythas, G.; Fonias, S.; Wang, L.; De Maerschalck, B.; Vanlede, J.; Mostaert, F. (2021). Modelling Belgian Coastal zone and Scheldt mouth area: Sub report 14: Scaldis-Coast model - Model setup and validation of the morphodynamic model. *FHR Series*, 15_068_14. Flanders Hydraulics Research: Antwerp

Kolokythas, G.; Wang, L.; Fonias, S.; De Maerschalck, B.; Vanlede, J.; Mostaert, F. (2018). Modelling Belgian Coastal zone and Scheldt mouth area, Sub report 6 – Progress report 2: Evaluation of numerical modelling tools and model developments. Versie 3.0. *FHR Reports*, 15_068_6. Flanders Hydraulics Research: Anwterp

Smolders, S.; Maximova, T.; Vanlede, J.; Plancke, Y.; Verwaest, T.; Mostaert, F. (2016). Integraal plan Bovenzeeschelde: Subreport 1. SCALDIS: a 3D Hydrodynamic model for the Scheldt Estuary. *WL Rapporten*, 13_131. Flanders Hydraulics Research: Antwerp

Appendix 1 Bringing TELEMAC and Gmsh meshing tool closer

Generally, the TELEMAC-MASCARET model suite is used in combination with in a basic triangular mesh generator called Blue Kenue. However, in the current project a more advanced and flexible mesh generator Gmsh developed by Geuzaine & Remacle (2009) was adopted to construct the model grid.

One of the main advantages of Gmsh is the accurate specification of the target element size based on different conditions such as the local bathymetry, the bathymetry gradient, the distance from specified boundary lines, etc.. In addition to this, the possibility to run Gmsh using a batch file makes it proper for running morphodynamic simulations on an adaptive computational grid. On the other hand, it cannot create a mesh to be used directly in a TELEMAC simulation, therefore some effort has to be put to bring this two software products closer. At Flanders Hydraulics Research a Matlab toolbox[3] has been developed to make Gmsh compatible to TELEMAC (Gourgue *et al.*, 2015).

This chapter is divided in two main parts: first the procedure of the mesh construction of the Zeebrugge (ZB) TELEMAC model (De Maerschalck *et al.* 2016) is presented step-by-step and then the preparation of the TELEMAC input files, i.e. the geometry (SLF) and the boundary conditions (CLI) files, follows. Detailed presentation of GMSH capabilities (even though incomplete), can be found on the web (gmsh.info) and in Gourgue *et al.* (2015). The latter contains an application for the grid construction of a continental shelf model. Gmsh software can be downloaded from gmsh.info for free. For this exercise version 3.0.0 for Windows was utilized.

Mesh construction by Gmsh

Defining the outline of the computational domain

The first step for our grid construction, is to define the outline of the computational domain in Gmsh. In this report, we assume that the outline of the domain is given in a shape file (SHP), so the task is to convert this SHP file into a GEO file which is accepted as input file by Gmsh. This conversion is achieved by use of a suitable Matlab script (***contour_shp_to_geo.m***[4]) developed specially to perform efficiently this task.

Note that the SHP file of the outline can be easily extracted by an existing TELEMAC SLF input file by means of Blue Kenue software: (1) select **BOTTOM** variable, 2) **Tools** → **T3 Mesh** → **Extract Edges**, 3) select **BOTTOM(Edges)** and 4) Save as SHP file.

Editing GEO file in Gmsh

The generated GEO file can be directly introduced (**File** → **Open…**) to the Gmsh software, which starts by simply double-clicking gmsh.exe file (Windows version). In Figure 52, the screen with the domain outline that appears after loading the GEO file is shown. GEO file is an ASCII file, so it can be opened either by any text editor or by Gmsh (in the task pane on the left: **Geometry** → **Edit script**). Note that any action/selection at the GUI will be transcribed to the GEO file and the other way around.

[3] https://wl-subversion.vlaanderen.be/!/#repoSpNumMod/view/head/Matlab/PUG
[4] https://wl-subversion.vlaanderen.be/!/#repoSpNumMod/view/head/Matlab/PUG/Branch/15_068

The generated GEO file contains some elementary entities, i.e. Points and B-Splines (points are connected by B-Splines). In order to be able to create a mesh inside the domain defined by those entities, first we have to connect the lines creating Line Loops and then to define a Plane Surface.

Figure 52 – Gmsh GUI screenshot with the domain outline after introducing the GEO file.

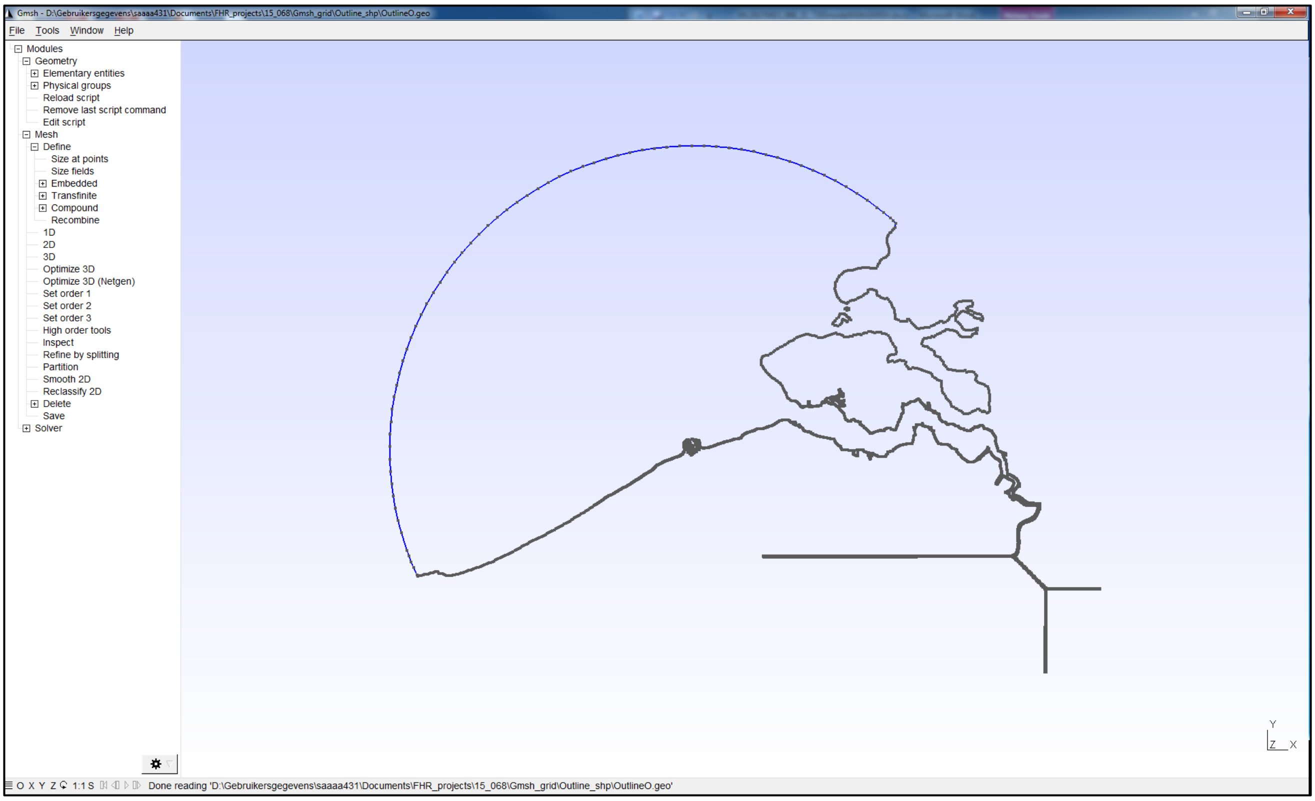

Uniform mesh construction

After finishing with the elementary entities we are ready to create the mesh. For setting the mesh parameters is easier to use the Gmsh GUI. A uniform mesh can be easily created by the commands of the left task pane taking the following actions:

1) Define the grid size
   - **Mesh → Define → Size fields → New → MathEval**
   - Replace what is in the box with the grid size in meters
   - Turn on the **Set as background field** option and click on **Apply** button

2) Create and save the mesh
   - **Mesh → 1D** (wait a bit, having a look at the horizontal bar below the main window)
   - **Mesh → 2D** (wait a bit more.. you can click on the same horizontal bar to see more information)
   - **File → Export…** (*.msh)

A uniform mesh of grid size equal to 1000 m resulting from the procedure above is shown in Figure 53.

Figure 53 – Gmsh GUI screenshot with a uniform mesh of element size equal to 1000 m.

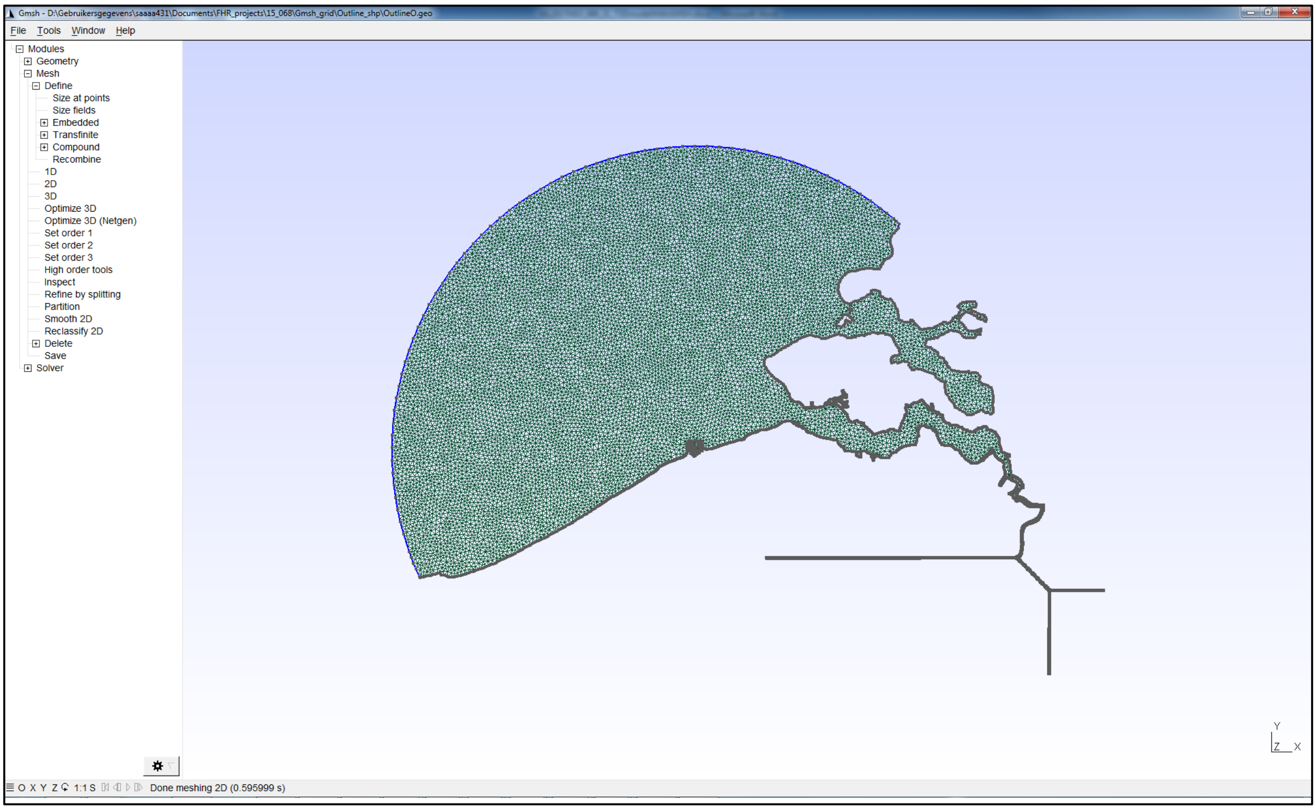

Adaptive mesh construction

Apparently a uniform mesh is not adequate for our morphodynamic simulations, therefore an adaptive mesh refinement has to be performed in order to achieve more accurate predictions close to the shoreline and especially at the areas of interest.

As shown in the previous section, the mesh density is determined by the tab **Size fields** on the left task pane (**Mesh** → **Define** → **Size fields**). After pushing **New** button, 26 options for prescription of the characteristic size of the elements composing a field are provided, as shown in Figure 54. The properties of each field can be seen after selecting it and pressing the **Help** tab (next to **Options** tab). In the present exercise eight (8) options for size prescription were utilized:

1) *MathEval*: A value that defined the uniform mesh size was entered here. It was also multiply used for operations among other fields. In general mathematical expressions can be defined in this field.
2) *Threshold*: This field is always complementary to another field. Two element sizes (Lcmin, Lcmax) and two distances (DistMin, DistMax) have to be prescribed here. Lcmin size will be imposed up to a distance DistMin from an entity and Lcmax beyond the DistMax distance. Between DistMin and DistMax interpolation of the element size is applied.
3) *Attractor*: A list of edges (parts of the outline) and/or node numbers of the outline are introduced in this field. In order to have an effect on the element size it has to be combined with a *Threshold* field, which will be imposed only at the specified by the *Attractor* outline parts.
4) *Structured*: Bathymetric data on a structured grid provided in an input text file (with specific format) are interpolated linearly on the unstructured mesh. This input file is generated by a Matlab script (***Bathymetry_write_gmsh_struct.m***) developed especially for this task. Bathymetry based grid size can be achieved if *Structured* field is combined with a *Threshold* field. In this case the DistMin and DistMax parameters correspond to depths and not to horizontal distances.

5) *Gradient*: This field makes use of the bathymetric data in the *Structured* field in order to calculate the bathymetry gradients. Gradient based grid size can be achieved if *Gradient* field is combined with a *Threshold* field. In this case the DistMin and DistMax parameters correspond to gradients and not to horizontal distances.
6) *Box*: The coordinates (XMax, XMin, YMax, YMin) of a tetrahedron, a value of the grid size inside it (VIn) and a value outside of it (VOut) have to be given. It can be used as part of a *MathEval* expression multiplied by another field in order to impose the size of the second field inside the box (VIn has to be 1 and VOut a very large number).
7) *Restrict*: This field restricts the application of another field to a given list of edges and/or surfaces. To take full advantage of *Restrict* field capabilities, one elliptic arc (center points at Zeebrugge port) and a line at the mouth of Western Scheldt were drawn (see Figure 55). The element size in the sub-surfaces of the domain could be easier defined in this way.
8) *Min*: A list of fields has to be introduced here. The minimum value of the element size from all the selected fields will be selected. Normally this is the last field to define and since the merging of the selected fields is desirable, **Set as background field** option should be turned on.

<u>Attention:</u> Each time you modify one of the fields the **Apply** button has to be clicked in order for these changes to be applied.

After defining the Size Fields, the final step is to create and save the mesh (Figure 56):

- **Mesh → 1D**
- **Mesh → 2D**
- **File → Export…** (*.msh)

Figure 54 – **Size fields** tab after pressing **New** button.

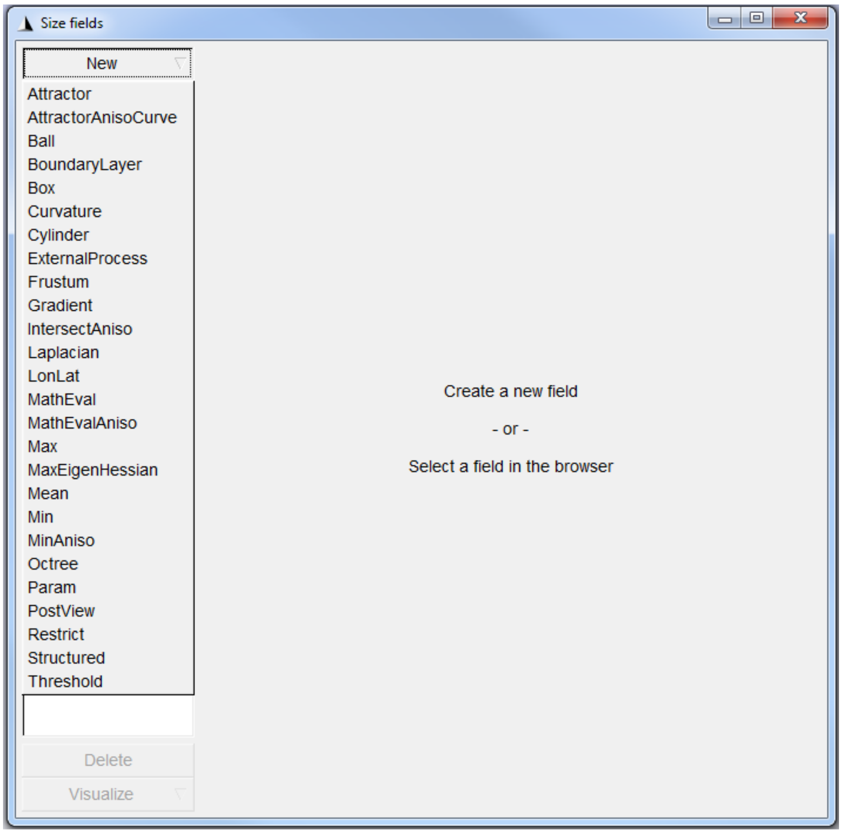

Figure 55 – Division of the computational domain for better determination of the element size.

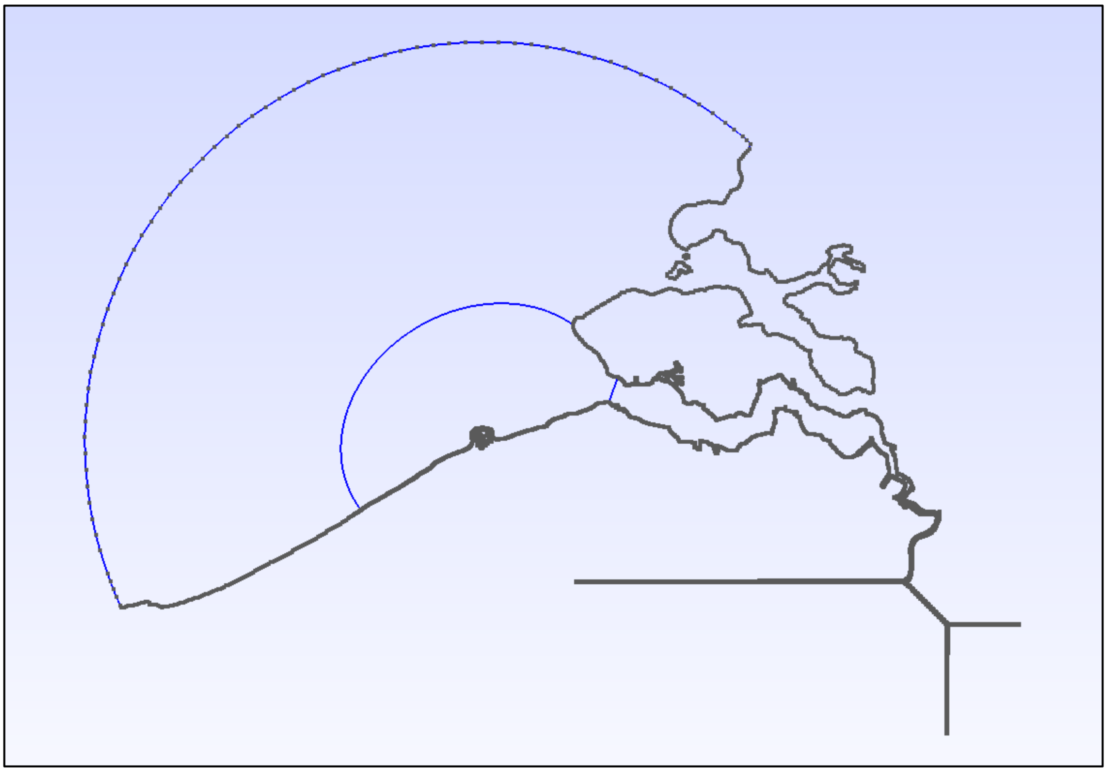

Figure 56 – Adaptive mesh refinement by Gmsh by means of selected Size Fields.

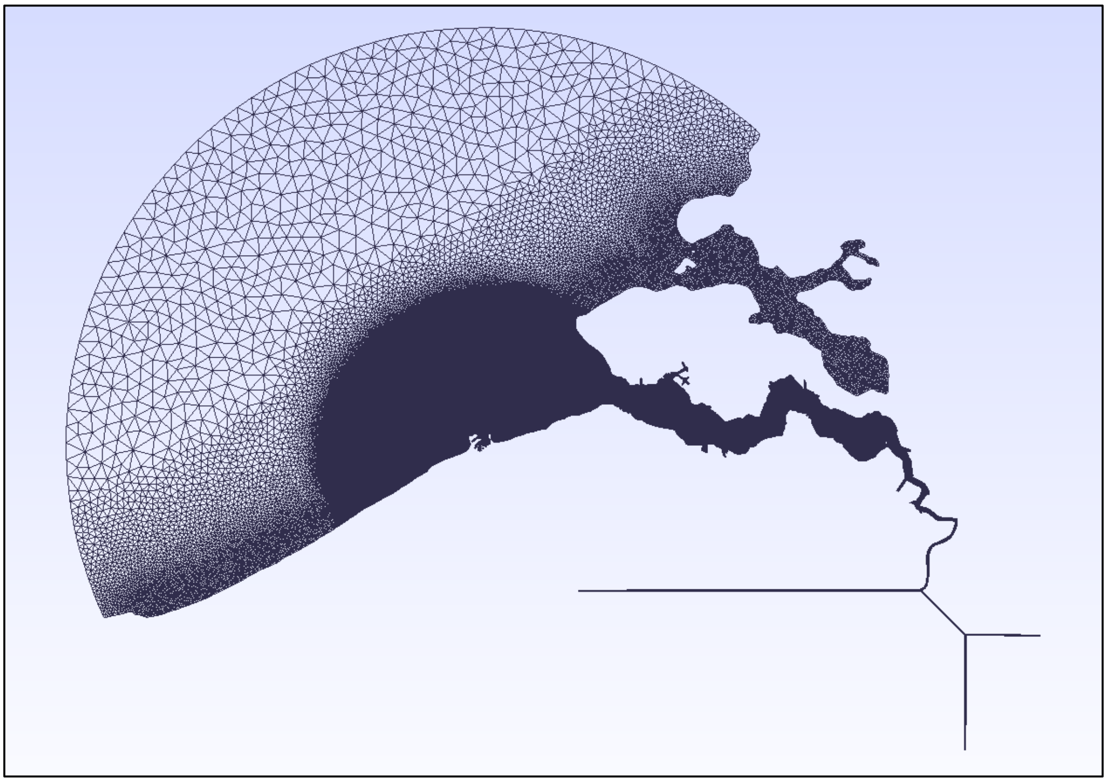

Preparation of TELEMAC input files

In this section the preparation of the necessary input files for a simulation by TELEMAC model, i.e. the geometry (SLF) and boundary conditions (CLI) files, is presented. A typical SLF file for hydrodynamic simulations contains bathymetry and bottom friction data interpolated on the nodes of the computational domain. The CLI file contains information about the type of boundary condition (wall, discharge, water level, etc.) at each node of the domain outline.

Both the aforementioned input files are created by use of the following Matlab script:

telemac_input_files.m

First the bathymetry and the bottom friction data, which in the specific case come from and old SLF file created in Blue Kenue, are interpolated on the mesh (*.msh) file exported by Gmsh. Then the CLI file is written based on the type of the outline segments defined by a *Physical Line ID* in Gmsh.

Sometimes scenarios of coastal interventions have to be simulated. In these cases only local bathymetric data are provided by the client, which have to be incorporated in the computational domain. This local interpolation to an existing SLF file can be done by using the Matlab script:

telemac_input_files_local_interp.m

Attention: In case that the new scenario demands extra modification of the existing grid (as in the case of the dunebelt scenarios) then the generation of the TELEMAC input files has to be done in two steps:

1. Use ***telemac_input_files.m*** to interpolate the original bathymetry (without the interventions) to the modified mesh. For the next step you need the generated SLF file and the modified mesh file (*.msh).
2. Use ***telemac_input_files_local_interp.m*** to perform the local bathymetry interpolation and create the new SLF and CLI files. As input file you have to insert both the SLF file created in Step 1 and the modified mesh (*.msh) from GMSH.

Mesh Quality

The quality of the generated mesh can be checked using the Matlab script[5]:

Telemac_Mesh_Quality.m

The only input file needed is the geometry SLF file.

The mesh quality control is based on the calculation of the following three basic metrics, i.e. skewness, aspect ratio and smoothness. A table with the major mesh properties and histograms of element angles, and number of neighbouring nodes are also exported. A warning message pops up in case of over-constrained elements (triangles with nodes on the boundaries) existence.

[5] Part of the Flanders Hydraulics Research Matlab toolbox:
https://wl-subversion.vlaanderen.be/!/#repoSpNumMod/view/head/Matlab/Telemac_WL_toolbox

Appendix 2 Definitions of Statistics

Water levels

The **Bias** of water level represents the average deviation of the differences between model predicted water level and measurement.

The **RMSE** of water level is a measure of the spread of the predicted values level around the measurement. It corresponds to a sample standard deviation.

The **RMSE0** is the bias corrected root mean square error which describes the forecast errors not associated with the bias.

The mathematical expressions are listed below. *y* and *x* represent modeled and measured values respectively and *n* is the number of samples.

$$Bias = \overline{y} - \overline{x}$$

$$RMSE = \sqrt{\frac{\sum_{1}^{n}(y_i - x_i)^2}{n}}$$

$$RMSE0 = \sqrt{\frac{\sum_{1}^{n}((y_i - x_i) - (\overline{y} - \overline{x}))^2}{n}}$$

ADCP velocities

Average velocity magnitude and direction for each transect are calculated as the magnitude and direction of the average vector (based on the average U and V components), (average means the combination of the depth average and average over the transect). This means that both magnitude and direction of velocities are taken into account. For example, a direction of the velocity with a higher magnitude has more weight in the calculation of an average direction than a direction of the velocity with a smaller magnitude.

$$\overrightarrow{V_{met}}(x,z,t) = \overrightarrow{e_x} U_{met}(x,z,t) + \overrightarrow{e_y} V_{met}(x,z,t)$$

$$\overrightarrow{V_{\mathrm{mod}}}(x,z,t) = \overrightarrow{e_x} U_{\mathrm{mod}}(x,z,t) + \overrightarrow{e_y} V_{\mathrm{mod}}(x,z,t)$$

where $\overrightarrow{V_{met}}(x,z,t)$ is the vector of the measured velocity and $\overrightarrow{V_{\mathrm{mod}}}(x,z,t)$ is the vector of the modelled velocity.

Average velocity magnitude and direction:

$$MAG_{met}(t) = \left\| \frac{\sum_x \left\langle \overrightarrow{V_{met}} \right\rangle}{n} \right\| \qquad DIR_{met}(t) = dir\left(\frac{\sum_x \left\langle \overrightarrow{V_{met}} \right\rangle}{n} \right)$$

$$MAG_{\mathrm{mod}}(t) = \left\| \frac{\sum_x \left\langle \overrightarrow{V_{\mathrm{mod}}} \right\rangle}{n} \right\| \qquad DIR_{\mathrm{mod}}(t) = dir\left(\frac{\sum_x \left\langle \overrightarrow{V_{\mathrm{mod}}} \right\rangle}{n} \right)$$

where $\left\langle \overrightarrow{V_{\mathrm{mod}}} \right\rangle(x,t)$ and $\left\langle \overrightarrow{V_{met}} \right\rangle(x,t)$ are depth average modeled and measured velocities.

The **bias of magnitude and direction** is calculated as the difference between the calculated and measured average velocity magnitude and direction.

$$BIAS_{mag}(t) = MAG_{\mathrm{mod}} - MAG_{met}$$

$$BIAS_{dir}(t) = DIR_{\mathrm{mod}} - DIR_{met}$$

The **RMSE of velocity magnitude and direction** is calculated based on the depth average velocity magnitude and direction for each point along the transect. Magnitude is not taken into account for the calculation of the RMSE of velocity direction and vice-versa. Therefore, the RMSE plots show more variation between the model and measurements than the plots of average velocity magnitude and direction for all transects.

$$RMSE_{mag}(t) = \sqrt{\frac{\sum_x \left(\left\| \left\langle \overrightarrow{V_{\mathrm{mod}}} \right\rangle \right\| - \left\| \left\langle \overrightarrow{V_{met}} \right\rangle \right\| \right)^2}{n}}$$

$$RMSE_{dir}(t) = \sqrt{\frac{\sum_x \left(dir\left(\left\langle \overrightarrow{V_{\mathrm{mod}}} \right\rangle \right) - dir\left(\left\langle \overrightarrow{V_{met}} \right\rangle \right) \right)^2}{n}}$$

Stationary and ADCP velocities

The **MAE** (mean absolute error) is calculated based on the calculated (Y_1,Y_2) and observed (X_1,X_2) components of the current. The **RMAE** (relative mean absolute error) is derived to identify the order of magnitude of the error compared to the observed velocities. A table was proposed in which the RMAE was used to identify the model quality to represent the current.

$$MAE = \left\langle \left\| \vec{Y} - \vec{X} \right\| \right\rangle = \frac{1}{N} \sum_{n=1}^{N} \sqrt{\left(Y_{1,n} - X_{1,n} \right)^2 + \left(Y_{2,n} - X_{2,n} \right)^2}$$

$$RMAE = \frac{\left\langle \left\| \vec{Y} - \vec{X} \right\| \right\rangle}{\left\langle \left\| \vec{X} \right\| \right\rangle} = \frac{MAE}{\left\langle \left\| \vec{X} \right\| \right\rangle}$$

Appendix 3 Bed roughness testing

This appendix the additional roughness sensitive tests are presented. Two empirical friction laws are considered for the determination of the friction force at the bottom, i.e. the Manning's law and the Nikuradse's law. The main reason for conducting these additional bed roughness tuning tests, was to improve the predictions of Scaldis-Coast for peak flood velocities, which seem to be underestimated for some of the stationary measurement station of *Meetnet Vlaamse Banken:* MP0-Wandelaar, MP4-Bol van Knokke.

Theoretical background

Bottom friction is introduced in the Saint-Venant equations (equations of motion) as a source term $\vec{F}^f$ (m/s^2):

$$\vec{F}^f = -G_i \frac{\vec{u}}{\cos a}\sqrt{u^2+v^2}$$

where u, v (m/s) are the depth-averaged velocity components in the two horizontal dimensions, and a (-) is the local slope. Factor G_i (m^{-1}) depends on the utilized friction law:

1) Manning's law:

$$G_1 = \frac{gn^2}{h^{4/3}}$$

where n (m$^{1/3}$/s) is the Manning's roughness coefficient, g (m/s^2) is the gravitational acceleration and h (m) is the bottom depth.

2) Nikuradse's law:

$$G_2 = \frac{g}{hC^2}$$

where C is a coefficient obtained by the formula:

$$C = 7.83\ln\left(12\frac{h}{k_s}\right)$$

where k_s (m) is the Nikuradse's roughness coefficient.

Bottom roughness tuning

Base roughness field

The first calibration stage of the Scaldis-Coast model presented in Kolokythas *et al.* (2018) was strongly based on the calibration of the existing Scaldis model reported in Smolders *et al.* (2016). For the schematized upstream part the calibration of the Zeebrugge model (IMDC, 2015) was taken into account. The roughness coefficient (according to Manning's law) distribution over the computational domain that was finally selected, is presented in Figure 57. In the main part of the domain the coefficient is constant and equal to

0.022 $m^{1/3}/s$. Downstream of the Western Scheldt and in the Low Sea Scheldt reduces to values equal to 0.012 $m^{1/3}/s$. This will be called as the base roughness field.

The comparison of the numerical results with corresponding measurements at several stations in the Belgian coast and in the Western Scheldt showed in general good performance of Scaldis-Coast model. However, the comparison of predicted depth-averaged velocities with stationary measurements showed that peak flood velocities seem to be underestimated in some of the considered locations. The improvement of the predicted peak flood velocities is the main motivation for the extra effort put on the bed roughness tuning.

Figure 57 – Base roughness field (Manning's law) on the computational domain of Scaldis-Coast model.

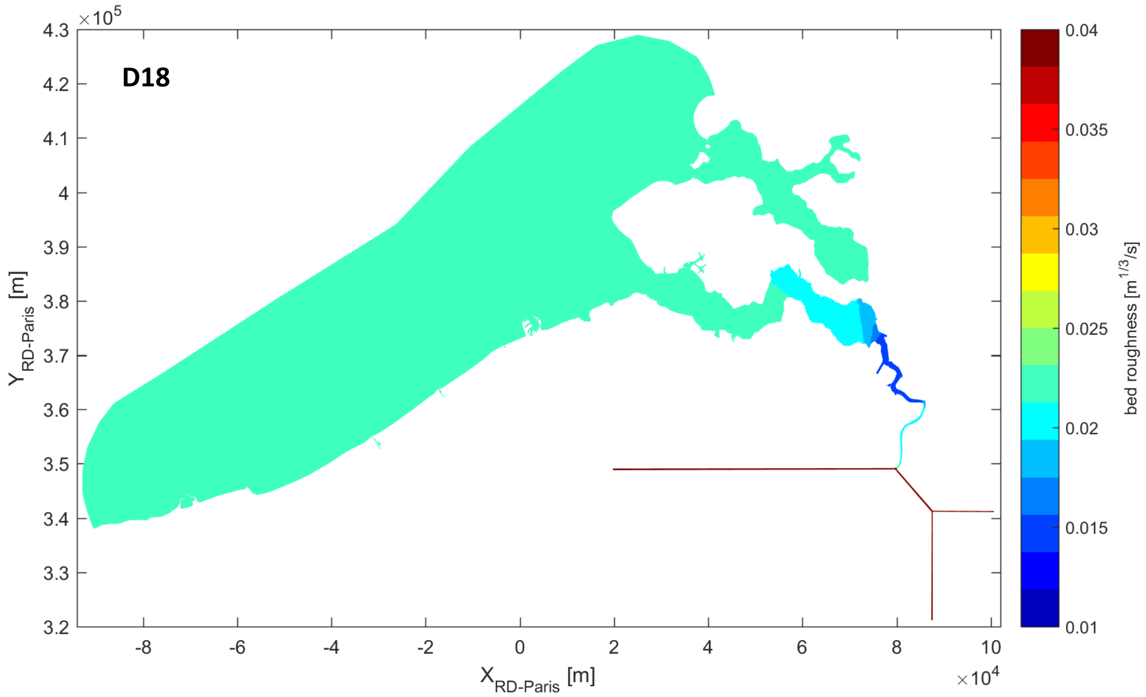

Bed roughness coefficient tuning tests

A series of hydrodynamic simulations were conducted keeping all the settings identical except for the bed roughness coefficient. Tests included the consideration of both Manning's and Nikurades's laws (see Table 18).

The idea was to reduce the bottom friction using lower values for the Manning's coefficient, n, (keeping them as realistic as possible) in order to improve the prediction of the peak flood velocities. Then Nikuradse's law was also tested using k_s values that lead to almost the same friction forces F_f at a certain range of bottom depths (i.e. from 5 to 10 m).

In Figure 58, the friction factor G_i that was discussed in the previous section is plotted versus the bottom depth for (most of) the tested n and k_s values. It is shown that reducing n from 0.022 (base run) to 0.018 leads to a 33% decrease of factor G_i and therefore of the friction force applied in the equations of motion. It is also observed that the lower coefficients n and k_s (i.e. 0.018 and 0.005) present a deviating behavior for depths lower than 5 m, while this behavior starts from deeper (around 10 m) for the higher coefficients n and k_s (i.e. 0.024 and 0.05).

Table 18 – Numerical experiments for the bed roughness coefficient tuning.

Run	Friction law	Coefficient n / k_s – description
D18	Manning	n=0.022 up to Ossenisse – upstream varying (Scaldis) / Base run
D20	Manning	n=0.018 up to HPW* – upstream varying (same as D18)
D20a	Manning	n=0.015 up to HPW then n=0.024 (constant)
D20b	Manning	n=0.018 up to Scheldeoord then n=0.024 (constant)
D20c	Manning	n=0.018 up to HPW then n=0.024 (constant)
D20d	Manning	n=0.018 up to HPW then n=0.024 and 0.035 at schematized part
D17d	Nikuradse	ks=0.005 up to Breskens then ks=0.05
D21	Nikuradse	ks=0.001 up to HPW then ks=0.05
D21a	Nikuradse	ks=0.005 up to Scheldeoord then ks=0.05
D21b	Nikuradse	ks=0.005 up to HPW then ks=0.05
D21c	Nikuradse	ks=0.005 up to HPW then ks=0.05 and 0.5 at schematized part

* HPW: Hooge Platen West

Figure 58 – Friction factor G_i versus bottom depth for different values of Manning's and Nikuradse's coefficients for a depth range equal to 1 to 5 m (top figure) and a depth range equal to 5 to 20 m (bottom figure).

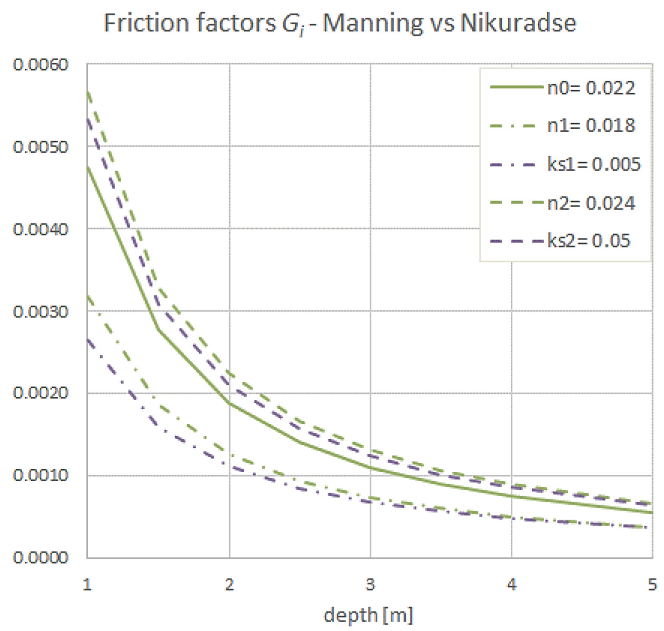

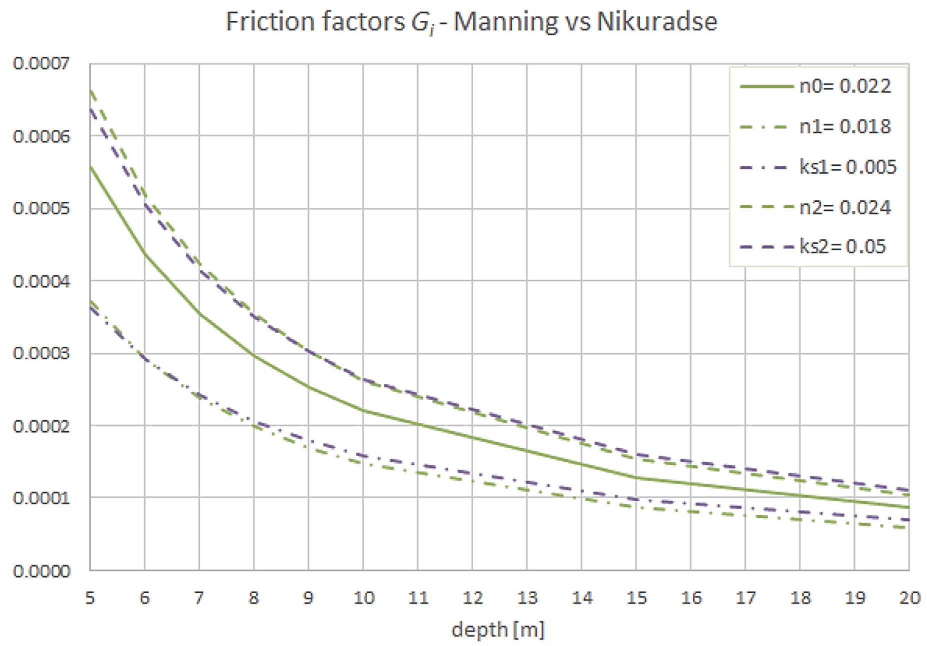

The most important roughness distributions (both Manning's and Nikuradse's coefficients) that were tested, are shown in Figure 59, Figure 60 and Figure 61.

In Figure 59 the Manning's roughness field is shown for the test Run D20, where n = 0.018 for the main part of the domain, i.e., offshore, coast, mouth of Western Scheldt and Eastern Scheldt up to Hooge Platen West (HPW), while a varying n identical to D18 run is considered in the rest upstream part.

In Figure 60 the Manning's & Nikuradse's roughness fields are shown for the test Runs D20d & D21c, respectively. In these configurations n = 0.018 and k_s = 0.005 downstream and up to HPW, while n = 0.024 and k_s = 0.05 up to the schematized upstream part, where n = 0.035 and k_s = 0.5. Test Runs D20c & D21b are identical to D20d & D21c, respectively, except for the schematized upstream part where *n* and k_s values remain equal to 0.024 and 0.05, respectively, as in the Western Scheldt.

Figure 59 – Bed roughness field (Manning's law) on the computational domain of Scaldis-Coast model for Run D20 (see Table 18).

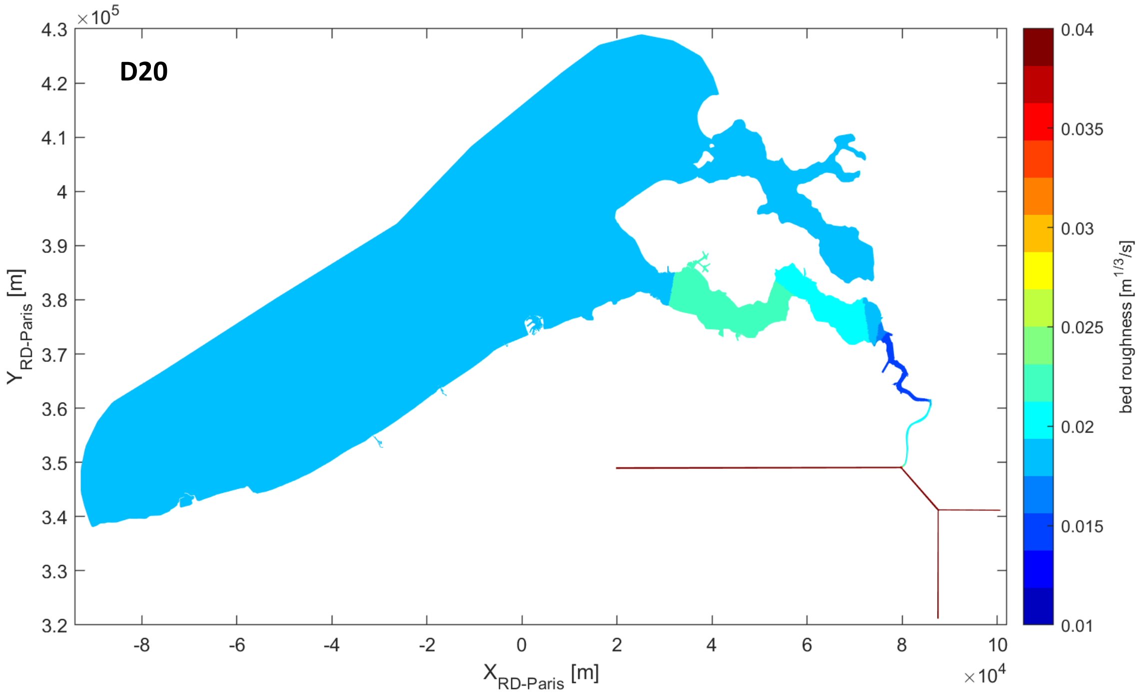

Figure 60 – Bed roughness field on the computational domain of Scaldis-Coast model for Run D20d (Manning's law) and Run D21c (Nikuradse's law) (see Table 18).

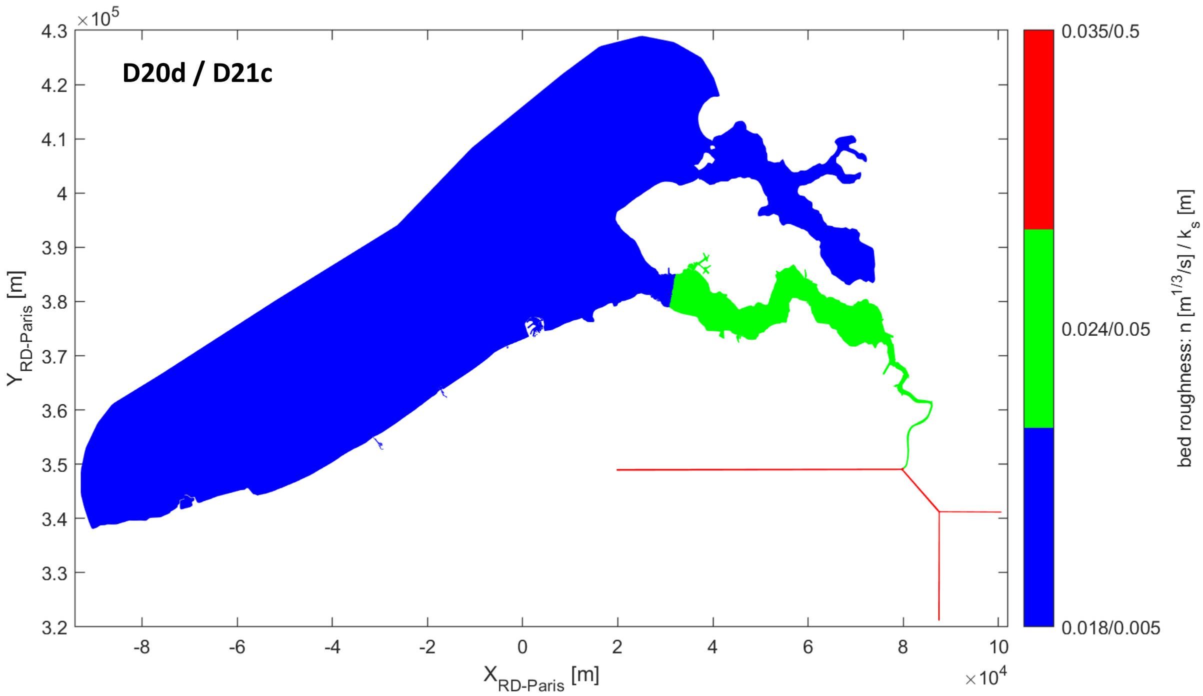

Finally, in Figure 61 the Manning's & Nikuradse's roughness fields are shown for the test Runs D20b & D21a, respectively. In these configurations n = 0.018 and k_s = 0.005 downstream and up to Scheldeoord, while n = 0.024 and k_s = 0.05 for the remaining upstream part.

Figure 61 – Bed roughness field on the computational domain of Scaldis-Coast model for Run D20b (Manning's law) and Run D21a (Nikuradse's law) (see Table 18).

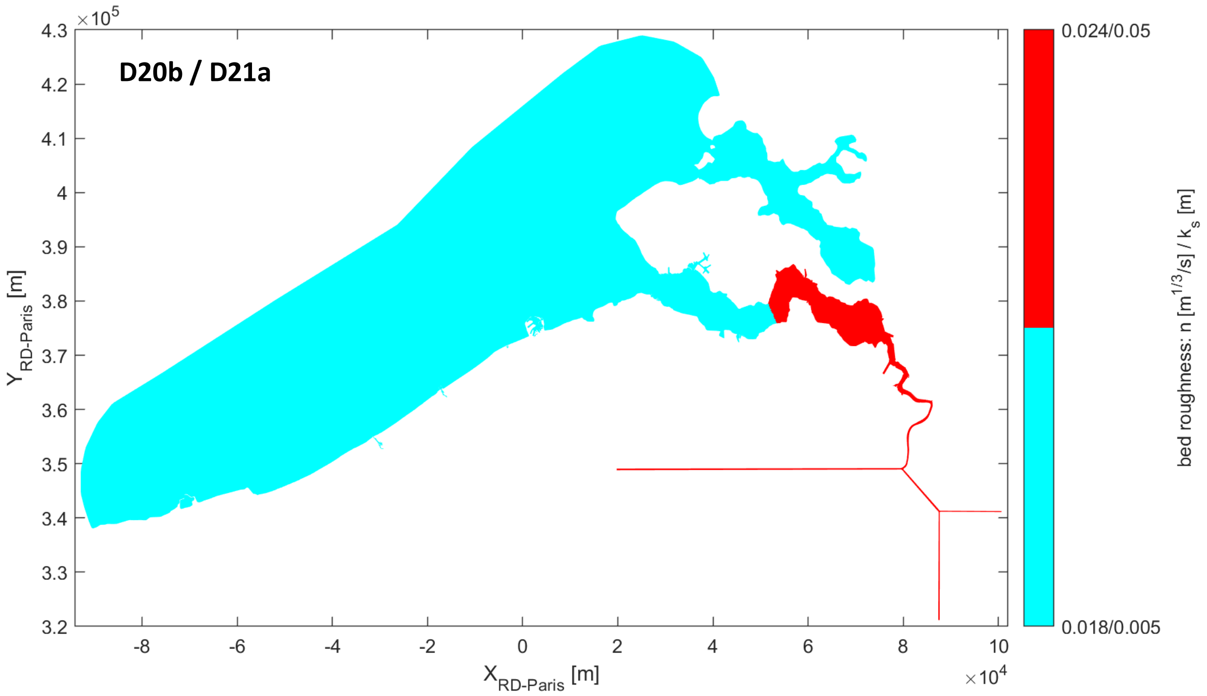

Results of Manning's coefficient tuning

Stationary velocities

The depth-averaged velocities from Scaldis-Coast are compared with 6 stationary velocity measurements from 2013 at the locations shown in Figure 62, i.e. at Wandelaar, Bol van Knokke, Bol van Heist, WZ buoy and at Hooge Platen West. Note that the velocities at the three first locations resulted from depth averaging of the middle bin of the current profiler (bin 3) ranging from 5.0 m to 7.5 m below the water surface. At WZ buoy, velocity profile is averaged within a distance of about 3 m from the bottom and at Hooge Platen West depth averaged velocities are used for the comparison.

Figure 62 – Locations of the stationary velocity measurements on the computational domain of Scaldis-Coast.

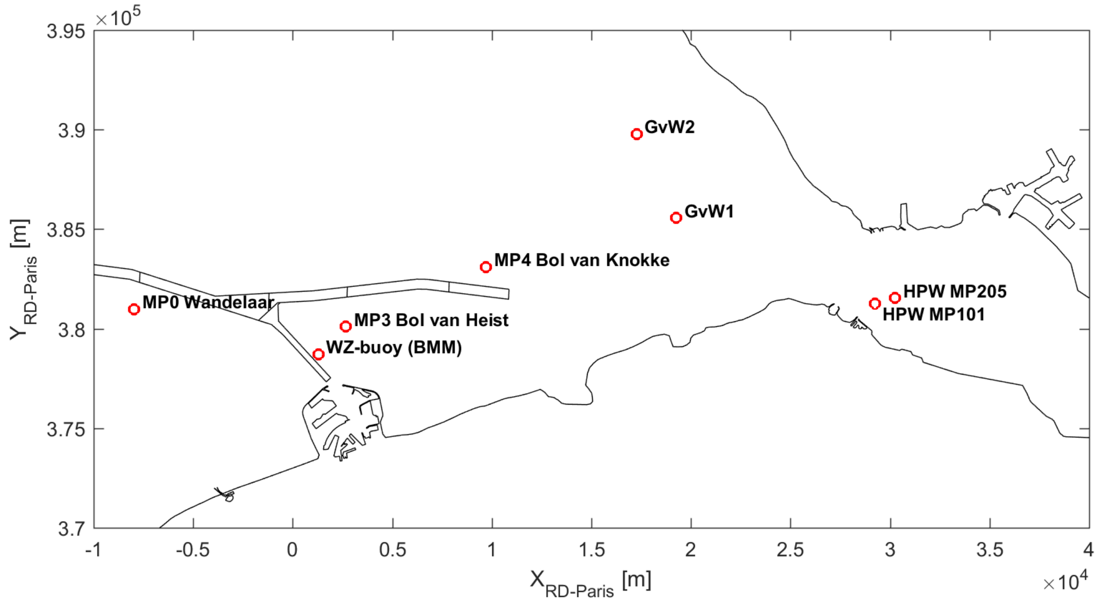

Figure 63 to Figure 65 show the time series of velocity magnitude and direction for a period of 5 days (18-09-2013 and 23-09-2013) at the aforementioned locations for the reference run (D18), the Manning's *n* test runs (D20*, only those with *n*=0.018 up to HPW) and the measurements. It is found that, in general, the reduced *n* coefficient tests can achieve an increase of the peak flood and ebb velocities around 10 to 15 cm/s compared to the reference run. The highest increase of the peak ebb velocities is observed at Wandelaar station (Figure 63), i.e., about 10 cm/s, while the highest increase of the peak flood velocities is found at HPW MP0205 (Figure 65) and Bol van Heist (Figure 63), i.e. 15 cm/s and 10 cm/s, respectively.

Figure 63 – Magnitude and direction of the measured and modelled velocity time series at Wandelaar (top figure) and at Bol van Heist (bottom figure).
Measured velocities at both stations come from averaging from 5.0 m to 7.5 m below water surface.
D18: reference run; D20*: Manning's *n* test runs.

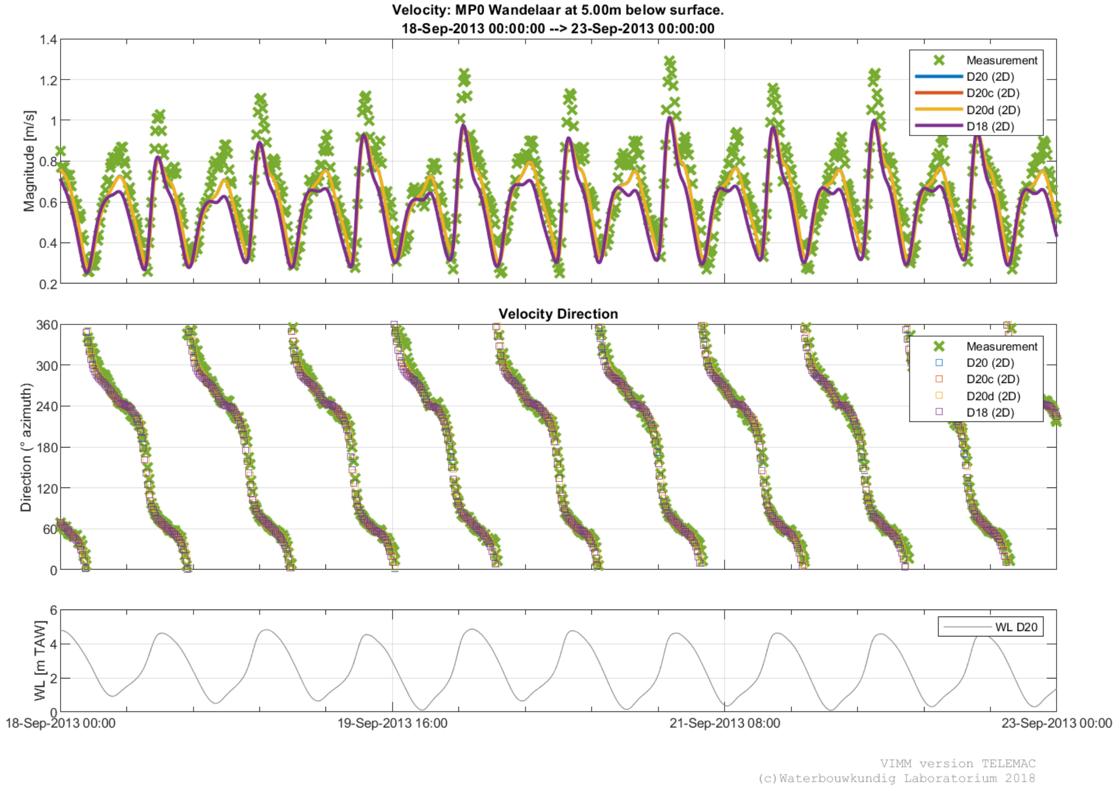

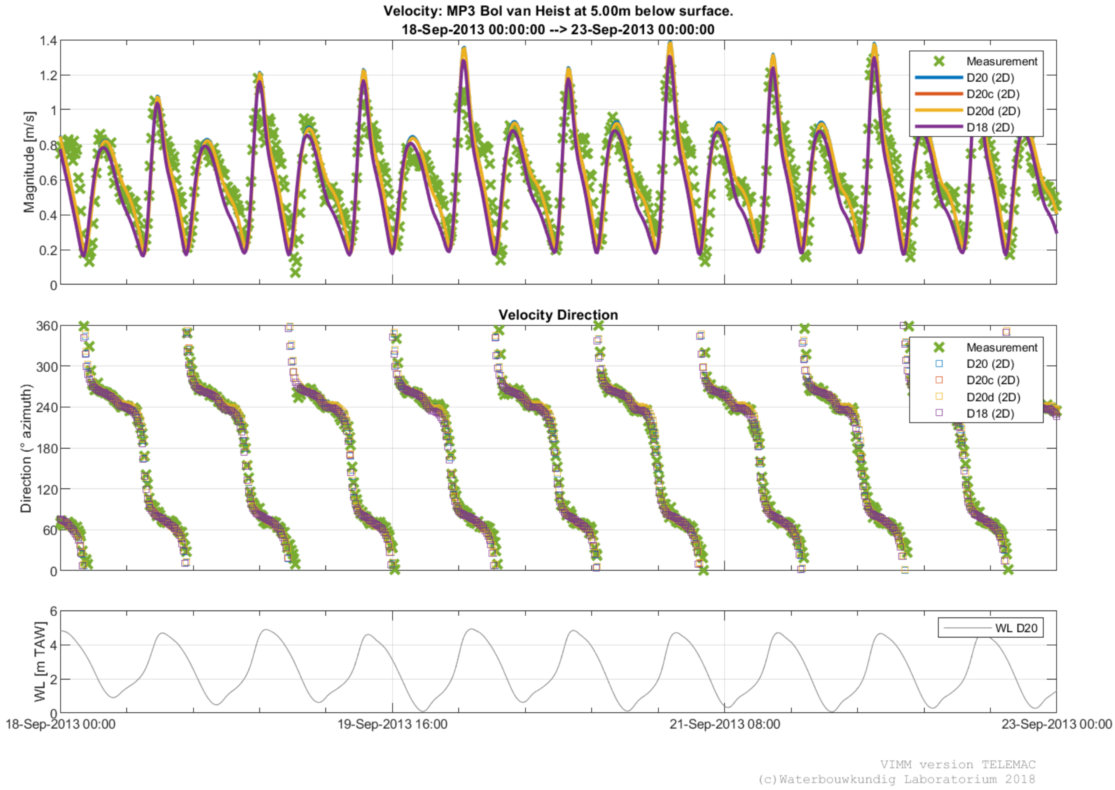

Figure 64 – Magnitude and direction of the measured and modelled velocity time series at Bol van Knokke (top figure) and at WZ buoy (bottom figure).
Bol van Knokke: Depth-averaged measurements from 5.0 m to 7.5 m below water surface;
WZ buoy: profile-averaging up to 3.0 m from the bottom. D18: reference run; D20*: Manning's *n* test runs.

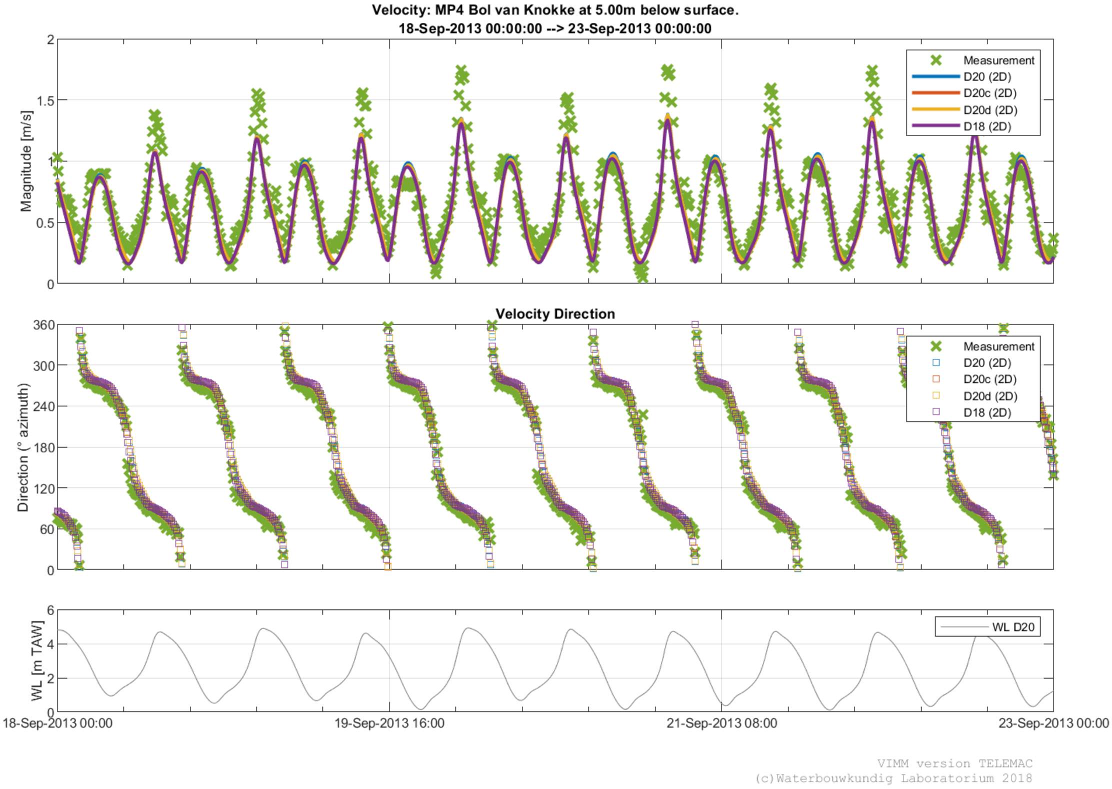

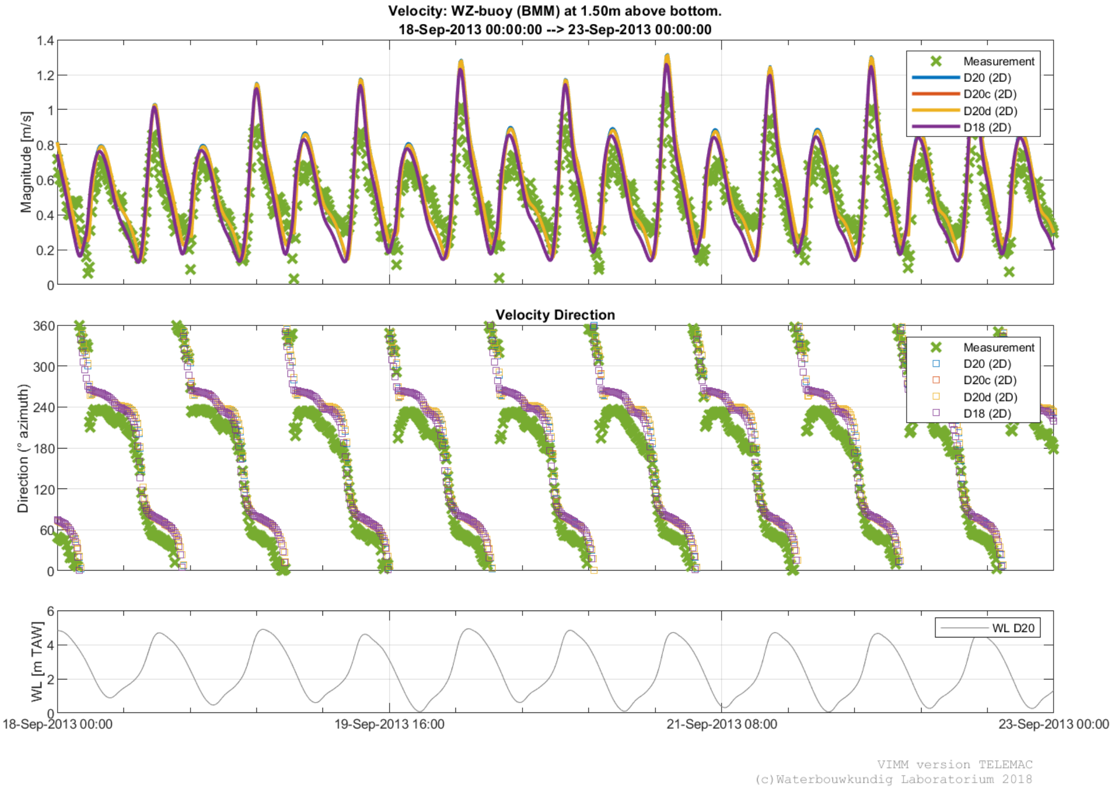

Figure 65 – Magnitude and direction of the measured (depth-averaged) and modelled velocity time series at HPW MP101 (top figure) and at HPW MP205 (bottom figure).
D18: reference run; D20*: Manning's *n* test runs.

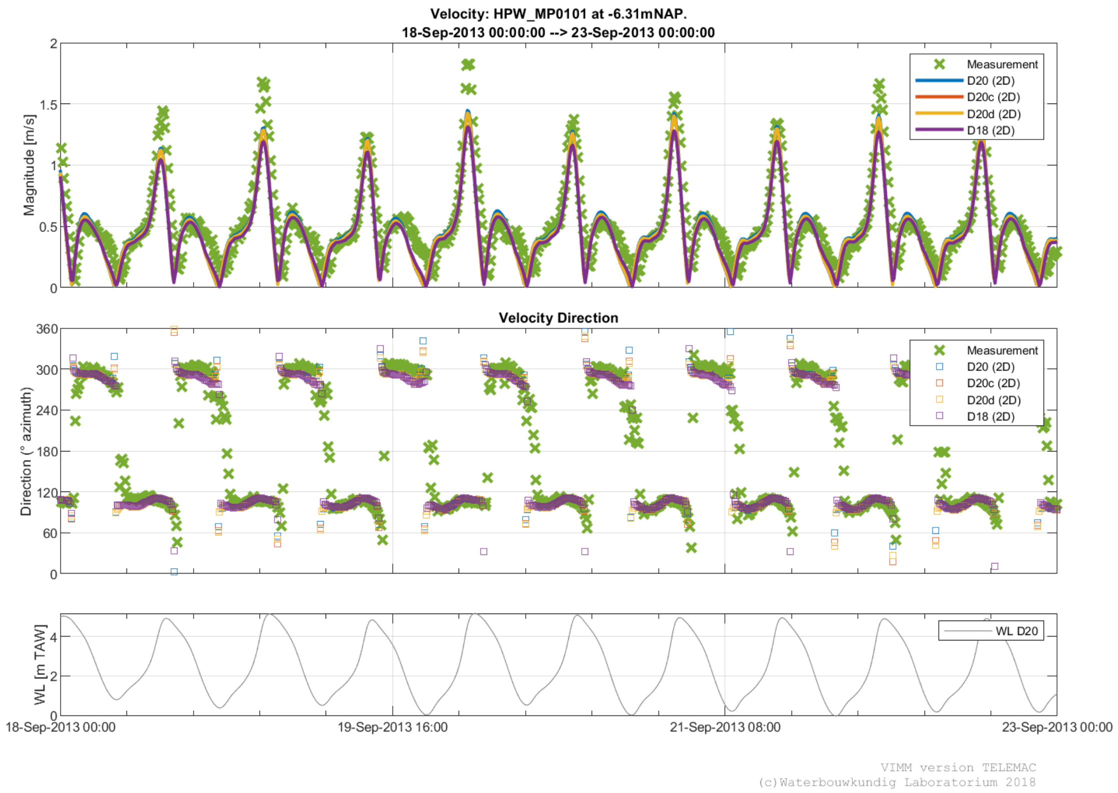

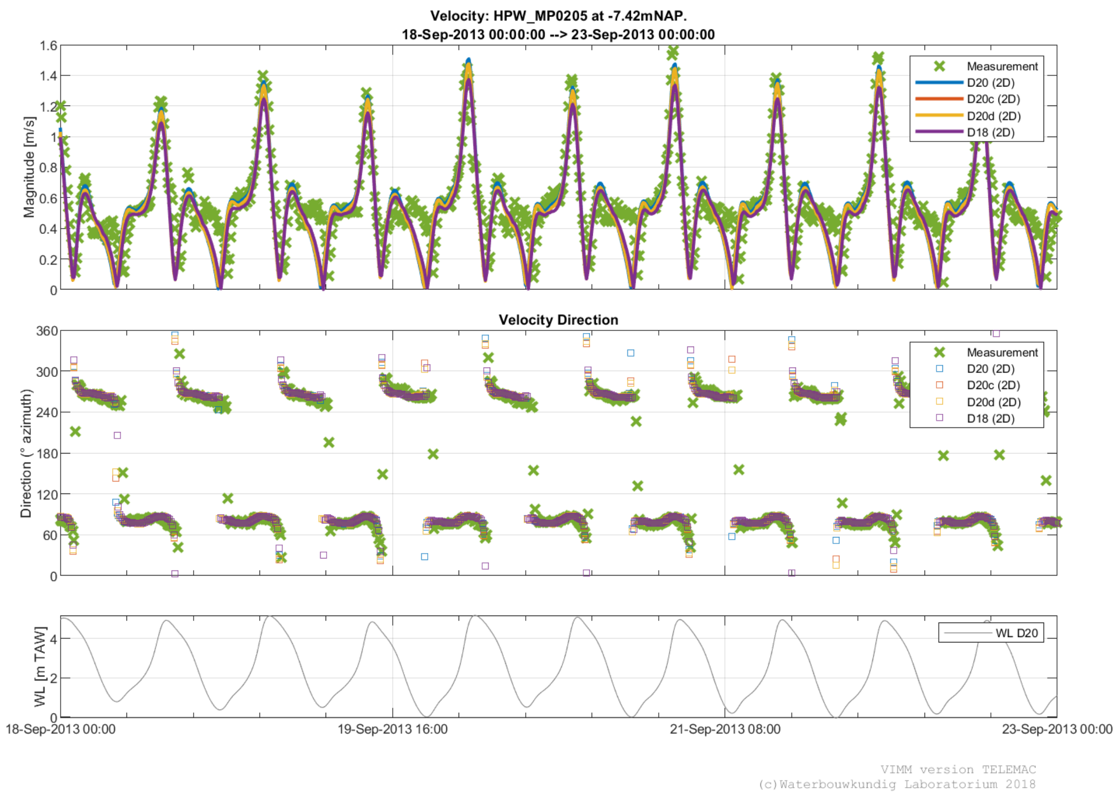

The statistical parameter RMAE (Relative Mean Absolute Error) for the velocity vector is utilized for the model qualification as shown in Table 12. The definition of RMAE and of all the other statistical parameters utilized for the validation of the model are given in Appendix 2. Note that the RMAE includes both the magnitude and direction errors. It is used as a qualification parameter in this study, following the work that has been done by Sutherland *et al.* (2004).

Table 19 – Model qualification based on RMAE (Sutherland *et al.*, 2004).

Model qualification		**RMAE [-]**
Excellent		**<0.2**
Good		**0.2-0.4**
Reasonable/fair		**0.4-0.7**
Poor		**0.7-1.0**
Bad		**>1.0**
Not Applicable		**-**

The RMAE parameter for the stationary velocities at the considered locations in the North Sea and the Western Scheldt, is presented in Figure 66. It is found that the reduction of the Manning's *n* coefficient at the coast (D20* Runs) leads to slightly improved results for the stations at North Sea and to slightly worse results at HPW stations compared to the reference run (D18). In general the performance is good, except for WZ buoy where the predictions are characterized as reasonable. The reason is that the amplitude of velocities is overestimated because the compared measured velocities are relatively close to the bottom.

Figure 66 – RMAE of the velocity vectors at the selected stations on the computational domain of Scaldis-Coast.
D18: reference run; D20*: Manning's *n* test runs.

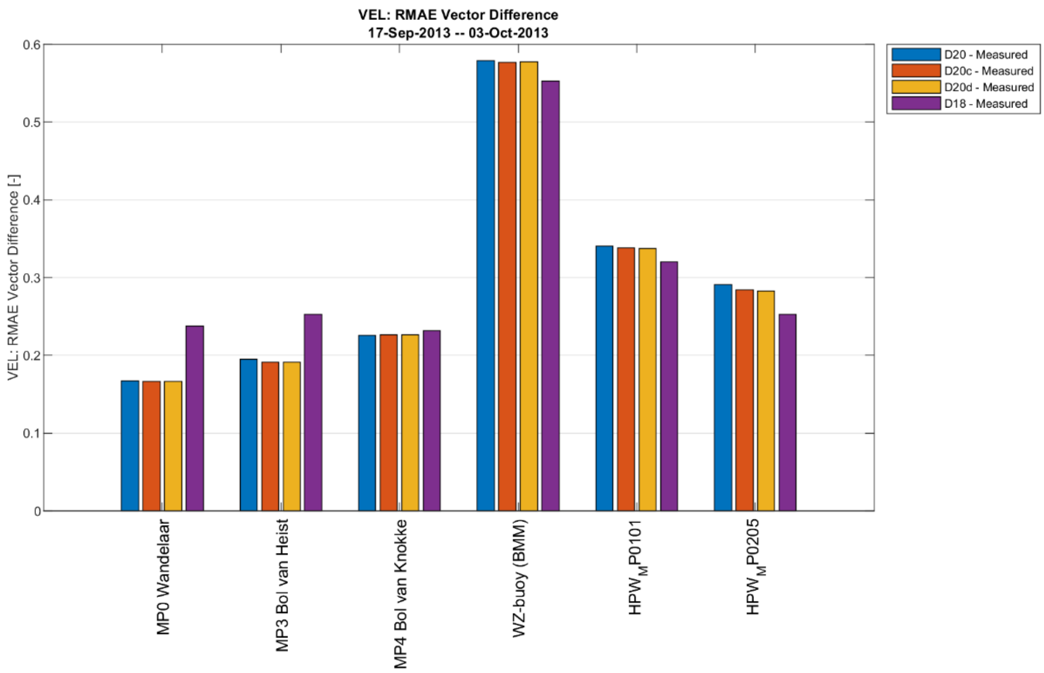

Water levels

The tidal amplitude characteristics predicted by the numerical tests were compared with the corresponding measured ones at the locations depicted in Figure 67. These are the high and the low water levels and their time of occurrence.

Figure 67 – Locations of the water level measurement stations on the computational domain of Scaldis-Coast.

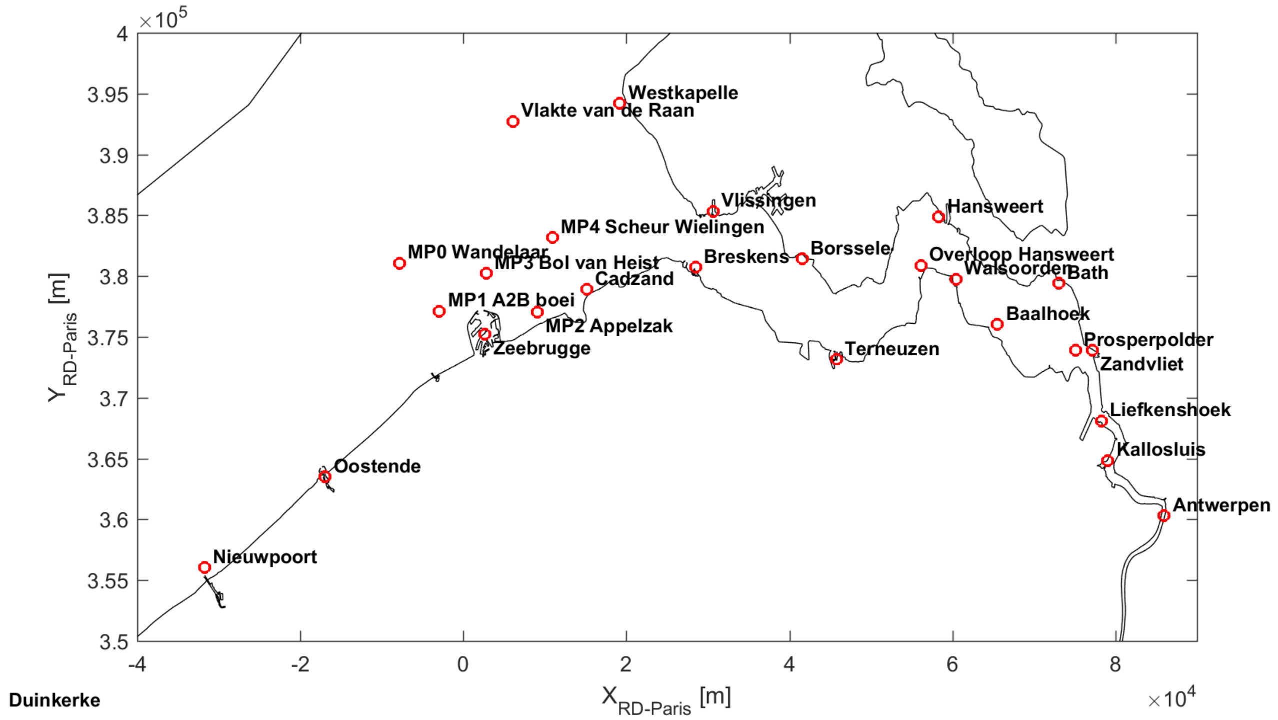

The bias in the high (HW) and low water (LW) levels between the numerical predictions of all runs and the measurements at the selected observation points, are shown in Figure 68, while in Figure 69 the bias in the complete water level time series is given. It is found that the D20* test runs perform similarly or slightly better than the reference run (D18) in predicting HW and LW levels for the majority of the coastal stations. The HW biases are increasing for the stations located close to the mouth of Western Scheldt and become much greater than that of D18 run for the stations Vlissingen up to Terneuzen. Note that these stations are the closest to the area of transition from $n = 0.018$ to a higher n. For the rest upstream stations, the runs with a constant n=0.024 (D20c, D20d) seem to perform slightly better than D18, while run D20 (varying n) performs relatively bad. The impact of increased n (=0.035 for D20d) at the upstream part is very low, observed only at the upstream stations. The aforementioned differences cannot be indicated in Figure 69 of the bias of the complete water level time-series.

Figure 68 – Bias in the High Water levels (top figure) and the Low Water levels (bottom figure) between the numerical predictions and the measurements. D18: reference run; D20*: Manning's *n* test runs.

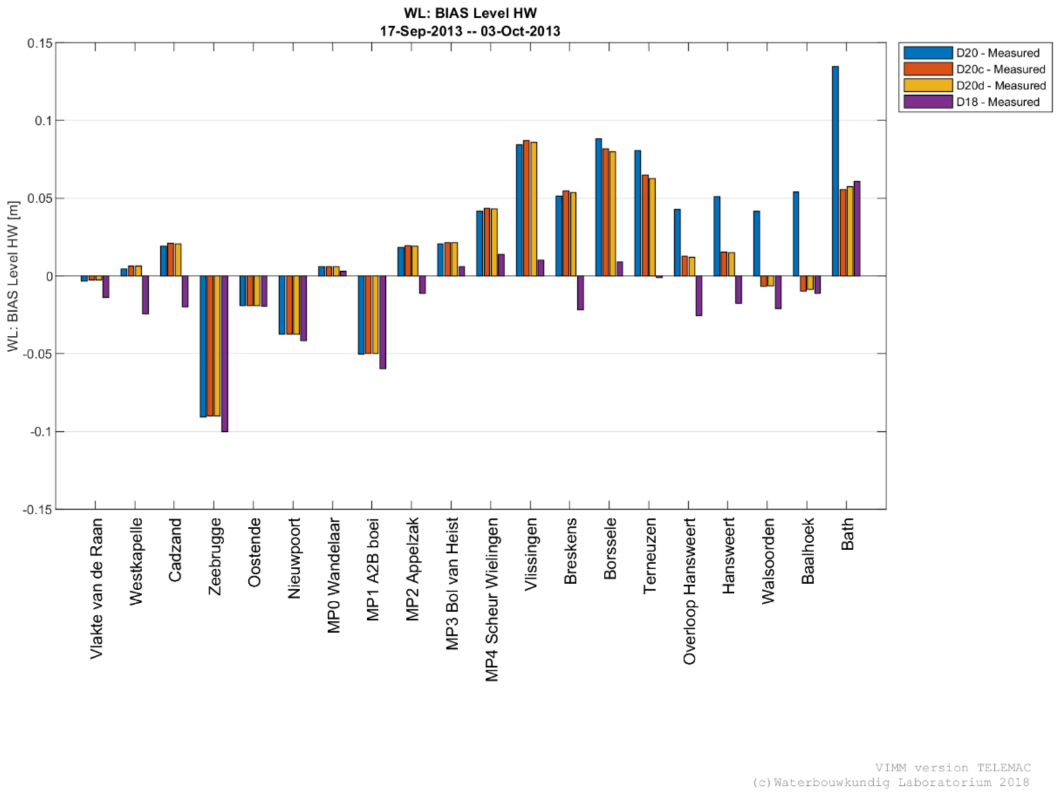

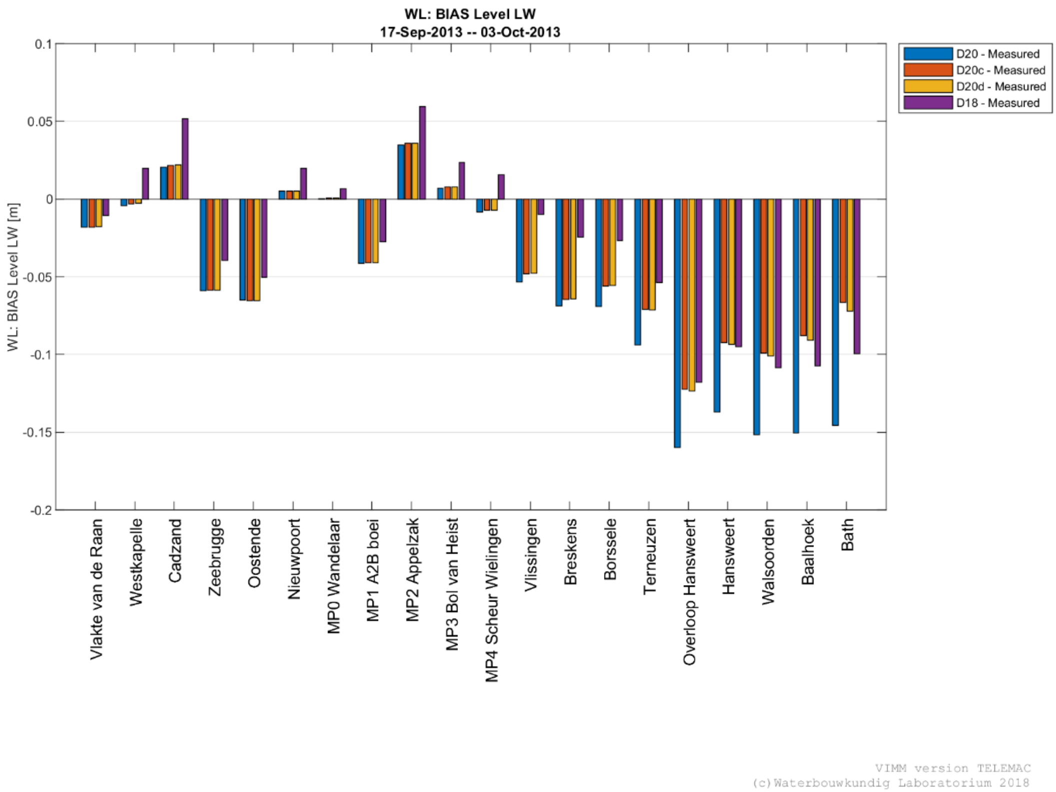

Figure 69 – Bias in the complete water level time-series between the numerical predictions and the measurements. D18: reference run; D20*: Manning's *n* test runs.

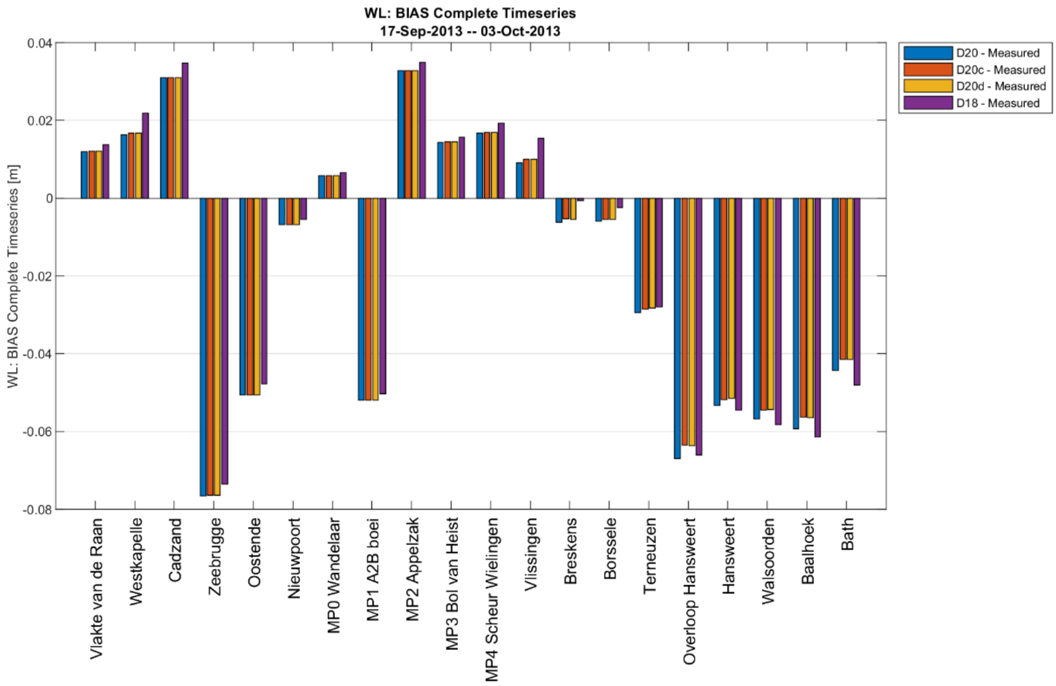

In Figure 70 the bias in the time of occurrence of high and low water between the numerical predictions of all runs and the measurements at the selected observation points are shown. It is found that the D20* test runs generally predict accelerated tidal waves compared to D18 reference run, presenting a backward shift in time from 2 min at the coast to 6 min in the Western Scheldt for both HW and LW levels. The highest differences are observed at the Western Scheldt stations Vlissingen to Walsoorden. The acceleration of the tidal wave is attributed to the lower *n* values utilized in D20* runs compared the D18 ones. The highest backward shift in time is observed for LW levels predicted by D20a run due to the varying low *n* values (up to 0.012) upstream (see Figure 59).

In Figure 71 the RMSE in the complete water level time series is given and it is shown that the D20* test runs perform similarly or slightly worse than the reference run (D18) in predicting water level variation at the coast. The results of D20* runs become worse at the stations in Western Scheldt, specifically at stations between Vlissingen and Walsoorden, where the differences reach values up to 5 cm. However the D20c and D20d runs lead to RMSE values around 15 cm (reasonable) and moreover give lower RMSEs at Baalhoek and Bath compared to D18. Once again it is shown that the concept of the varying (low) *n* values in Western Scheldt coupled with a lower *n* = 0.018 at the coast (D20 run), leads to bad performance of the model in the Western Scheldt.

Figure 70 – Bias in the time of High Water levels (top figure) and the time of Low Water levels (bottom figure) between the numerical predictions and the measurements. D18: reference run; D20*: Manning's *n* test runs.

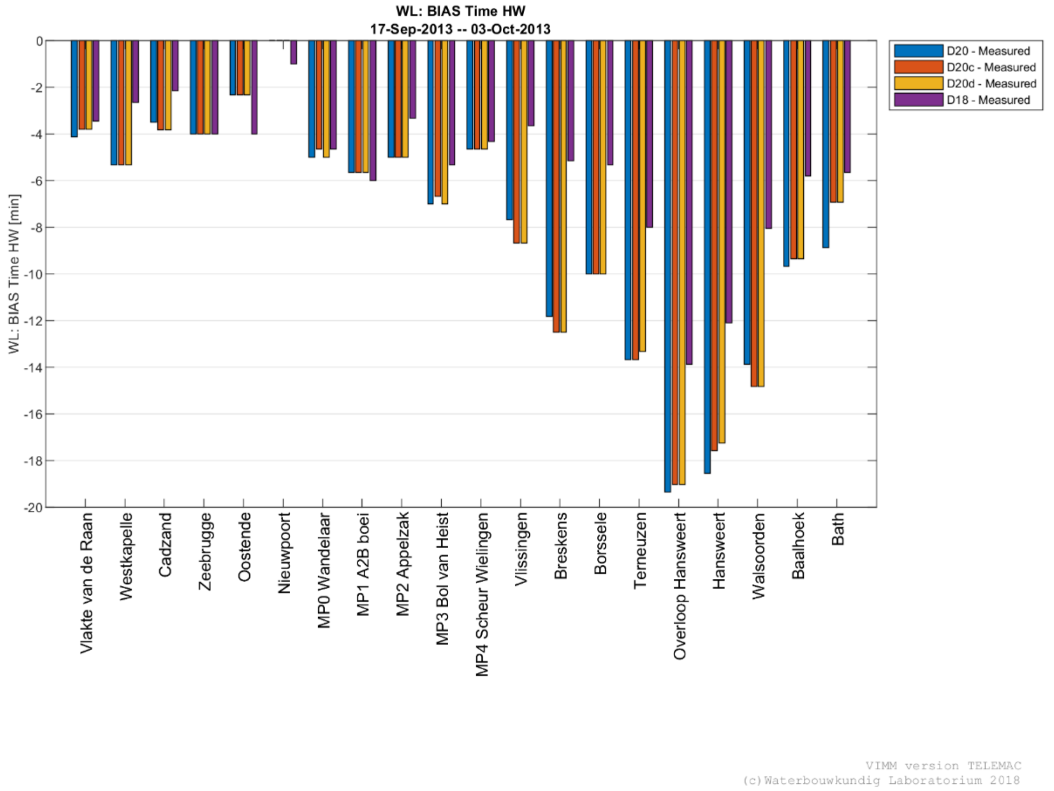

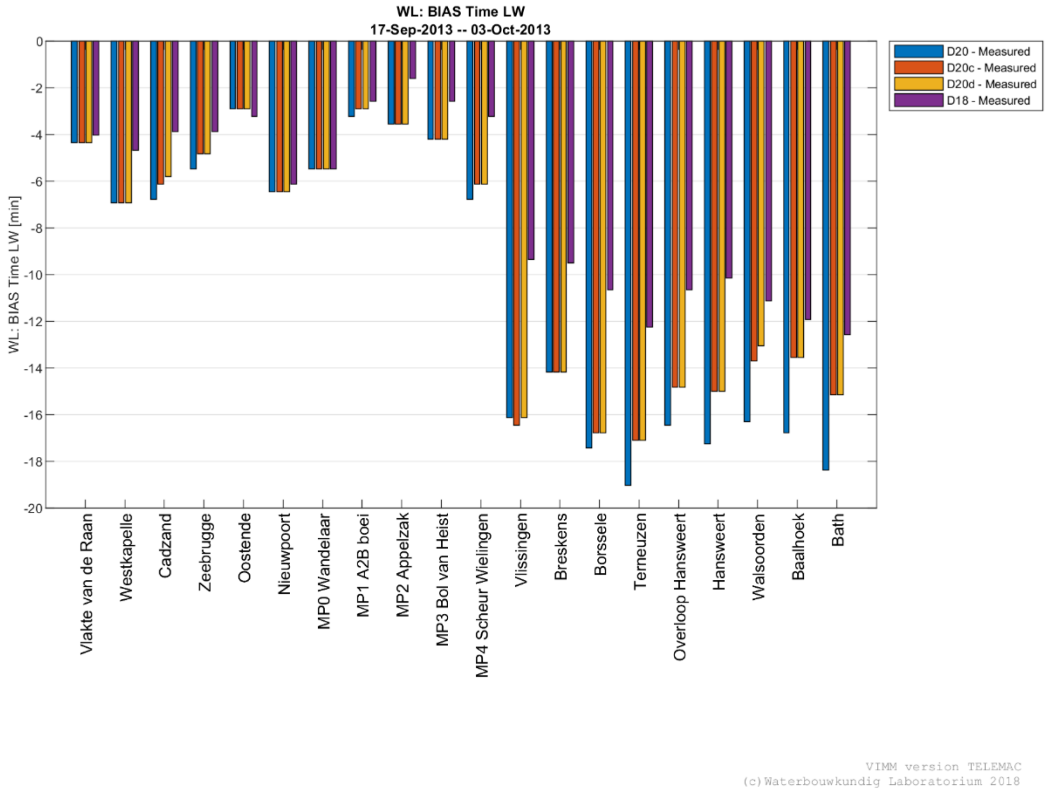

Figure 71 – RMSE in the complete water level time-series between the numerical predictions and the measurements. D18: reference run; D20*: Manning's *n* test runs.

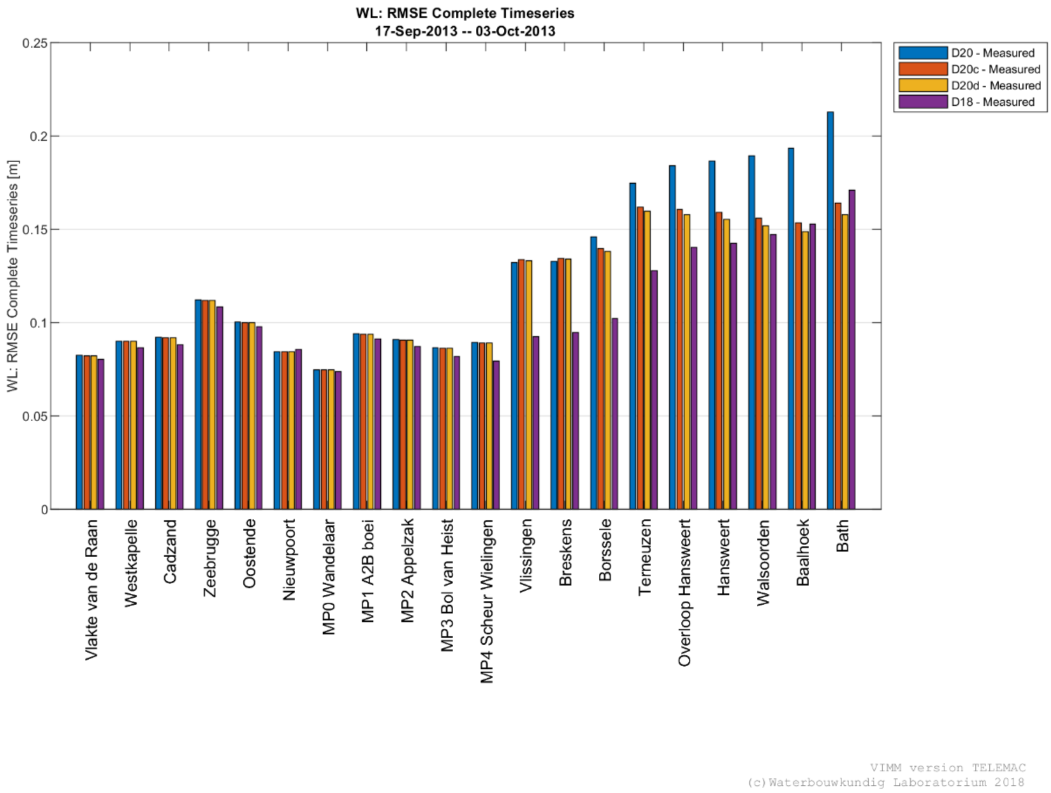

Comparison of Manning's and Nikuradse's laws

Stationary velocities

Figure 72 to Figure 74 show the time series of velocity magnitude and direction at the selected stations for the reference run (D18), the Manning's run D20d (best performing one), the Nikuradse's run D21c (with k_s values corresponding to the n values from D20d) and the measurements. The reader can refer to Figure 60 as a reminder for the utilized n and k_s field. It is found that, in general, the two approaches (Manning and Nikuradse) lead to quite similar results, however D21c run leads to slightly lower peak velocities compared to the ones of D20c.

The RMAE parameter for the stationary velocities at the considered locations in the North Sea and the Western Scheldt, is presented in Figure 75. As expected, it is indicated that the Nikuradse's run (D21c) gives results very close to those of the Manning's run (D20d).

Figure 72 – Magnitude and direction of the measured and modelled velocity time series at Wandelaar (top figure) and at Bol van Heist (bottom figure).
Measured velocities at both stations come from averaging from 5.0 m to 7.5 m below water surface.
D18: reference run; D20d: Manning's *n* test run; D21c: Nikuradse's *n* test run.

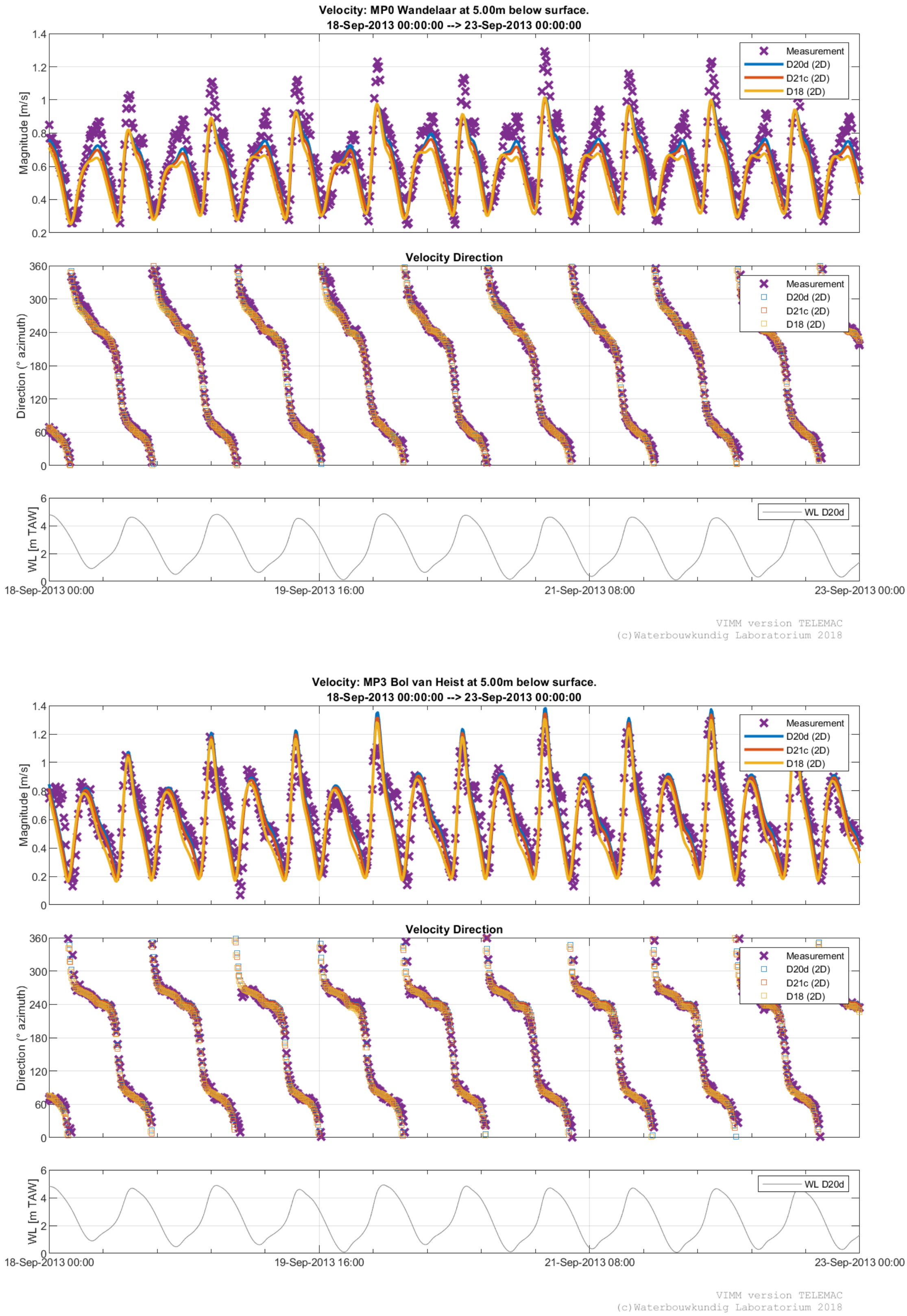

Figure 73 – Magnitude and direction of the measured and modelled velocity time series at Bol van Knokke (top figure) and at WZ buoy (bottom figure).
Bol van Knokke:Depth-averaged measurements from 5.0 m to 7.5 m below water surface; WZ buoy: profile-averaging up to 3.0 m from the bottom. D18: reference run; D20d: Manning's *n* test run; D21c: Nikuradse's *n* test run.

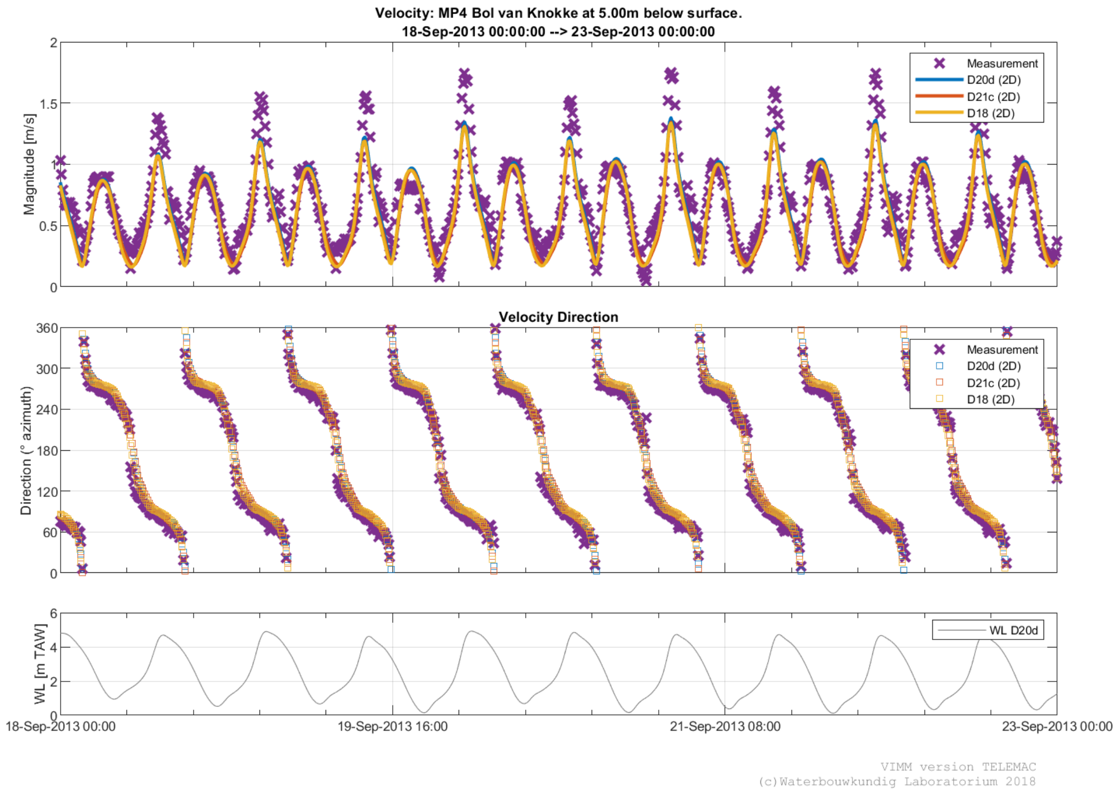

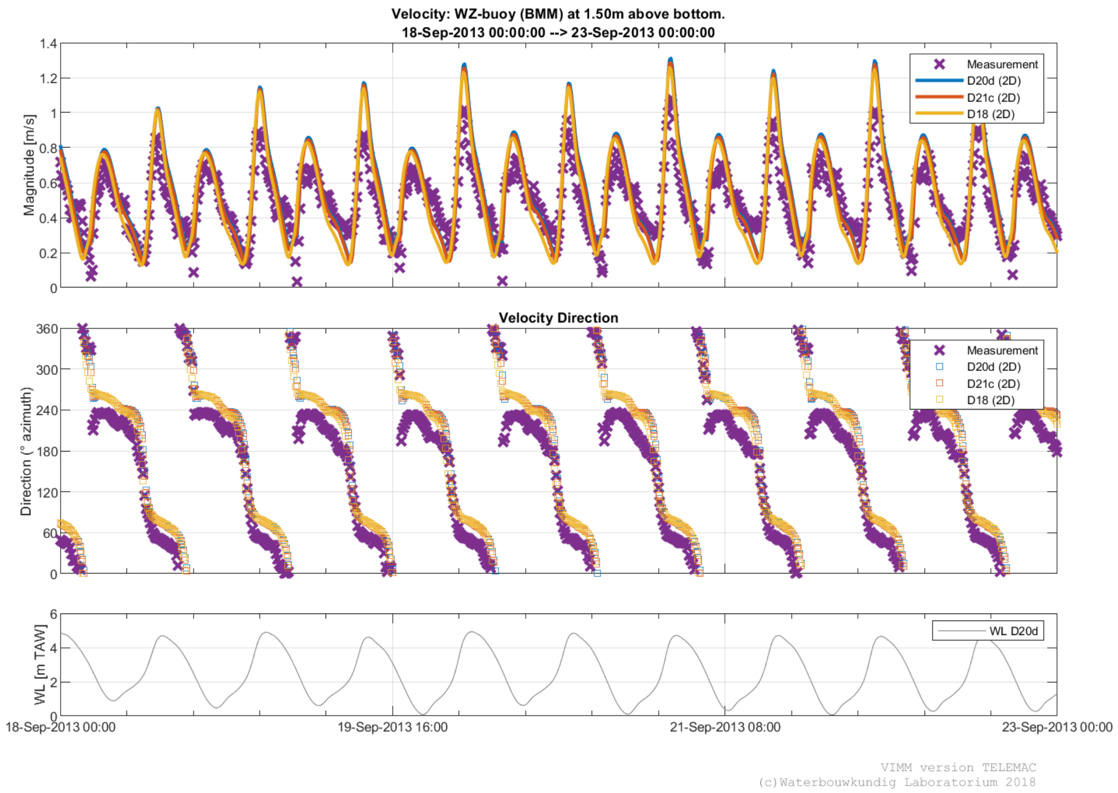

Figure 74 – Magnitude and direction of the measured (depth-averaged) and modelled velocity time series at HPW MP101 (top figure) and at HPW MP205 (bottom figure).
D18: reference run; D20d: Manning's *n* test run; D21c: Nikuradse's *n* test run.

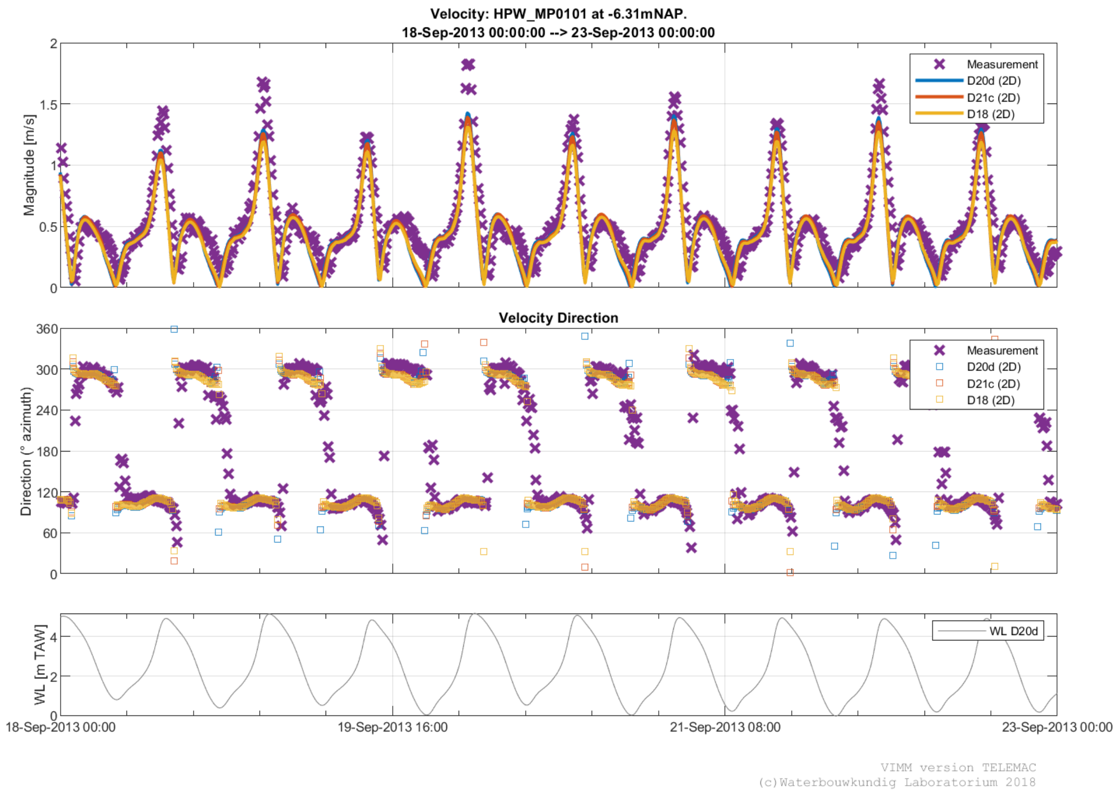

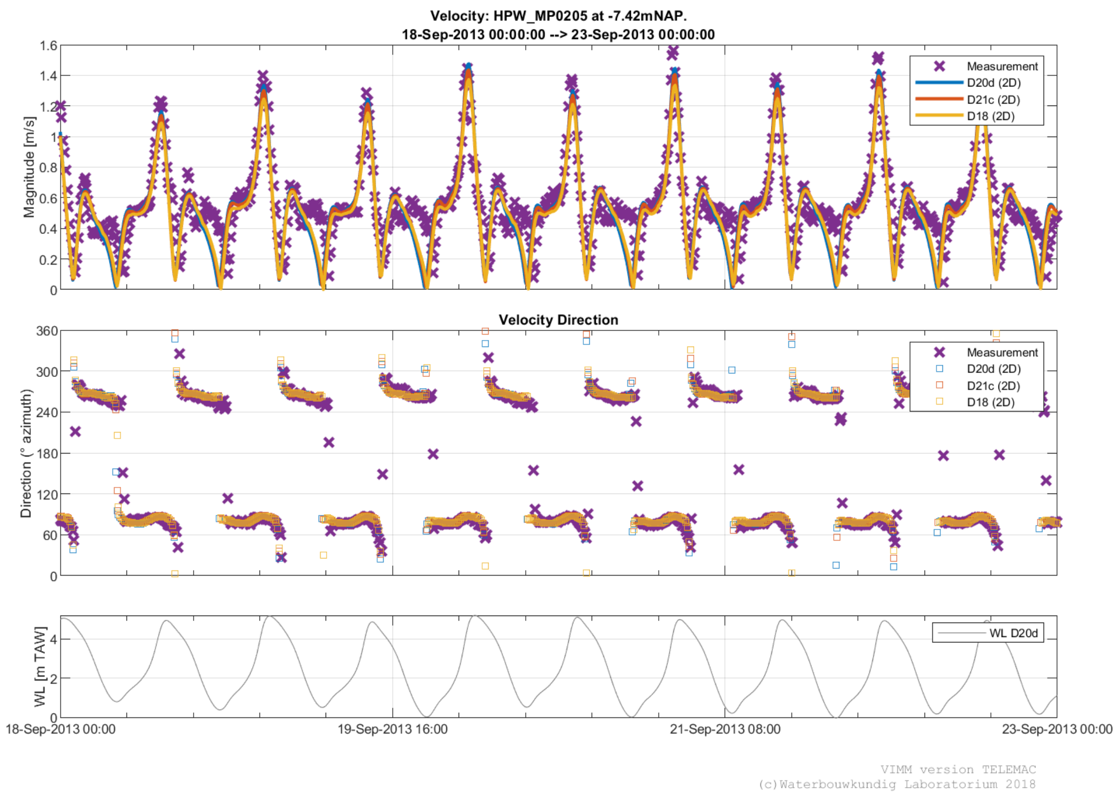

Figure 75 – RMAE of the velocity vectors at the selected stations on the computational domain of Scaldis-Coast. D18: reference run; D20d: Manning's *n* test run; D21c: Nikuradse's *n* test run.

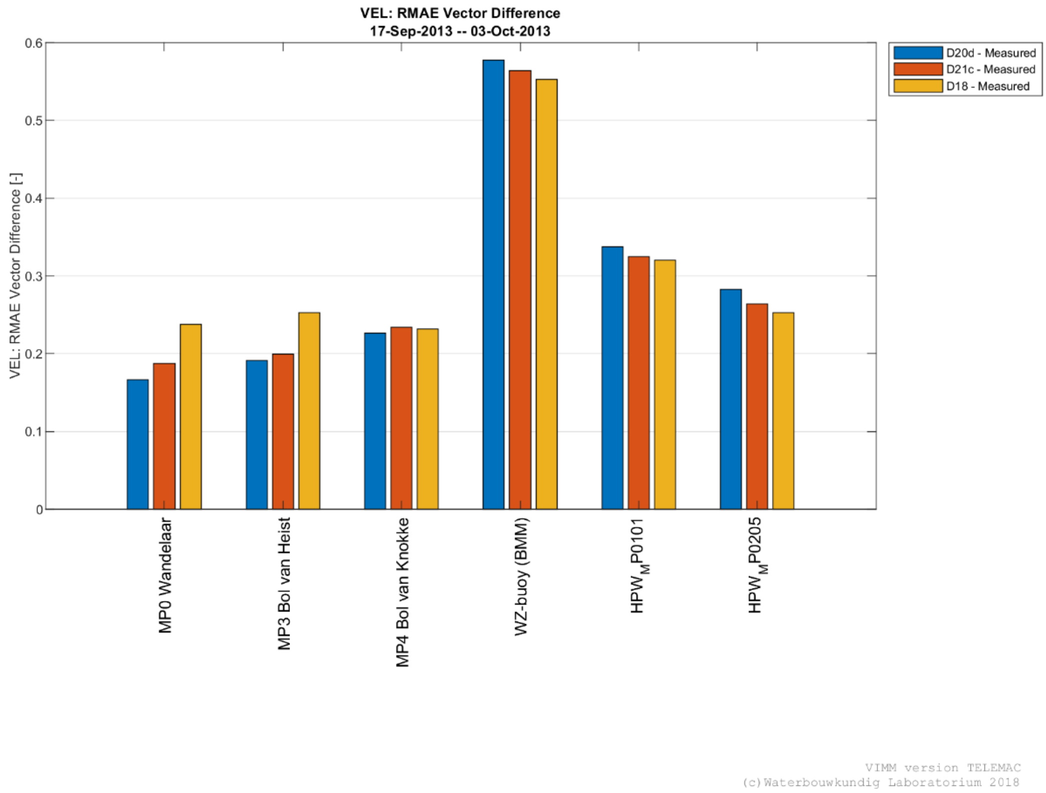

Water levels

The bias in the high (HW) and low water (LW) levels between the numerical predictions of Manning's and Nikuradse's runs and the measurements at the selected locations, are shown in Figure 76, while in Figure 77 the bias in the complete water level time series is given. Overall the Nikuradse's run presents better behavior than the Manning's run in predicting HW and LW levels. Specifically, it is found that the Nikuradse's run (D21c) performs similarly or better than the Manning's run (D20d) in predicting LW levels for the majority of the stations. As for the HW levels, D21c run underestimates them compared to D20d only at two upstream stations (Walsoorden and Baalhoek). The aforementioned differences cannot be indicated in Figure 77 of the bias of the complete water level time-series, where the two set-ups give similar results.

Figure 76 – Bias in the High Water levels (top figure) and the Low Water levels (bottom figure) between the numerical predictions and the measurements.
D18: reference run; D20d – Manning's *n* test run; D21c: Nikuradse's *n* test run.

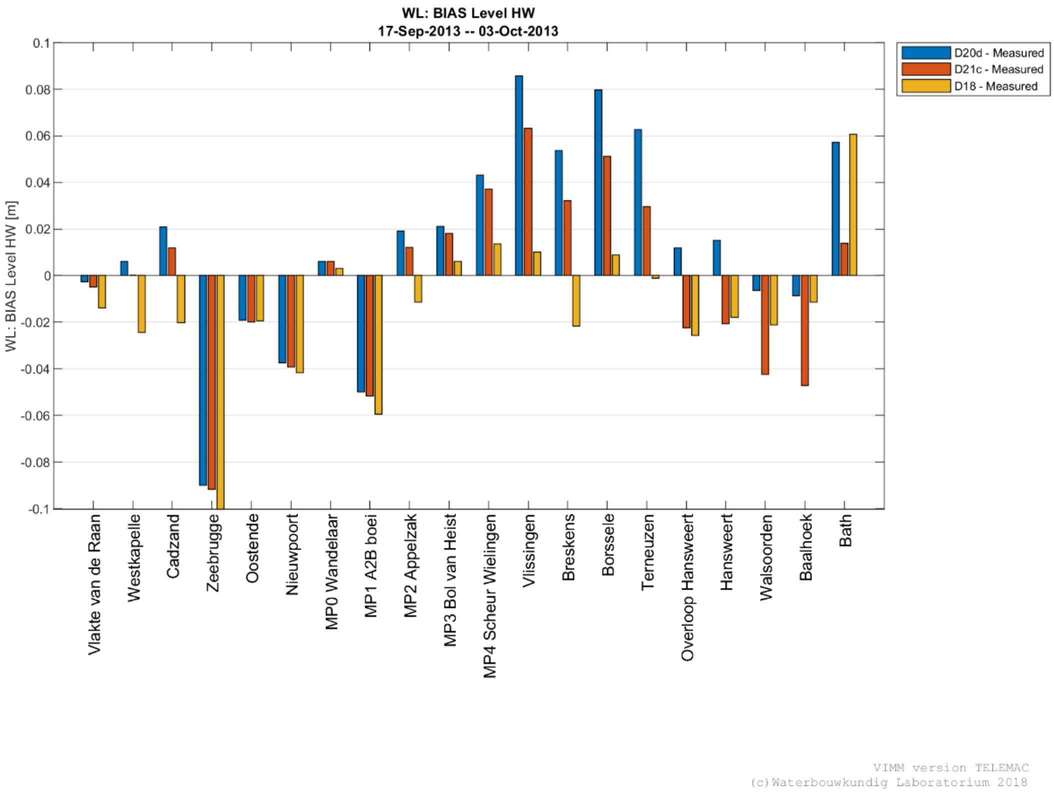

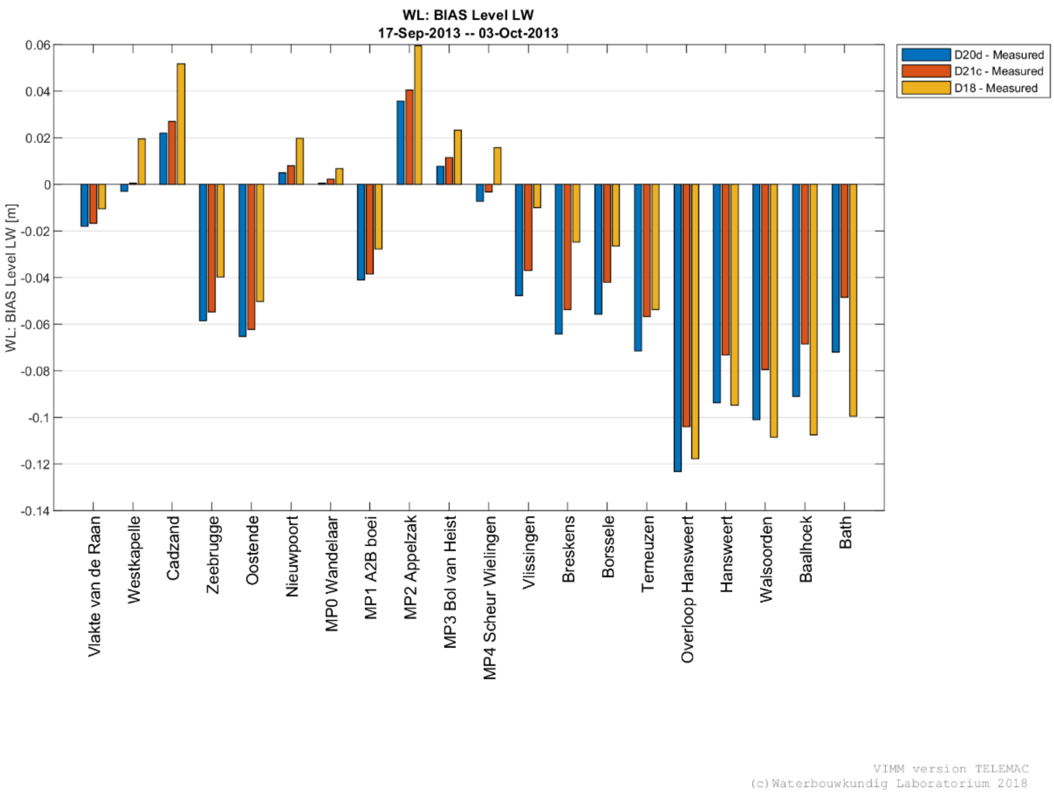

Figure 77 – Bias in the complete water level time-series between the numerical predictions and the measurements. D18: reference run; D20d: Manning's *n* test run; D21c: Nikuradse's *n* test run.

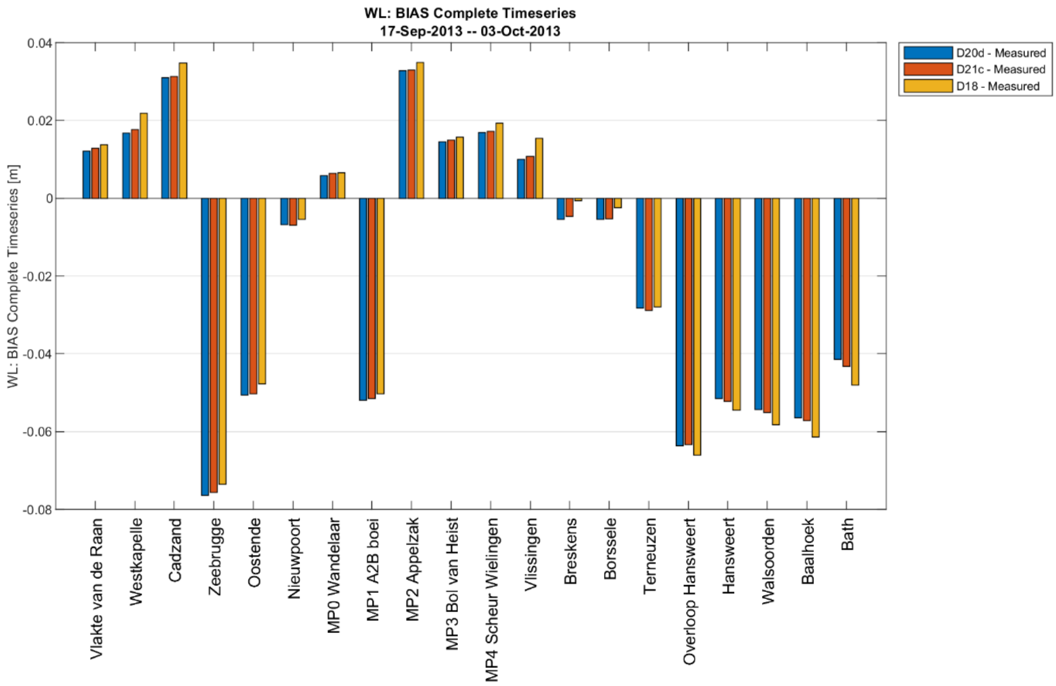

In Figure 78 the bias in the time of occurrence of high and low water between the numerical predictions of Manning's and Nikuradse's runs and the measurements at the selected locations, are shown. It is found that the D21c run also predicts accelerated tidal waves compared to D18 reference run, but this backward shift in time is now lower from 1 min to 3 min for both HW and LW levels compared to the Manning's run (D20d). It is shown that the differences between D20d and D21c become larger in the upstream stations compared to the coastal ones.

In Figure 79 the RMSE in the complete water level time series is given and it is shown that the D21c run performs better than D20d in The Western Scheldt keeping the RMSEs always lower than 15 cm. However D21c still performs worse than the reference run D18 at stations between Vlissingen and Terneuzen, where the differences now reach values up to 3 cm. For the most upstream stations D21c performs even better that the reference run D18.

Figure 78 – Bias in the time of High Water levels (top figure) and the time of Low Water levels (bottom figure) between the numerical predictions and the measurements.
D18: reference run; D20d: Manning's *n* test run; D21c: Nikuradse's *n* test run.

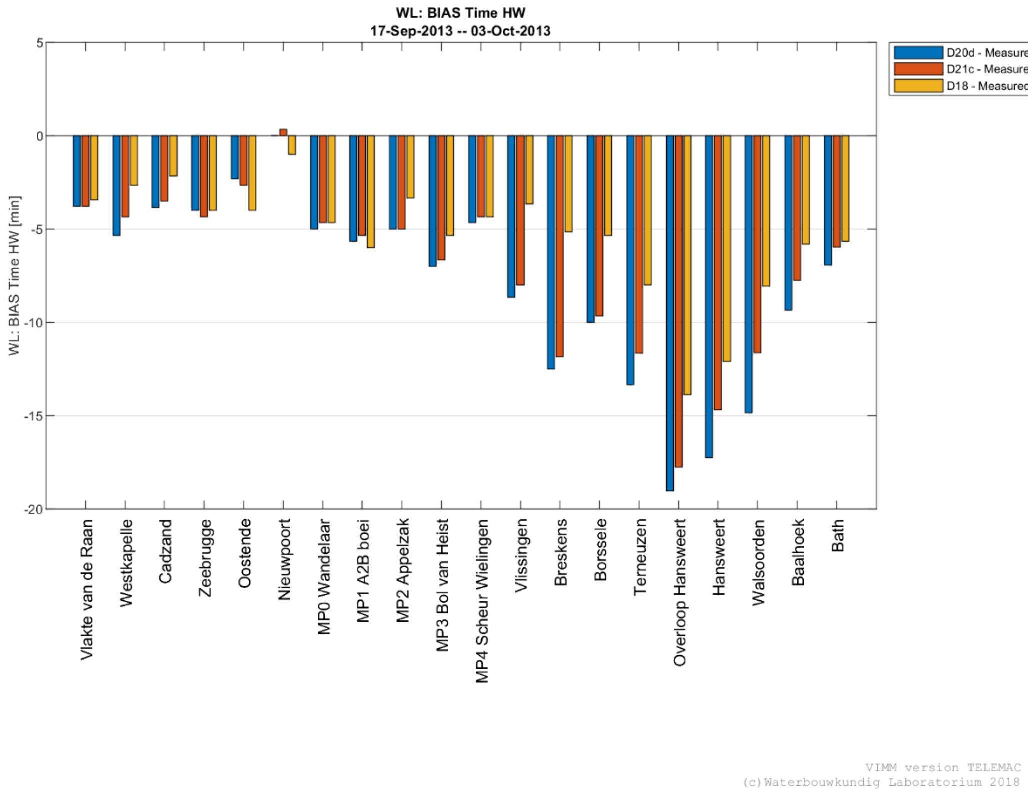

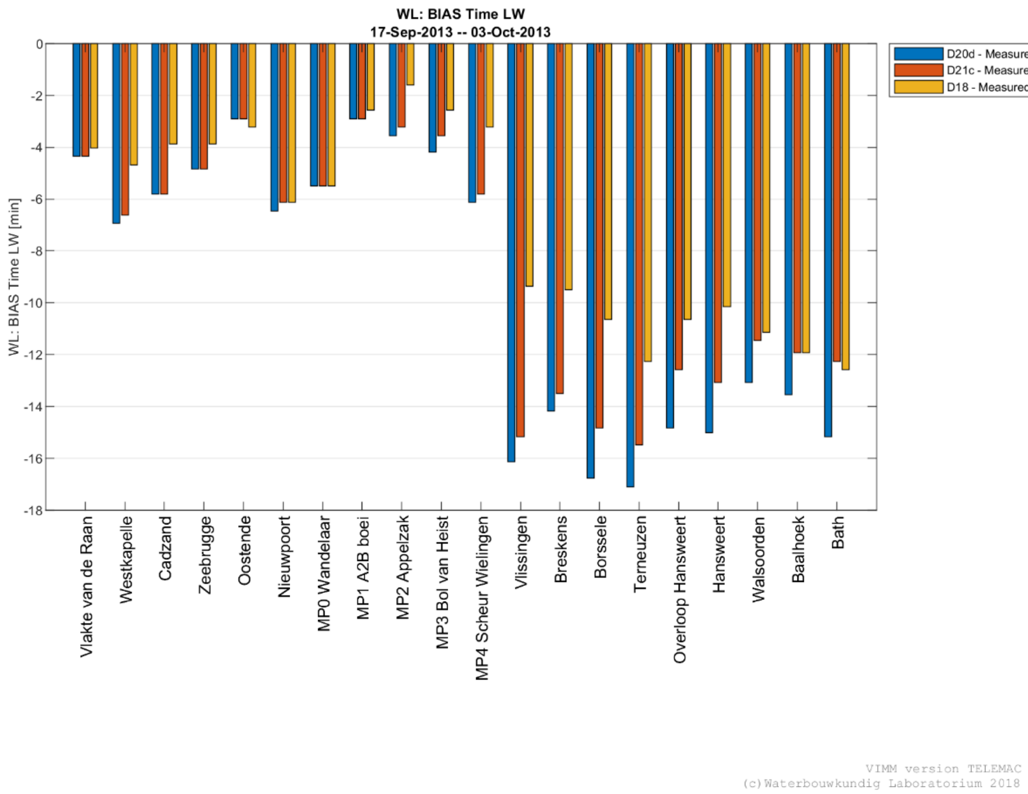

Figure 79 – RMSE in the complete water level time-series between the numerical predictions and the measurements. D18: reference run; D20d: Manning's *n* test run; D21c: Nikuradse's *n* test run.

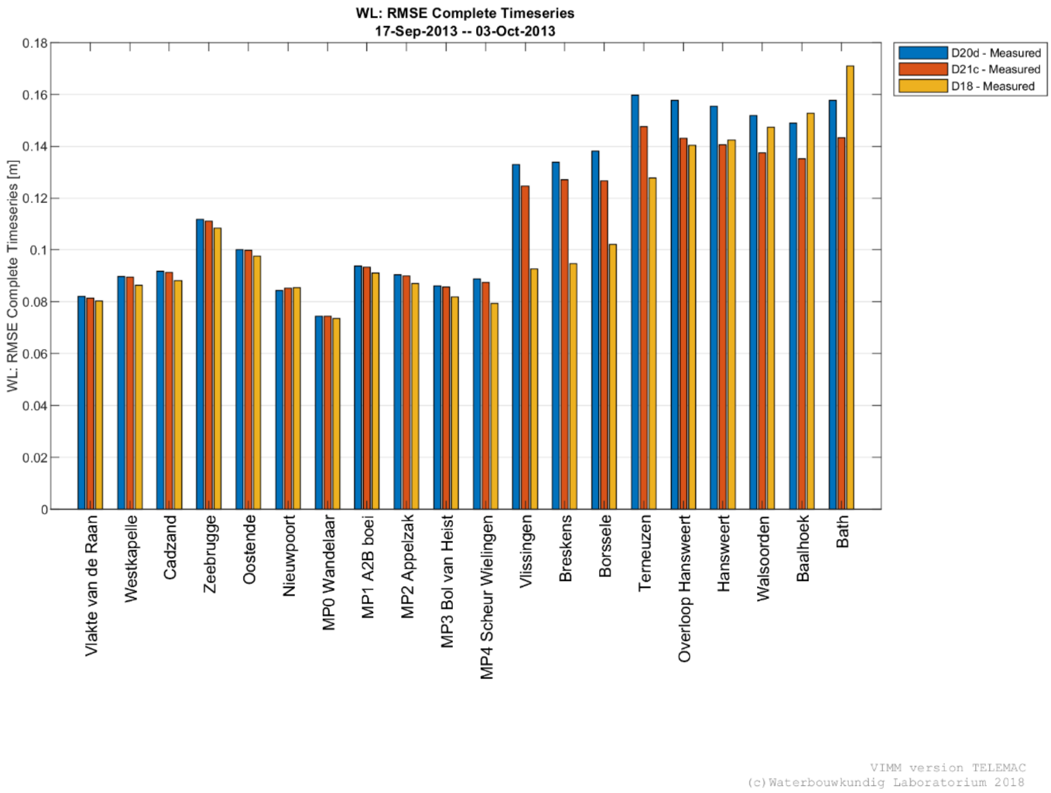

Other bed roughness tests

Stationary velocities

Figure 80 to Figure 82 show the time series of velocity magnitude and direction at the selected stations for the reference run (D18), the two Manning's runs D20a (*n* = 0.015 up to HPW), D20b (*n* = 0.018 up to Scheldeoord) and the measurements. It is found that the lower *n* value at the coast (D20a) can achieve an increase of the peak flood and ebb velocities around 15 to 20 cm/s compared to the reference run. The highest increase of the peak ebb velocities is observed at Wandelaar station (Figure 80), i.e., about 15 cm/s, while the highest increase of the peak flood velocities is found at HPW MP0205 (Figure 82) and Bol van Heist (Figure 80), i.e. 20 cm/s and 15 cm/s, respectively. A slight time shift of velocity time-series predicted by run D20a can also be observed especially in Figure 80. Note that run D20b gives almost identical results with D20d (*n* = 0.018 up to HPW) at the coastal stations and that is the reason that it is not plotted on the figures.

Figure 80 – Magnitude and direction of the measured and modelled velocity time series
at Wandelaar (top figure) and at Bol van Heist (bottom figure).
Measured velocities at both stations come from averaging from 5.0 m to 7.5 m below water surface.
D18: reference run; D20a: Manning's *n* =0.015 up to HPW; D20b: Manning's *n* =0.018 up to Scheldeoord.

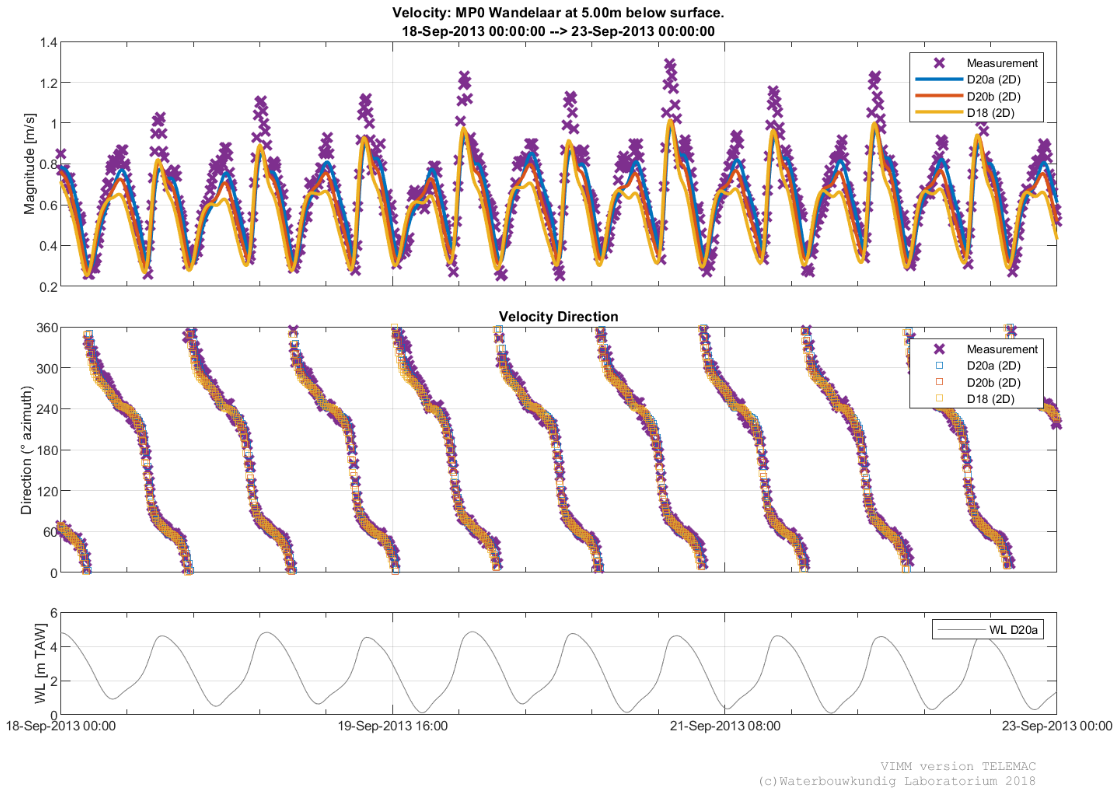

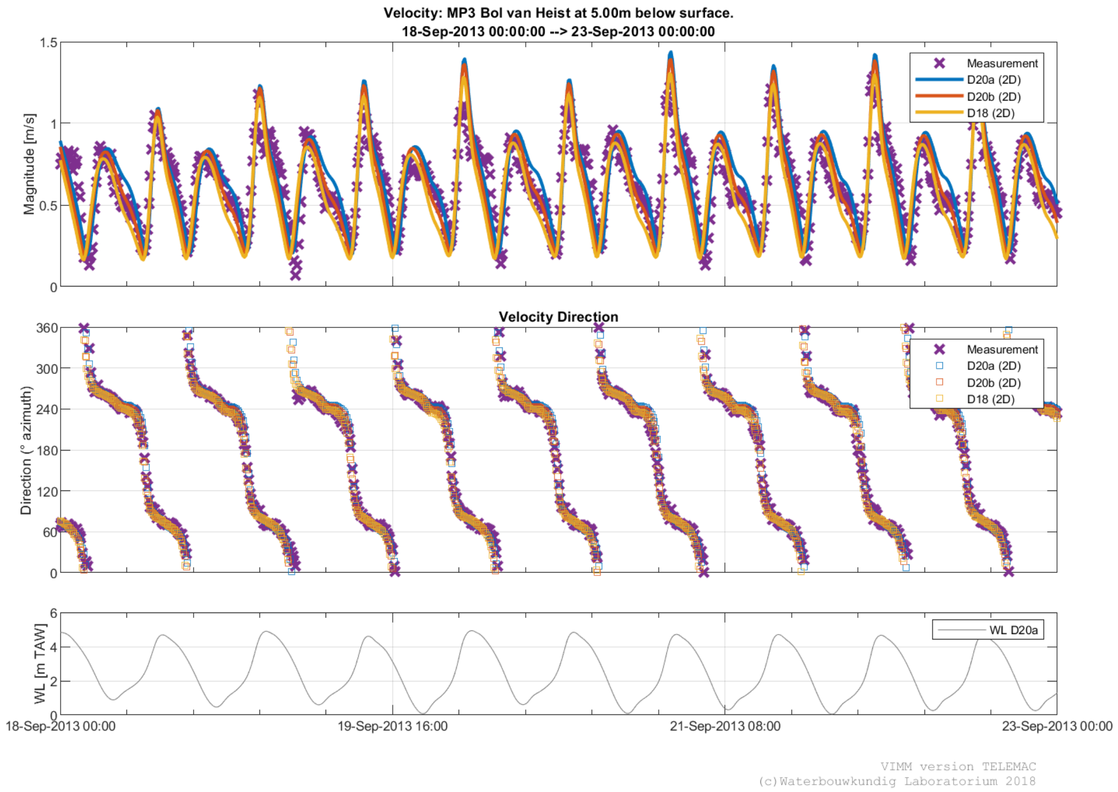

Figure 81 – Magnitude and direction of the measured and modelled velocity time series at Bol van Knokke (top figure) and at WZ buoy (bottom figure).
Bol van Knokke: Depth-averaged measurements from 5.0 m to 7.5 m below water surface; WZ buoy: profile-averaging up to 3.0 m from the bottom. D18: reference run; D20a: Manning's *n* =0.015 up to HPW; D20b: Manning's *n* =0.018 up to Scheldeoord.

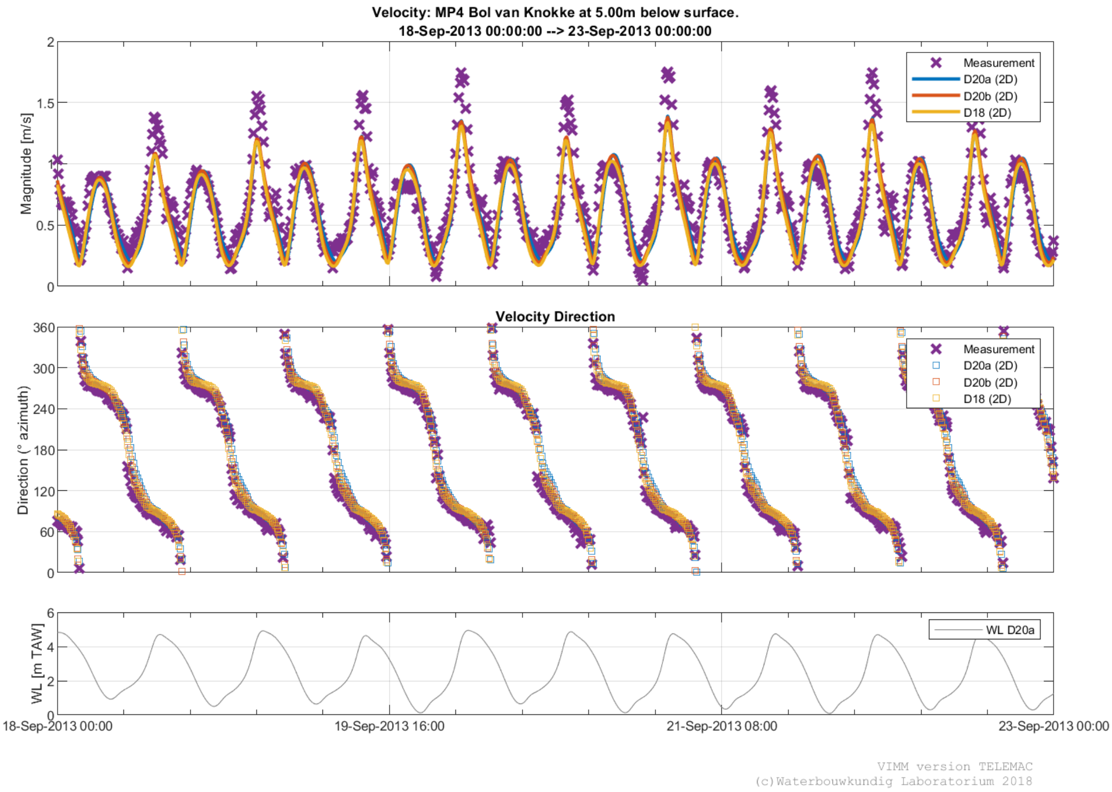

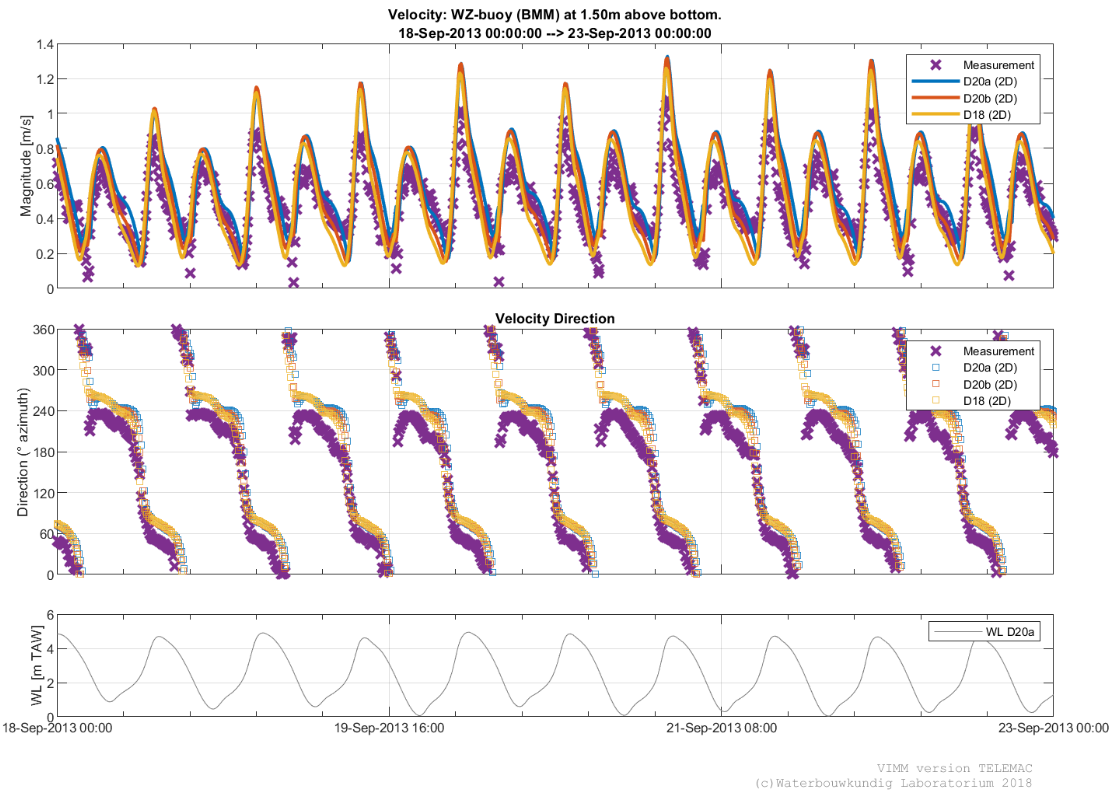

Figure 82 – Magnitude and direction of the measured (depth-averaged) and modelled velocity time series at HPW MP101 (top figure) and at HPW MP205 (bottom figure).
D18: reference run; D20a: Manning's *n* =0.015 up to HPW; D20b: Manning's *n* =0.018 up to Scheldeoord.

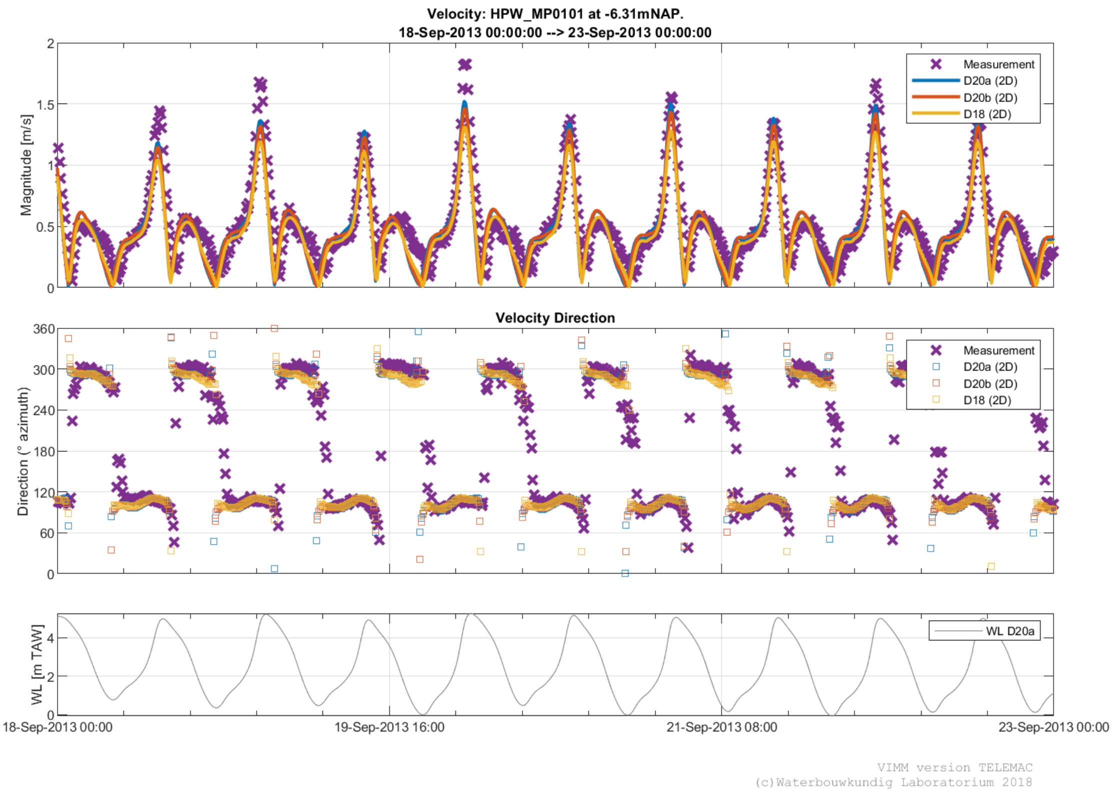

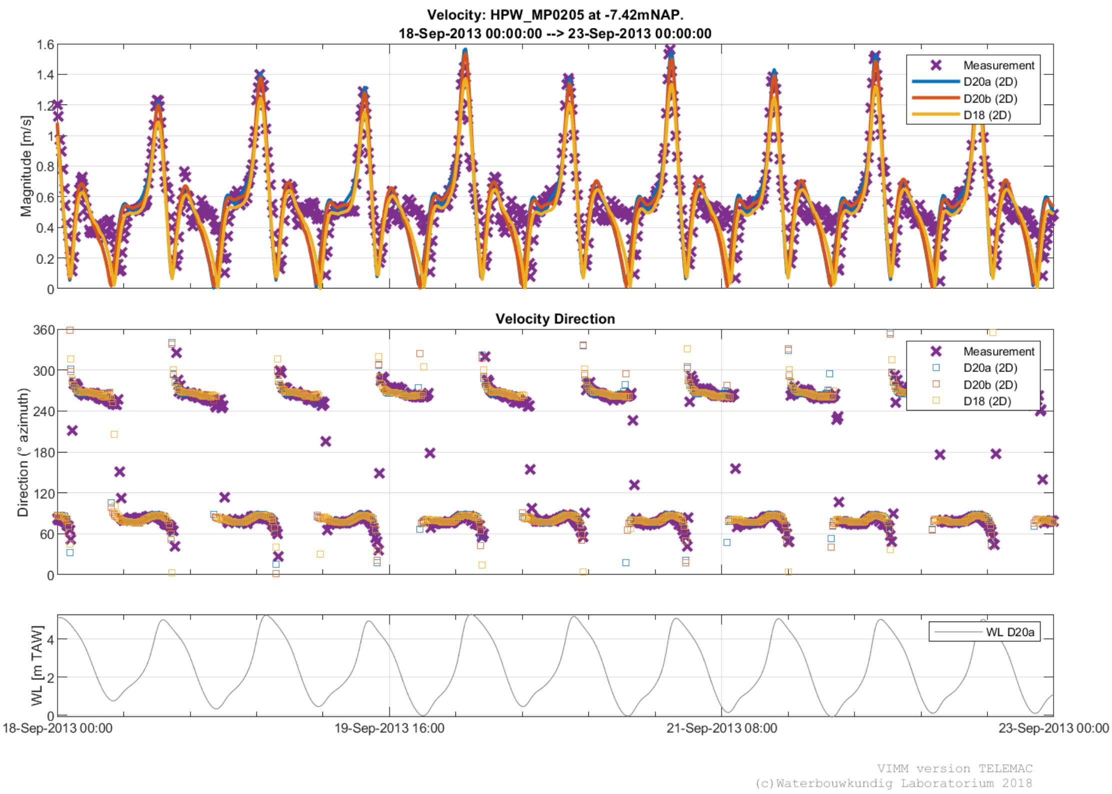

Water levels

The bias in the high (HW) and low water (LW) levels between the numerical predictions of the Manning's runs D20* (except for D20c which leads to almost identical results with D20d) and the measurements at the selected locations, are shown in Figure 83.

Figure 83 – Bias in the High Water levels (top figure) and the Low Water levels (bottom figure) between the numerical predictions and the measurements.
D18: reference run; D20a: Manning's *n* =0.015 up to HPW; D20b: Manning's *n* =0.018 up to Scheldeoord; D20d: Manning's *n* =0.018 up to HPW.

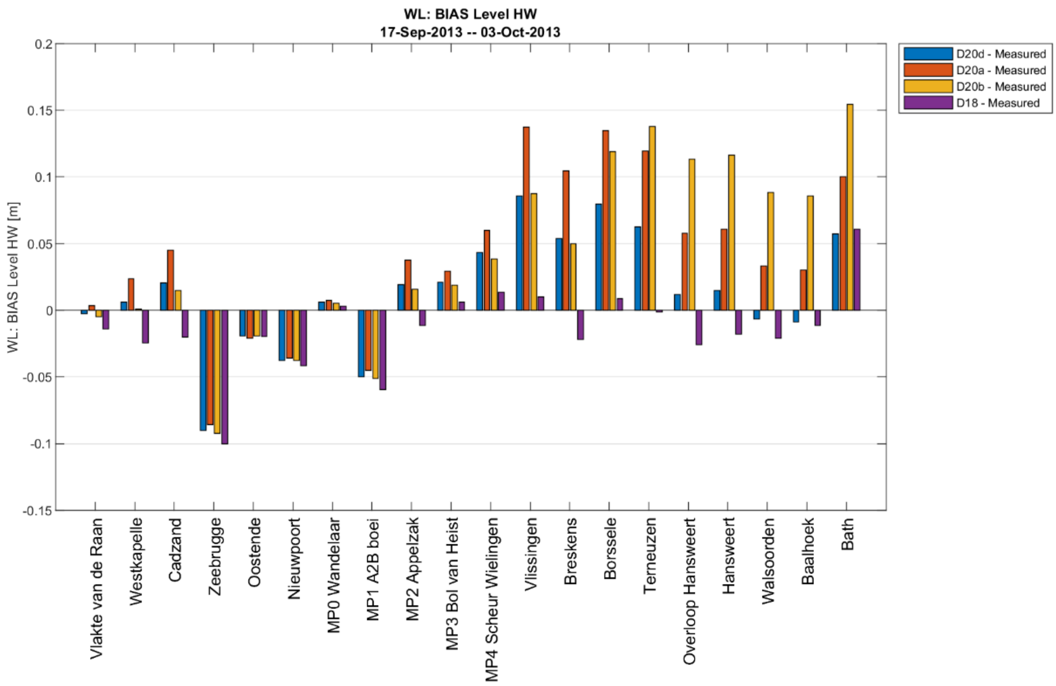

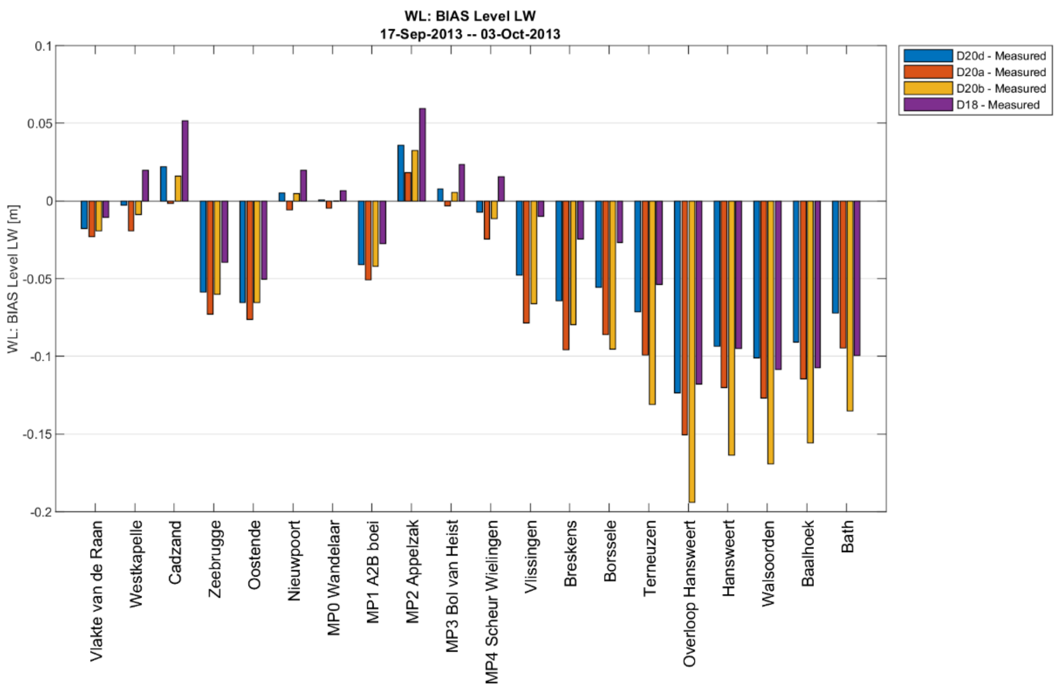

In general the performance of all the D20* Manning's runs is similar in predicting HW and LW levels at the majority of the coastal stations. In the Western Scheldt, the performance of D20b becomes worse reaching LW values close to -20 cm at Overloop Hansweert. This behavior indicates that the extension of a low *n* value to the upstream direction (Scheldeoord) causes unwanted increase of the tidal amplitude. The HW and LW levels predicted by D20a show also (a smaller) increase of the tidal amplitude, indicating that an additional reduce of *n* is not optimal.

The aforementioned differences cannot be indicated in Figure 84 of the bias of the complete water level time-series, where the D20* set-ups give similar results.

Figure 84 – Bias in the complete water level time-series between the numerical predictions and the measurements.
D18: reference run; D20a: Manning's *n* =0.015 up to HPW; D20b:
Manning's *n* =0.018 up to Scheldeoord; D20d: Manning's *n* =0.018 up to HPW.

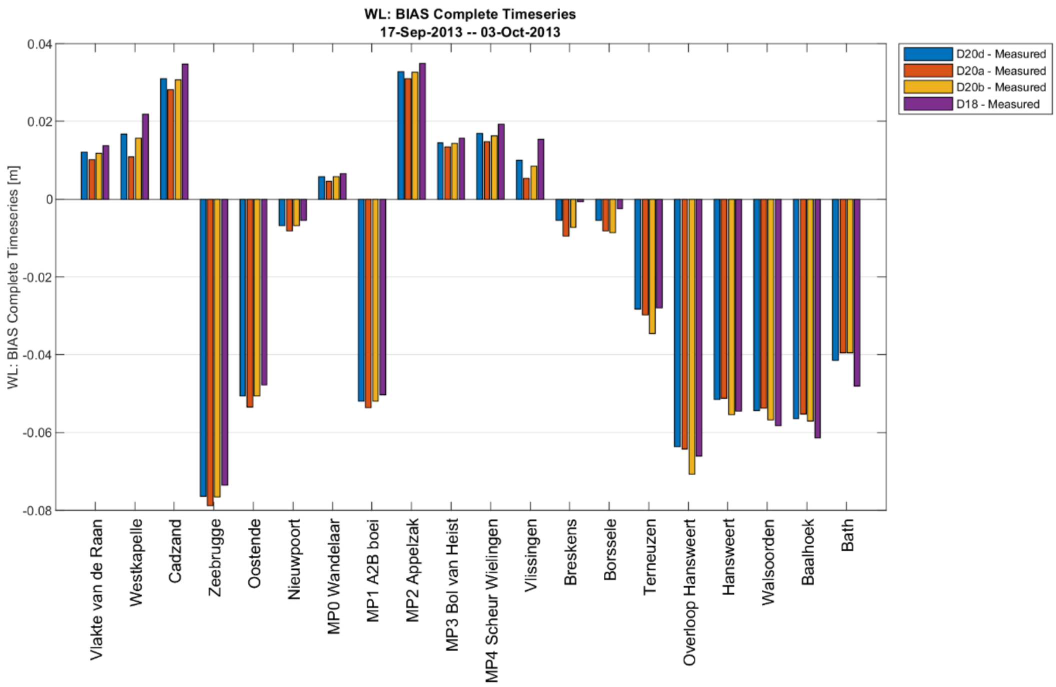

In Figure 85 the bias in the time of occurrence of high and low water between the numerical predictions of the Manning's runs D20*and the measurements at the selected locations, are shown. Overall it is shown that the acceleration of the tidal wave in the Western Scheldt is higher for both the extra reduced *n* = 0.015 (D20a) and for the extended low *n* (= 0.018) up to Scheldeoord (D20b). Compared to the D18 (reference) run, the backward shift in time for LW levels reaches values up to 12 min for both D20a and D20b runs. Note that the highest acceleration for D20a run is observed at the area of Vlissingen, while for D20b it is observed at more upstream stations. As for HW levels, the D20b run performs well up to Borselle compared to D20d, which shows that the extension of low *n* values can have a positive effect when the water is relatively deep. However the big differences in HW and LW time shift may be an indication that the formula for the variation of G_1 factor (and therefore the friction force F_f) as a function of the depth needs improvement.

In Figure 79 the RMSE in the complete water level time series is given and it is shown that both the D20a and D20b runs perform worse than D20d and D18 in The Western Scheldt. However for the D20a run the RMSEs are always less than 20 cm, while for D20b reach values up to 25 cm for the most upstream stations.

Figure 85 – Bias in the time of High Water levels (top figure) and the time of Low Water levels (bottom figure) between the numerical predictions and the measurements.
D18: reference run; D20a: Manning's *n* =0.015 up to HPW; D20b:
Manning's *n* =0.018 up to Scheldeoord; D20d: Manning's *n* =0.018 up to HPW.

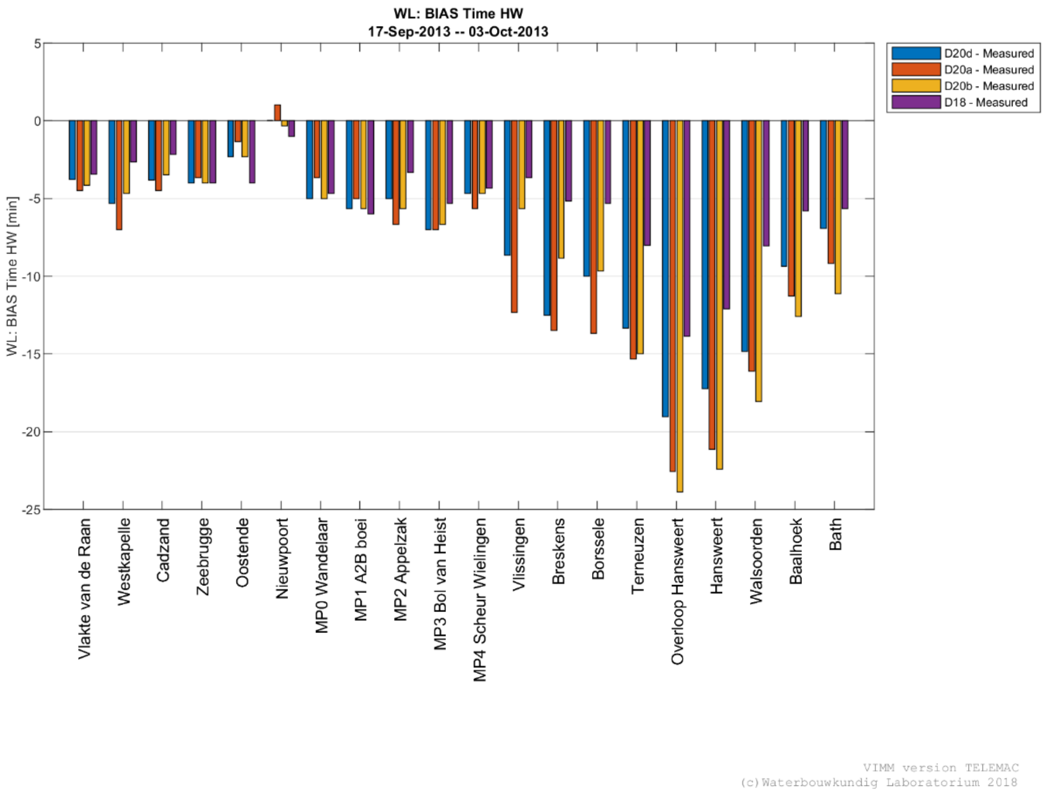

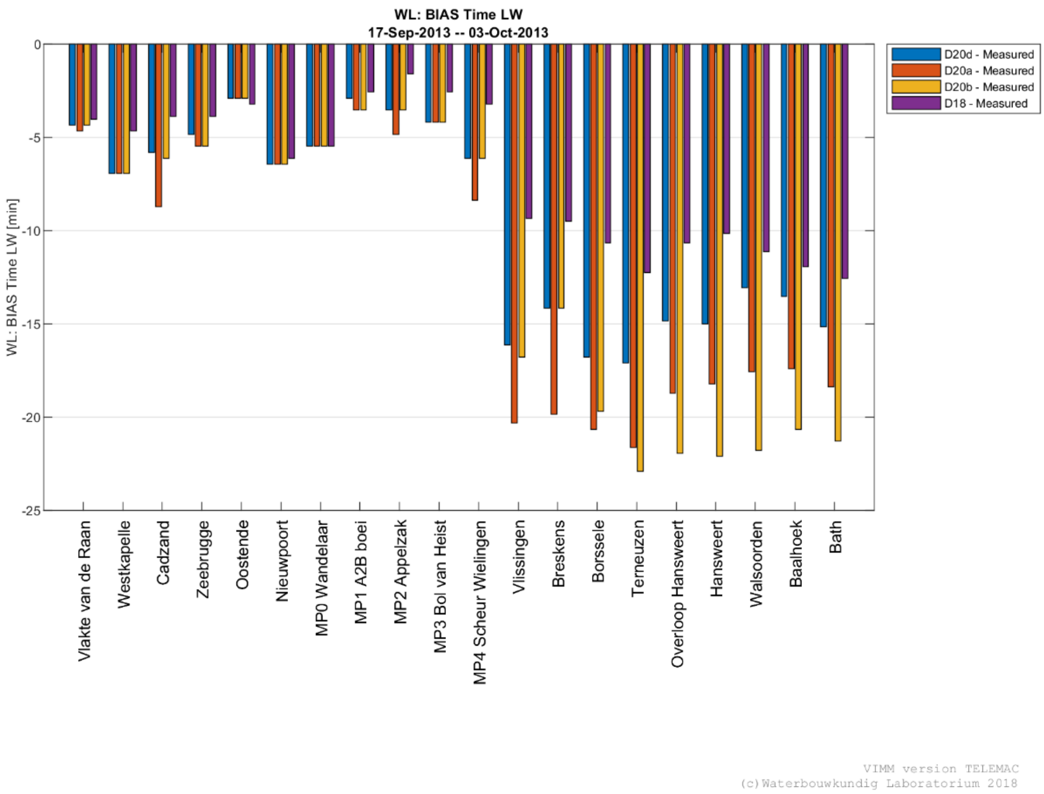

Figure 86 – RMSE in the complete water level time-series between the numerical predictions and the measurements. D18: reference run; D20a: Manning's *n* =0.015 up to HPW; D20b: Manning's *n* =0.018 up to Scheldeoord; D20d: Manning's *n* =0.018 up to HPW.

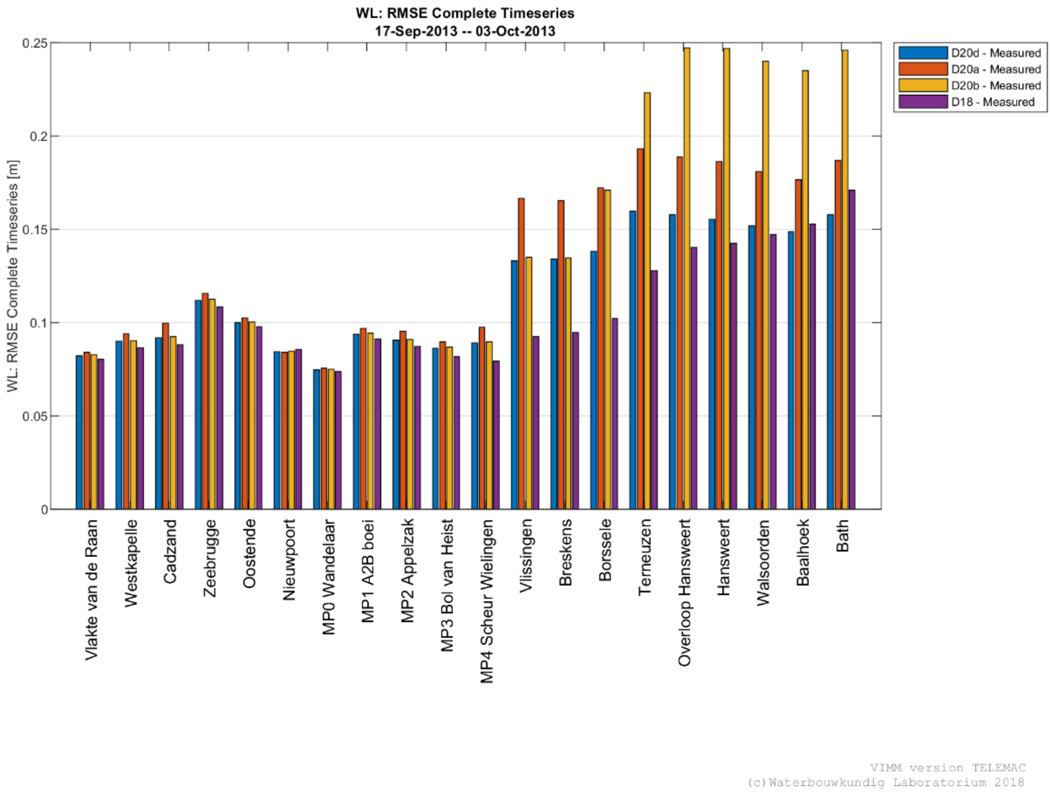

Conclusions

A series of hydrodynamic simulations were conducted for the bottom roughness tuning of the Scaldis-Coast model (Kolokythas *et al*., 2018). Tests included the consideration of both Manning's and Nikurades's laws. The main idea was to reduce the bottom friction using lower values for the Manning's coefficient, *n*, (or Nikuradse's k_s) in order to improve the prediction of the peak flood velocities.

It is found that:

- the reduced *n* coefficient tests can achieve an increase of the peak flood and ebb velocities around 10 to 15 cm/s compared to the reference run
- the high water (HW) levels affected the most by the reduction of *n* are those located at the area of the mouth of Western Scheldt (especially Vlissingen to Terneuzen). The low water (LW) levels are affected in a lesser extent.
- there is an acceleration of the tidal wave observed at the Western Scheldt which is attributed to the lower *n* values at the coast. The highest backward shift in time is observed for LW levels.
- the Nikuradse's test run (with k_s values corresponding to the reduced *n* values, D21c) lead to quite similar results for the velocities as the Manning's corresponding test (D20d). As for the water levels the Nikuradse's run presents better behavior in predicting the time of occurrence of HW and LW levels in the Western Scheldt. However, the reference Manning's run (D18) performs better in water level prediction at all stations downstream of Hansweert.
- an additional reduction of *n* at the coast (from 0.018 to 0.015) can increase up to 5 cm/s the predicted peak flood velocities. However accelerated tidal waves and increased tidal amplitudes are observer in the Western Scheldt indicating that an additional reduce of *n* at the coast is not optimal.
- the extension of the reduced *n* field (0.018) from Hooge Platen West (HPW) to Scheldeoord deteriorated the tidal wave characteristics especially at the most upstream Western Scheldt stations

To sum up, the most balanced behavior was exhibited by the Manning's test run D20d, in which the bed roughness field is composed by:

n = 0.018 up to HPW, *n* = 0.024 for the upstream part and *n* = 0.035 at the schematized part.

Note that the impact of increased *n* at the schematized part is very low.

DEPARTMENT **MOBILITY & PUBLIC WORKS**
Flanders hydraulics Research

Berchemlei 115, 2140 Antwerp
T +32 (0)3 224 60 35
F +32 (0)3 224 60 36
waterbouwkundiglabo@vlaanderen.be
www.flandershydraulicsresearch.be